Abstract of "Development of a Liquid Crystal Biosensor for the Detection of Endotoxin" by Maureen K. McCamley, Ph.D., Brown University, May, 2009.

This dissertation describes translational research conducted to develop a rapid diagnostic for the detection of endotoxin using liquid crystal sensor technology. Due to the elastic nature of bulk nematic liquid crystal, small changes in surface anchoring at the interface between the liquid crystal sensor and the targeted biomolecule (endotoxin) are amplified, allowing optical detection through polarizing microscopy. Theoretical simulations, using a phenomenological Landau-de Gennes approach, were applied to understand and predict the behavior of the confined nematic. Simulated optical micrographs were compared with experiments to understand the nematic profiles and to control and optimize the sensor in a specific regime. Distinct optical patterns were detected when the sensor was exposed to air and to water. A structural transition in the nematic structure was observed, driven by changes in the anchoring strength at the open surface of the sensor. This change was leveraged and used to detect the presence of both a model surfactant and the targeted biomolecule at the open surface. The response of the sensor can be controlled by changing certain experimental parameters, such as the depth, aspect ratio, anchoring strength and nematic material. Isolated lipopolysaccharide (LPS) was detected in concentrations varying from 1 mg/mL to 10 μg/mL, giving a very strong and quantifiable response of the sensor.

Development of a Liquid Crystal Biosensor for the Detection of Endotoxin

by

Maureen K. McCamley

B.S., New Mexico State University, 2002

Sc.M, Brown University, 2004

Submitted in partial fulfillment of the requirements

for the Degree of Doctor of Philosophy in the

Division of Engineering at Brown University

Providence, Rhode Island

May, 2009

This dissertation by Maureen K. McCamley is accepted in its present form by the Division of Engineering as satisfying the dissertation requirement for the degree of Doctor of Philosophy.

Date _____ _____
Gregory P. Crawford, Director

Recommended to the Graduate Council

Date _____ _____
Andrew W. Artenstein, Reader

Date _____ _____
Steven M. Opal, Reader

Date _____ _____
Anubhav Tripathi, Reader

Date _____ _____
Slobodan Žumer, Reader

Approved by the Graduate Council

Date _____ _____
Sheila Bonde
Dean of the Graduate School

Vita

Maureen Kathryn McCamley was born in Pusan, South Korea. She grew up in northern Virginia before moving to New Mexico in 1992. After graduating from New Mexico State University with a Bachelor's of Science in Mechanical Engineering in 2002, she moved to Rhode Island to begin graduate studies at Brown University. She received a Master's degree in Engineering in 2004, submitting a thesis on her research entitled "Effects of Lorentz Force Actuation on Turbulent Channel Flow." In 2005, she joined the Display and Photonics Laboratory and began working in the field of Biomedical Engineering. She was funded through a NASA GSRP fellowship for her graduate studies, and was selected in 2008 for the Christine Mirzayan Science and Technology Policy Fellowship at the National Academy of Sciences in Washington, D.C.

Publications

1. M. K. McCamley, M. Ravnik, A. W. Artenstein, S. M. Opal, S. Žumer, G. P. Crawford,"Detection and optimization of alignment changes at the open surface of a nematic liquid crystal sensor," *Journal of Applied Physics* , Accepted for publication

2. M. K. McCamley, M. Ravnik, A. W. Artenstein, S. M. Opal, S. Žumer, G. P. Crawford,"Optical detection of anchoring at free and fluid surfaces using a nematic liquid crystal sensor," *Applied Physics Letters* 91, 141916

3. Author: M. K. McCamley, A. W. Artenstein, G. P. Crawford, "Liquid Crystal Biosensors: A new approach for medical diagnostic devices," in S. J. Woltman, G. D. Jay, and G. P. Crawford (eds.), *Liquid Crystals: Frontiers in Biomedical Engineering* (World Scientific, 2007).

4. M. K. McCamley, A. W. Artenstein, S. M. Opal, G. P. Crawford, "Optical detection of sepsis markers using liquid-crystal based biosensors," *Proceedings of the SPIE - Photonics West* 6441, 64411Y (2007).

5. M. K. McCamley, C. Henoch, K. S. Breuer, "Structure and dynamics of turbulent flows subjected to Lorentz force control," *Proceedings of the AIAA* 2006-3191. San Francisco, CA. (2006).

6. M. K. McCamley, "Effects of Lorentz Force Actuation on Turbulent Channel Flow". *Sc. M*

Thesis, Division of Engineering, Brown University (2004).

7. J. Park, C. Henoch, M. K. McCamley, K. S. Breuer, "Lorentz Force Control of Turbulent Channel Flow," *Proceedings of AIAA* 2003-4157. Orlando, FL. (2003).

Acknowledgments

I would like to thank my family and friends who have been supportive through this long process. My parents, brother and other family have supported this endeavor from start to end. My friends and fellow graduate students: Mikey, Jean, Patrick, Don, Chris, Katie, Kevin and Missy,

Barus and Holley staff who have been wonderful through the course of my studies: Charlie, Mike, Tina, Cheryl, Lauren, Jonathon, Nancy, Estelle and Ginny.

My colleagues in the Display Lab who have been very giving of their time and knowledge: Matt Sousa, Jim Eakin, Fred Biga, Scott Woltman, John McMurdy, Leslie Shelton and Neil Rajan.

And finally my deepest appreciation goes to those who contributed most to this work: Professor Greg Crawford and Dr. Andrew Artenstein, my advisors; Miha Ravnik, without whom this collaboration would not have been possible; Professor Slobodan Žumer, who has provided invaluable guidance; and Dr. Steven Opal, who lent his expertise and experience with endotoxin.

Contents

List of Tables

List of Figures

Chapter 1

Medical Diagnostics: Background and Motivation

1.1 Introduction

The research work described in this dissertation began in a somewhat non-traditional manner. Typically, bench science is conducted for clarity and to satisfy scientific curiosity. This work began with the goal of identifying a clinical problem in medicine, and leveraging current scientific technology to find a solution. This translational process started by holding numerous meetings with physicians in a broad range of disciplines, which highlighted the absence of cutting edge technology in many medical settings. Due to the inherent nature of diagnostics, infectious disease was targeted as a field with an extensive range of opportunities. A collaboration was formed with infectious disease specialists at Memorial Hospital of Rhode Island, and at that first meeting, an idea was generated that later evolved into the work presented here. The particular areas of expertise of both the physicians and the engineers in the collaboration aligned, producing the basis for a liquid crystal based biosensor for the detection of endotoxin. This chapter presents background on sensors and a broad look at the problem of infectious disease, as well as current medical diagnostic methods. Chapter 2 provides a brief look at liquid crystals and their unique properties, particularly those that apply for use in a

biosensor. Previous work in the area of liquid crystal biosensors is covered in Chapter 3. Theoretical and Experimental processes and results are presented in Chapters 4 and 5, respectively. Chapter 6 provides a background on endotoxin and sepsis, and details experimental results for the detection of endotoxin with a liquid crystal biosensor. Conclusions and recommendations are discussed in Chapter 7.

Sensors, devices that receive and respond to a stimulus, have long been developed and used in clinical settings out of a necessity for advancement in diagnostics. The first stethoscope was developed in 1816 by Rene Laennec [2] due to his personal discomfort at placing his ear against the chest of a young female patient. While devoting much of his research to the measurement of the brain's electrical activity, Hans Berger recorded the world's first electroencephalogram (EEG) in 1924, shown in Figure 1.1. Experiments on patients with normal brain function, as well as those who suffered brain injuries, laid the basis for the EEG as a clinical diagnostic tool. Today, EEGs are used in the diagnosis of serious head injuries, brain tumors, cerebral infections, epilepsy, and degenerative diseases of the central nervous system. William Einthoven invented the electrocardiogram (EKG or ECG) in 1901 based on the hypothesis that the heart produces an electrical current with each beat; he was awarded the Nobel Prize in Medicine in 1924 for his work [3]. Each of the aforementioned examples represents a vital tool for modern physicians. Sensors, and their demand as a clinical diagnostic, have been burgeoning over the past 20 years as the pace of technological advancement has continued to rapidly expand. One of the most promising fields for incorporating biological sensors in today's clinical setting is in diagnosing infectious disease.

According to the US Department of Health and Human Services' *Centers for Disease Control and Prevention* there are 26 million office visits a year due to infectious and parasitic diseases in the United States alone. Adding hospital and emergency room visits increases that figure to well over 30 million [5]. Not only is the public health burden imposed by these visits considerable, but the financial cost associated with the diagnosis of these diseases is extraordinarily high. The urgent need for a reliable, clinically useful, rapid diagnostic cannot be more apparent than when considering *World Heath Organization* [6] statistics; there are 11 million annual deaths worldwide due

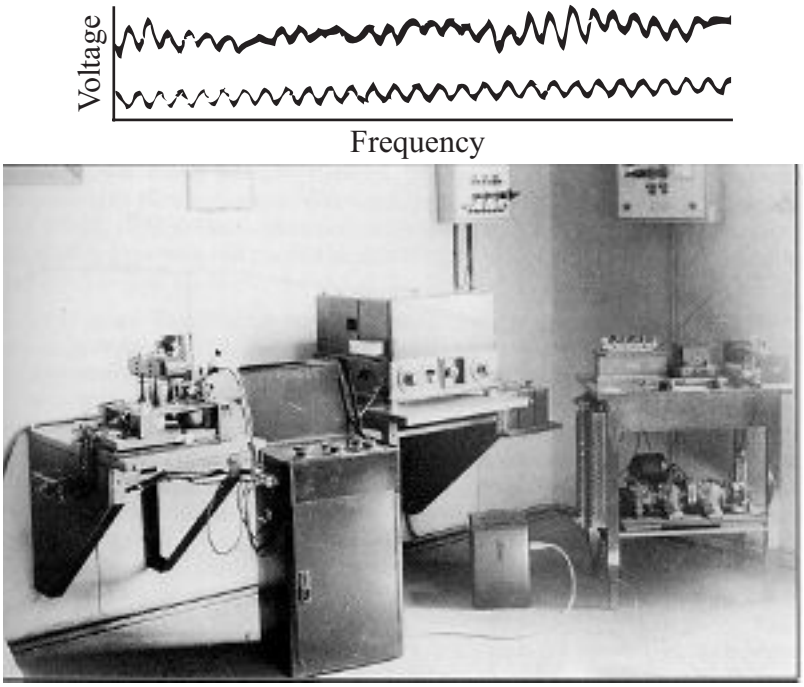

Figure 1.1: The world's first electroencephalogram (EEG), recorded by Hans Berger in 1924 and the setup used to capture the data. From [4].

to infectious diseases. The numbers are staggering when the impact of development and technology is included: 34% of deaths in developing countries were attributed to communicable diseases as opposed to only 6% in developed countries (Figure 1.2). The introduction of rapid, point-of-care infectious disease diagnostics will not entirely erase this burden, but will be a significant step forward in identifying victims and facilitating the start of proper treatment.

Infectious diseases, either emergent from nature or manipulated in the laboratory for malicious purposes, continue to be a major threat to global security. Although bioterrorism in one form or another has been practiced since the 14^{th} century, September 11th, 2001 changed the way terrorism was viewed in the modern world. Exactly one week after the attacks on the Pentagon and the World Trade Centers, the first letter containing anthrax was mailed from Trenton, NJ and changed the public's perception of bioterrorism. These attacks instilled fear and an acute awareness of our vulnerability to biological weapons.

The persistent threat of pandemic influenza on a scale not seen since 1918 represents an ongoing challenge. Viral mutations and emergences in animal species and humans must be continually studied

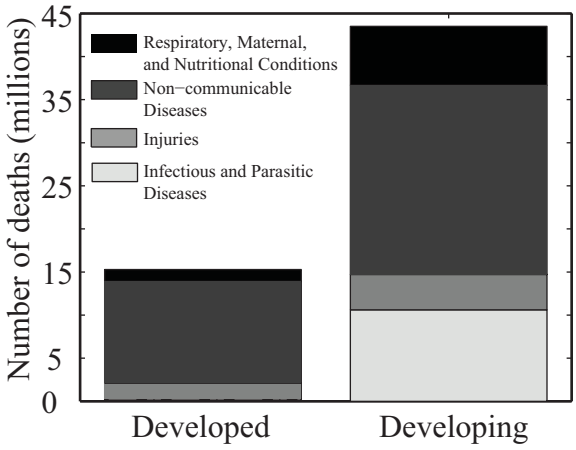

Figure 1.2: Causes of death worldwide for developed and undeveloped countries. Data from the *World Heath Organization*

and followed worldwide. The advancement of research and knowledge concerning infectious diseases has been considered a double edged sword: "...greater understanding and control over infectious diseases inevitably leads to greater opportunity for transforming those diseases into weapons" [7]. After the anthrax attacks, the shortcomings of our public health system were highlighted, spurring research into the development of not only vaccines but emergency plans for health care in the event of further attacks. In the midst of this preparation, it became evident that our ability to detect infectious diseases is sub-optimal: "In most parts of the world, the capacity to detect and respond to epidemics of infectious diseases is still lacking or rudimentary" [8]. These events again highlight the urgent need for rapid infectious disease diagnostics that function with equal accuracy both at a patient's bedside as well as in the field. One of the first steps in the aftermath of an attack of bioterrorism is to identify who has been exposed to potential pathogens and to quarantine those individuals. A handheld device to differentiate infected patients from those who are not at the entrance to a hospital or triage area can save time, money and, potentially, human lives. One of the earliest steps in tracking a novel epidemic virus is to rapidly delineate the extent of its transmission, necessitating a portable, accurate, rapid diagnostic device.

1.1.1 Scope of the Problem

With device technology advancing at a staggering pace, it is hard to believe that a workhorse diagnostic tool is not already ubiquitous in clinical use. Although hopes still exist that someday a *StarTrek* like tricorder device will spring to use, point of care diagnostics are currently somewhat crude, at best. Why is creating a device capable of identifying pathogens from a human sample so difficult? Currently, the gold standard for identification of bacteria is a laboratory culture: the sample is obtained, placed in culture medium, and incubated to facilitate growth; the latter leads to biochemical identification by a technician. This process generally requires at best 24 hours and involves significant financial cost, technical expertise, and scientific facilities. In the case of viruses, even more technical hurdles must be overcome, making viral isolation a procedure limited to specialty laboratories and unavailable in many hospital settings. In order for a rapid, portable diagnostic to succeed it must have the ability to quickly and accurately recognize biomolecules such as bacteria, viruses and parasites. Successful identification of these molecules involves trapping or labeling the target molecule and indicating its presence with a reliable, accurate and repeatable technique. Current methods will be discussed in depth later in the chapter.

1.1.2 Engineering a Solution

Recently, there has been a movement to combine medical need with engineering technology in order to facilitate useful, clinically relevant tools for medicine [9–14]. While much of the academic research in engineering aims to understand the basic underlying phenomena of scientific principles and is curiosity-driven, collaborations between engineers and physicians seek to provide useful solutions to clinically important problems. Instead of searching for an application for a novel engineering discovery, engineering technology is paired with existing problems presented by physicians in order to find a solution.

Biosensors are an ideal bridge between engineering and medicine; they allow the medical field to leverage the massive research and technological advances in engineering for use in clinical devices.

Currently, microfluidic devices are the focus of commercialization for a rapid diagnostic. A microfluidic device is commonly described as having a feature (such as a channel) with a size smaller than 1 mm. Microfluidic detection devices hold many advantages over conventional laboratory culture techniques. All aspects of the detection chip are miniaturized, requiring a very small sample size, on the order of nanoliters, allowing the chip itself to be portable. Flow patterns on the chip have been modeled, enabling the molecular identification of pathogens in a matter of seconds.

Although great strides have been made in the progression of microfluidic devices, a number of obstacles still remain. Most systems are extremely sensitive; while useful, this quality also leads to false positives, many due to contamination. The support equipment for these devices, such as pressure transducers and electrical stimuli, are cumbersome and expensive and hence hinder the portability of the system. Most microfluidic chips still require the target molecule to be marked or tagged, which in turn requires an advanced optical readout. Although the progress towards a clinically relevant microfluidic device has been promising, other technologies such as spectroscopic techniques and liquid crystal biosensors have recently emerged as competitors in this rapidly evolving field.

The focus of this research is on the use of liquid crystals in biological applications, specifically for use in diagnostics. Liquid crystal technology provides a striking example of a field that has been extensively studied and researched for commercial products, yet applications in biology and medicine have been slow in advancing. The unique properties of liquid crystals that make them enticing for biosensors, including birefringence [15, 16], surface alignment [17, 18], and electric switching [19, 20], have been studied in depth for applications such as flat panel displays. The ability to leverage this vast amount of existing knowledge for liquid crystal based biosensors provides promising advances in clinical diagnostics. Liquid crystals hold advantages over other materials currently used in diagnostic applications; the inherent birefringence of the molecule provides an optical signal enabling a sensor that doesn't require marking or labeling of the target biomolecule and amplifies the response, making detection simpler. The delicate response of surface interactions allow liquid crystal biosensors to be incredibly sensitive. Many of the qualities that make liquid crystals an attractive choice for

use in displays can be leveraged for biological sensors. Much of the translational potential for this technology, until this point in time, has been overlooked. Simply put, the engineering and medical communities can do better than the rapid diagnostics currently available. Recently, promising techniques have been investigated that will hopefully continue to be developed into a clinically useful product.

It should be noted that the scope of biological sensors currently being researched is broad. For the purpose of giving context for the background of this thesis, this chapter will focus on the application of liquid crystal biosensors, specifically those targeted towards infectious disease diagnostics. A summary of other related liquid crystal chemical and biological sensors is presented in Chapter 3.

1.2 Current Diagnostic Techniques

There are multiple techniques available to screen for the presence of a pathogen or an immune response in a patient suspected of harboring an infectious disease. None of these methods are 100% accurate; occasionally they fail to signal the presence of a pathogen or they identify a pathogen when none is present. Briefly, current microbiological diagnostic techniques will be outlined, followed by a discussion of emerging rapid diagnostic techniques that are non-liquid crystal based. For a more detailed discussion of current laboratory techniques, the reader should consult the textbooks of Schoechter and colleagues [21] and Mandell and colleagues [1].

Clinical diagnostics can be subdivided into four major categories: microscopy, culture, detection of immune response and detection of microbial macromolecules. Due to their unique morphologies, certain pathogens can be identified using microscopic techniques. One of the most common techniques used to group potential pathogens is staining. The Gram stain differentiates between two major groups of bacteria. Due to structural differences in the outer cell membrane, Gram-positive bacteria stain purple and Gram-negative bacteria stain pink. While this can help narrow the diagnostic possibilities and assist in the choice of empiric therapy, it is not considered definitive identification. Other stains used in clinical microbiology include the acid-fast, Giemsa, iodine and silver, each with different properties.

Laboratory culture is the most widely used and specific method of identifying a pathogen. In general, a suspected sample is grown *in vitro* in a nutrient rich environment. The sample is observed, and over time, a positive test results when a pathogen is cultivated. An open-ended culture provides an environment where all possible etiologic (causative) agents can be recovered. Open ended cultures are useful in cases where the biological sample is usually sterile, such as blood, cerebrospinal fluid, or joint fluid; non-sterile body sites contain many normal flora that may contaminate the sample and render the results difficult to interpret. Cultures from non-sterile body sites can be grown on selective media, where only specific classes of pathogens are enhanced. Various techniques are employed to improve the yield from cultures: subculturing for species identification, or lysis centrifugation, where blood is collected directly into a tube that lyses the blood cells. All culture methods require interpretation by a physician to correlate the results with the clinical setting and to determine if the pathogen is an etiologic agent or a component of normal flora. Many pathogens cannot be cultured in a typical hospital or commercial laboratory setting, and require specialized technical resources and personnel. All require a minimum of $12-24$ hours for pathogen growth and additional time for reliable identification.

Serologic assays detect the body's immune response to an infection. Solid phase immunological assays measure the presence of specific antibodies in serum. A pathogen or antigens specific to that pathogen are fixed to a solid support where specific antibodies bind and are immobilized. This binding event is detected by adding a labeled antibody that binds to the human antibodies and catalyzes the production of a visible compound. Examples of these assays include the ELISA (enzyme linked immunosorbant assay) and the Western blot (immunoblot). Yacoub-George and colleagues [22] have used a capillary ELISA technique coupled with chemiluminescence as the detection principle to detect potential biological warfare agents. It may take up to four weeks to detect a serologic response to an infectious antigen; therefore, the use of serological tests is of limited value in the early stages of infection before the patient has developed the requisite antibodies.

Much like a forensic lab uses DNA to identify the perpetrator of a crime, molecular methods use microbial DNA to identify potential pathogens. One of the most common current methods for DNA

identification is the polymerase chain reaction (PCR). PCR amplifies targeted strands of microbial nucleic acid, which can then be detected based on size by gel electrophoresis or with fluorescence labeling. PCR techniques provide great sensitivity as they can detect very small concentrations of a potential pathogen. However, this also proves to be a limitation as any degree of contamination is exponentially amplified along with any targeted microbe. Both sides of the argument to replace cell culture in laboratories with molecular techniques are presented in a forum by Ogilvie [23] and Carman [24]. Recent publications have compared culture and PCR methods for specific pathogens [25, 26]. Applications of molecular diagnostics for rapid detection such as PCR diagnostics on microfluidic chips will be discussed in the next section, followed by other rapid diagnostic research areas.

1.2.1 Molecular Diagnostics and Microfluidics

Although applications of PCR and molecular diagnostics on microfluidic platforms will be discussed here, more detailed analyses and reviews can be found elsewhere [27–29]. The three main steps involved in molecular diagnostics are DNA extraction, amplification, and detection or sensing. In keeping with the long range view of a rapid, portable diagnostic presented earlier, we shall present research moving towards independent and accurate sensors.

Meningitis, an infection of the membranes lining the central nervous system and covering the brain, provides an example of an infectious disease where a rapid diagnostic could make an enormous impact. Bacterial meningitis is life threatening condition that can be rapidly fatal to even young, healthy individuals. Corless and colleagues [30] describe a real-time PCR based diagnostic capable of simultaneously identifing the three major pathogens that cause bacterial meningitis: *N. meningitidis, Streptococcus pneumoniae* and *Haemophilus influenzae* type b. DNA extraction took place separately from the PCR device (7700 Sequence Detection System, also known as Taqman^{TM}) by incubation and centrifugation. A large number of samples, 4113, from the British Meningococcal Reference Unit were screened for the three potential pathogens and any positive result was confirmed with a single primer set. Sensitivities for the three pathogens were all above 88%. Although limitations with the DNA primers were encountered, and degradation of the DNA due to long term storage

was noted, the multiplex assay used in this study enabled rapid identification for all three main pathogens and a high throughput of suspected cases of bacterial meningitis.

For cases of viral central nervous system (CNS) infections, Boriskin and colleagues [31] developed a microarray which focused on 38 gene targets for 13 viral causes of meningitis and encephalitis. The sensitivity and specificity of the assay were 93% and 100%, respectively, when results were verified using a single-target PCR. One of the limitations of the study was that it was difficult to target strain-specific nucleotide polymorphisms. Although the assay can be further refined, a PCR microarray assay has proven successful in screening for multiple pathogens in CNS infections. Real-time PCR assays have been developed for the detection of possible bioterrorism agents such as anthrax [32, 33] as well as other CNS infections caused by enteroviruses and herpesviruses [34].

After DNA amplification, different methods can be utilized for the detection of the target region. In a study by Deisingh and Thompon [35], PCR was combined with detection using a thickness shear mode (TSM) acoustic wave sensor. One of the advantages of using an acoustic wave sensor is that it can detect viable cells as opposed to the total bacterial load. Although the results of the study showed that long sequences specific for *E.coli* can be detected using PCR coupled with an acoustic wave sensor, the authors caution that a clinical sample was not used in the assay. It is hypothesized that other extraneous material present in a clinical sample will perhaps change the sensitivity and specificity of the assay. Another method used to rapidly detect the presence of pathogens is fluorescence polarization combined with DNA amplification. Tsuruoka and colleagues [36] developed a rapid test using oligonucleotide hybridization for the detection of agents such as *E.coli* and human hepatitis C virus (HCV). In optimizing conditions, such as temperature and salt concentration, they decreased the time required for the hybridization reactions. Although their focus was on specific DNA probes to induce higher hybridization of target molecules, the study highlights the use of DNA amplification combined with fluorescence detection as a rapid diagnostic tool.

The next logical step in developing a portable, rapid, PCR based diagnostic for infectious disease pathogen identification would be combining the preparation steps, such as DNA extraction, with PCR and detection. Lee and colleagues [37] have tested a microchip device that incorporates

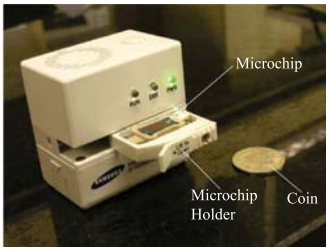

Figure 1.3: Portable LIMBS device with a single chamber and small laser diode for the real time detection of pathogens. From [37]. Permission for use to be requested.

pretreatment steps, such as cell lysis and purification. The Laser-Irradiated Magnetic Bead System (LIMBS) developed for this study (shown in Figure 1.3) uses magnetic beads combined with an 808 nm high power laser pulse and vibrations to disrupt the cells. The wavelength was chosen based on the absorption coefficients in water, so as to transmit as much energy as possible to the targeted pathogens. The combination of heat and mechanical shock from the vibrations leads to cell lysis of both Gram-positive and Gram-negative bacteria within 40 seconds. After the cells are lysed, the beads coated with cell debris and denatured proteins released from the cells are cleared with a magnet and real time PCR is performed on the remaining DNA in the chamber. The entire process, from sample preparation through cell lysis and PCR detection, takes less than 32 minutes. Research developments such as this are commonly referred to as lab-on-a-chip technologies, integrating many different processes and assays from a conventional laboratory setting onto a microchip.

Microfluidic and lab-on-a-chip technologies for rapid infectious disease diagnostics have been extensively reviewed elsewhere [38–41]. Detection issues [42] as well as digital microchip technologies [43] have also been explored. Methods such as electrophoresis [44], dielectrophoresis [45–47], electrowetting [48] and interferometric devices [49] have all been studied for on chip manipulation and detection. The range of applications for microfluidic chips has been expanding to include the management of infectious diseases such as CD4 counting in AIDS patients [50], replacing conventional DNA microarrays [51], glucose detection [52], point-of-care cancer diagnostics [53], and the detection of cervical cancer cells [54].

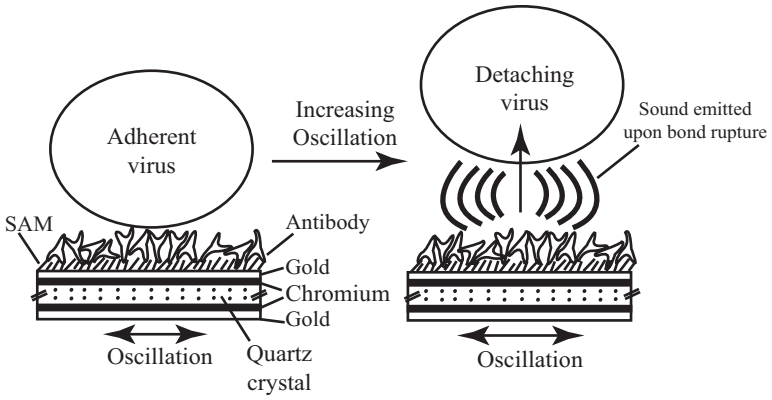

Figure 1.4: Schematic of the operation of a quartz crystal microbalance (QCM) device which uses periodic isolation to rupture the bonds at the surface and identifies the presence of targeted pathogens by detecting the acoustic emission.

1.2.2 Quartz Crystal Microbalance Assays

Another promising technique in the development of a rapid clinical diagnostic is the quartz crystal microbalance (QCM) method. Generally, the frequency of vibration of a crystal induced by an electric field changes proportionally when a mass is applied to its surface. QCM detection methods can be combined with immunological techniques for specific pathogen targeting. Lee and colleagues [55] used a QCM immunoassay to detect the presence of bacterial spores. A non-pathogenic simulant for *Bacillus anthracis* (the causative agent of anthrax) was detected in a constant flow cell sensor, which gives continuous real time monitoring. A frequency shift of about 20 Hz was seen from the anti-*B.subtilis* targeted sensor. Microscope images were taken after the flow cell experiment to verify attachment of the bacterial spores. A second experiment verified the sensor differentiated between bacterial spores and vegetative cells. One of the limitations of a one step direct QCM immunoassay is that the sensitivity of the assay depends on the molecular weight of the targeted analyte; lower molecular weight antigens result in lower sensitivities. A more detailed discussion of QCM based immunoassays is given in a review by Su and colleagues [56].

Other applications using a piezoelectric quartz crystal have been studied. Instead of targeting the surface with antigens for an immunoassay, a DNA probe can be immobilized on the surface. The corresponding mass and thus frequency change can be detected when hybridization occurs.

Recent studies targeting bacterial pathogens [57, 58] have been published. Another unique and very interesting approach proposed by Cooper and colleagues [59] involves driving the QCM with an alternating voltage. Targeted molecules adhere to the surface, which is oscillated with increasing amplitude. At a certain point, the force exerted on the particles by the surface is too high and the bonds rupture. This process is aptly named rupture event scanning (REVS). The QCM is then used as a sensitive microphone to capture the acoustic emission, which signals the presence of the particles (shown in Figure 1.4). The REVS system was able to detect $5x10^7$ particles/mL of HSV1 (herpes simplex virus) in 1 μL of calf serum. Advantages of this technique include no marking or labeling and high sensitivity, which make it appealing for a point-of-care diagnostic.

1.2.3 Non-liquid crystal Optical Techniques

Biosensors using optical detection methods measure a change in some characteristic of light based on the presence of a biomolecule or a binding event on the sensor's surface. One of the main advantages of optical detection is the lack of direct connections to the biosensor. Without signal output connections, the design of the biological fluid-sensor interface is simplified. Cunningham and colleagues [61] have developed a method known as the BIND system that utilizes a guided mode resonant filter to detect binding events on the sensor surface. A photonic crystal, which is composed of a periodic arrangement of dielectric materials, is tuned according to the attachment of biomolecules or cells to the surface. Each sensor output is read by a probe consisting of two optical fibers. One fiber emits a collimated white light source onto the sensor and the other collects the reflected light. Advantages of this method include mass fabrication, rapid detection time (approximately 20 ms), label free detection and an array format (eight targeted sensors can be detected simultaneously). Given the nature of the readout and analysis (robotic microplate handlers), this device would be difficult to use as a point of care diagnostic. However, this method could be applicable as a pharmaceutical device for screening, where cost per assay is an extremely important parameter and portability is not required. This technique for detection has been discussed in more detail [62] along with immunological results [63, 64]. Haes and colleagues [65] have demonstrated the use of triangular silver

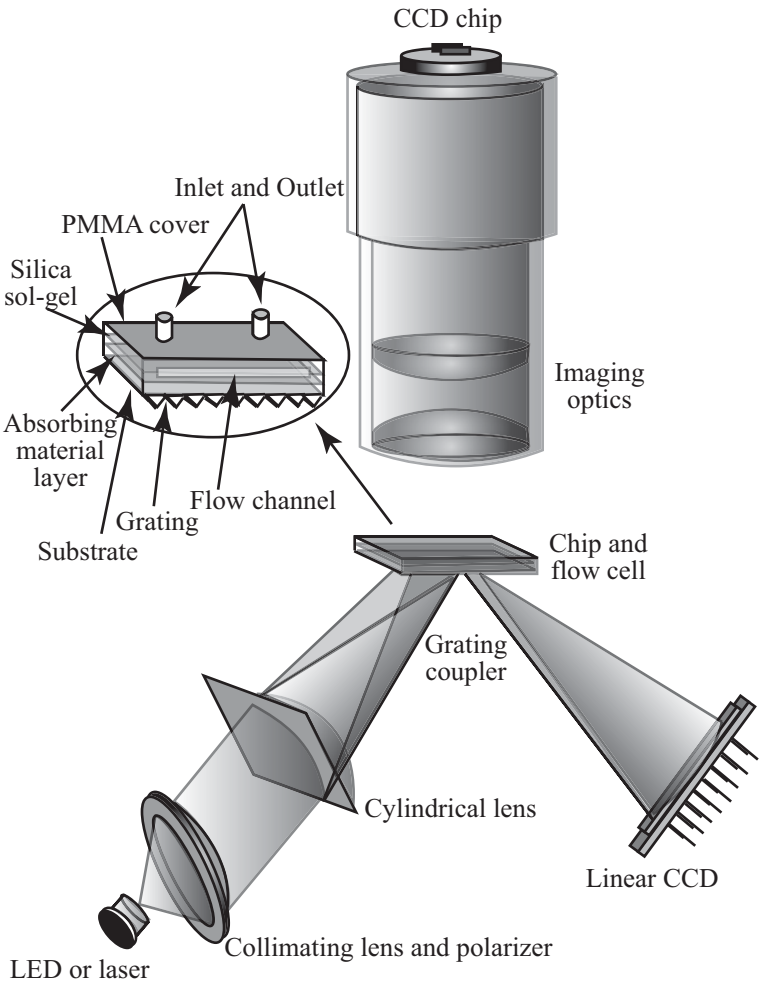

Figure 1.5: Instrumental setup for disposable optical leaky waveguide sensor for the detection of bacterial spores. From [60]. Permission for use to be requested.

nanoparticles combined with localized surface plasmon resonance (LSPR) to detect surface binding events. Small refractive index changes are measured near the surface of a metal and signal analyte binding. A protein receptor system (biotin-streptavidin) was used to demonstrate the capabilities of the sensor, with a limit of detection in the low-picomolar to high-femtomolar range.

Another optical technique with promising results for biosensing applications is the use of an evanescent field through metal clad leaky waveguide (MCLW) sensors (Figure 1.5) [60]. In order to increase the penetration depth of the evanescent wave to include the entire particle volume, a glass substrate was coated with a very thin layer of titanium (8.5 nm) followed by a layer of vacuum deposited silica (300 nm). The metal layer increases the penetration depth and propagation

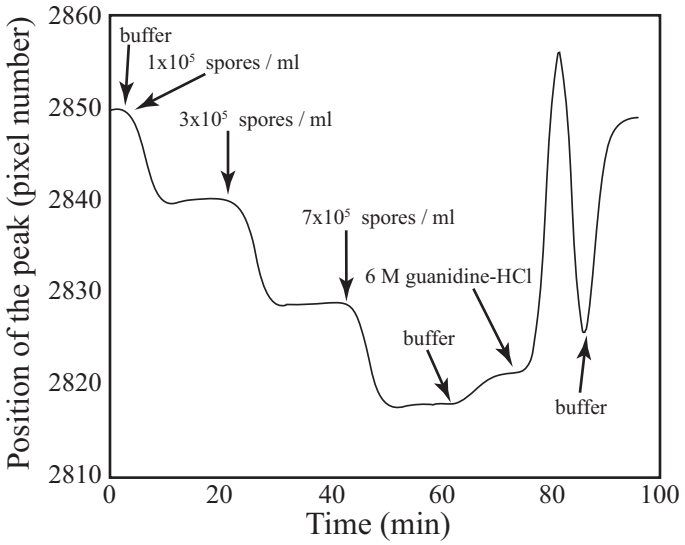

Figure 1.6: Refractive index changes for differing bacterial spores concentrations using the metal clad leaky waveguide sensor, arrows indicate solution addition. Data from [60].

length of the evanescent field. Refractive index detection was used to indicate the presence of varying concentrations of bacterial spores (shown in Figure 1.6), as well as the regeneration of the sensor. In order to achieve a higher sensitivity than evanescent wave detection alone, scattering and fluorescence were also measured to obtain data at lower concentrations of bacteria. Optimization of sensor parameters, such as the pH of the medium, immobilization and binding, and regeneration was completed to increase sensor performance.

Reviews of interferometric, SPR, luminescence [66], evanescent wave fluorescence [67] and fiber optic biosensors [68] have been published in the literature and provide more insight into the mechanisms, advantages and recent developments of each optical sensor type.

This chapter has discussed the scope and motivation of the problem of detecting infectious disease, as well as current techniques employed clinically. Progress in the use of liquid crystal sensors for biological applications will be discussed in Chapter 3, and a basic introduction to the physics of liquid crystals appears in Chapter 2.

Chapter 2

Liquid Crystal Physics:

Phenomena and Surface Anchoring

2.1 Background and Introduction

The goal of this research is to leveraging existing knowledge and technology from the Display and Photonics Laboratory at Brown University for application in the area of medical diagnostics. To that end, it is important to fully understand the specific theory and background of the intended technology. This chapter explains the basic nature of liquid crystals, including their structure and unique properties which can be applied to sensor applications. More detailed explanations are devoted to the interaction of liquid crystals with interfaces and surface anchoring, specifically aqueous solutions. The unique ability of a fluid, as well as surfactants distributed in that fluid, to change the orientational alignment at the interface, will be explored as the basis of a liquid crystal biosensor.

2.1.1 Molecular Structure

Liquid crystals are all around us: from the bottom of a soap dish to inside each and every cell membrane in the human body, the liquid crystal phase is an important yet seldom recognized phase

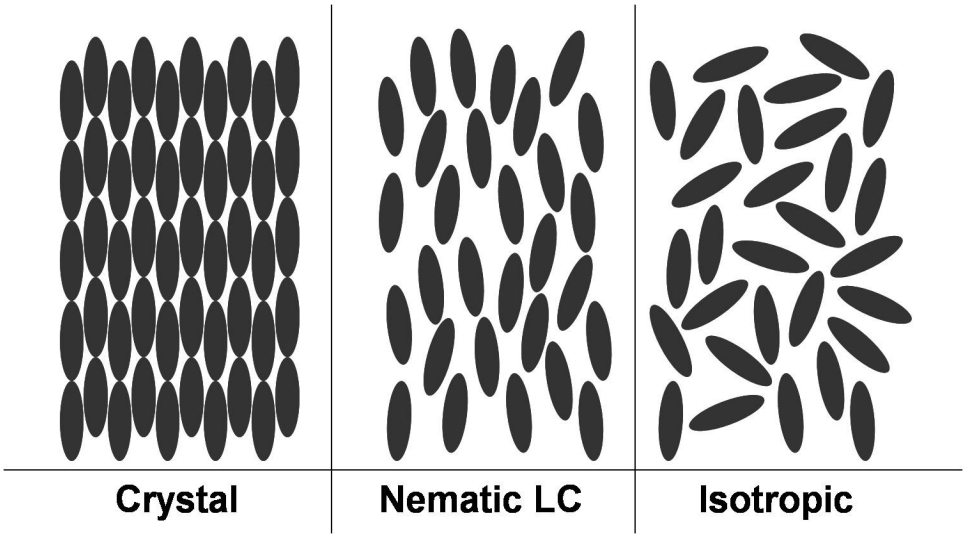

Figure 2.1: An illustration of the solid, liquid crystal, and liquid phases of matter.

of matter. Phases of matter are separated by the amount of order they contain, with the solid or crystalline phases containing the greatest order. Crystalline phases exhibit both positional and orientational order. Strong attractive forces hold these molecules in place, thereby requiring a large external force to deform the shape. In contrast, a liquid has no order; the molecules are completely random and their location can not be predicted. The attractive forces between these molecules allow the liquid to conform to the shape of their container. Gases contain even less order, and due to this, a gas can be easily deformed. Although less well known, the plasma phase and the liquid crystal phase are ubiquitous in technological applications. The plasma phase exists at temperatures well above those of a gas, while the liquid crystal phase is observed between a solid and a liquid, as seen in Figure 2.1.

The liquid crystal or nematic phase has no positional order, although it does display orientational order. Orientational order is the amount in which the molecules are oriented with regard to one another. The nematic director, shown in Figure 2.2, gives the average orientational order for molecules, as a function of the angle of deviation from a defined direction. The angle of deviation has a maximum of 180°, as the molecules are symmetric about one axis.

The basic rod-shaped structure of the liquid crystal molecule allows it to exhibit some exceptional properties. To maintain its unique shape, the molecule must be rigid for at least a portion of its

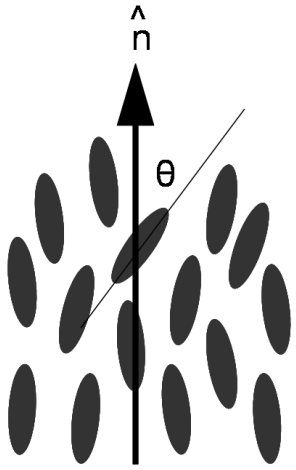

Figure 2.2: Molecules in the nematic liquid crystal phase. The preferred orientation is shown with a dashed line, and makes an angle θ with the nematic director.

length. The center of the molecule is formed by two or more rigid ring structures, with a hydrocarbon chain at each end. The number of rings and the length and composition of the hydrocarbon chains varies with different types of liquid crystal materials. This unique structure allows for many classes of liquid crystals as well as properties that can be exploited for a myriad of applications. Properties and structures of some commonly used nematic liquid crystal are given in Table 2.1.

2.1.2 Thermotropic Phase

Liquid crystal materials that are stable over a given temperature range are described as thermotropic liquid crystals. Compounds as well as mixtures of compounds can be classified in this group. The most common and simplest phase of thermotropic liquid crystals is the nematic phase, shown in the

Table 2.1: Properties and characteristics of cyanobiphenyls, a commonly used group of nematic liquid crystals.

Material	**Elastic Constants** [69] ($K_1 1$, $K_3 3$ **[pN], at 20**$^\circ C$)	**Clearing Point** $T_{n/i}[^\circ C]$	**Birefringence** Δn	**Structure**
5CB	7.21,10.0	35.1	0.212	
6CB	5.56,6.27	29.0	0.189	
7CB	10.40,12.90	43.8	0.199	
8CB	6.7,9*	41.0	0.178	

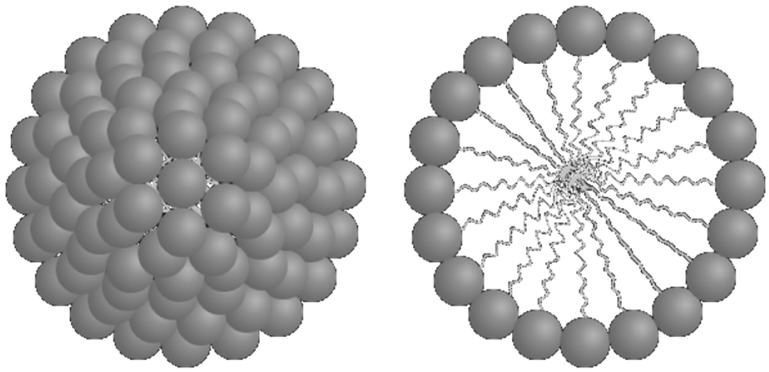

Figure 2.3: Schematic depiction of a micelle formed by amphiphilic molecules. The entire structure is shown on the left, with a cross section displayed on the right.

center of Figure 2.1. A preferred direction or orientation is maintained in this phase, yet there is no positional order. The molecules move around randomly, but on average the long axis of the molecule is aligned with the nematic director.

2.1.3 Lyotropic Phase

The liquid crystal phase also exists when two substances are mixed together, and is then dependent on the concentration (as opposed to the temperature). This class of liquid crystals are called lyotropics, and are commonly found in cell membranes. When lyotropic liquid crystals are placed in water, the hydrophobic ("water fearing") tails isolate themselves from the aqueous solution. Thus the hydrophillic heads ("water loving") are facing the outside and a structure called a micelle is formed, shown in Figure 2.3. The molecules and hence the structures move about randomly, but still maintain the orientational order required for the liquid crystal phase.

2.1.4 Order Parameter

The degree of order of a material in the liquid crystal phase is difficult to quantify, due to the three dimensional, random nature of the phase. The order parameter, S, defined below describes the amount of order for a uniaxial system. This definition assumes a system of rigid rods, and cylindrical symmetry, so only the distance from the preferred axis is included.

$$S = \langle \frac{3}{2} cos^2\theta - \frac{1}{2} \rangle \tag{2.1}$$

For a perfectly ordered system (one in which the long axis of the molecules are all aligned in the exact same direction) the order parameter, $S = 1$. In a completely random system with no orientational order, $S = 0$. The order parameter varies with temperature; most liquid crystals have order parameter values between 0.3 and 0.8. Many important liquid crystal parameters have a rough proportionality to the order parameter, as shown in Table 2.2, which is useful information for the development of liquid crystal based applications.

If external fields (such as electric, surface or magnetic) break the rotational symmetry of the molecular orientational fluctuations around the director, then the order parameter becomes biaxial. External constraints, such as a rigid flat surface, can limit the phase space of the possible molecular orientations and require inclusion of the polar angle ϕ. The additional preferred direction of ordering is introduced as the secondary director $e^{(1)}$, and the degree of ordering around $e^{(1)}$ as the biaxiality P. The secondary director $e^{(1)}$ lies in the plane perpendicular to the regular director **n** and is a spatial field in elastically distorted samples. The uniaxial order parameter tensor is expanded into the full order parameter Q_{ij} in order to account for the biaxiality as:

$$Q_{ij} = \frac{S}{2}(3n_i n_j - \delta_{ij}) + \frac{P}{2}(e_i^{(1)} e_j^{(1)} - e_i^{(2)} e_j^{(2)}) \tag{2.2}$$

where S is the degree of the nematic order, P is the biaxiality and $e_i^{(m)}$ are the secondary nematic directors. Further discussion is included in Chapter 4.

Table 2.2: Liquid crystal parameters and their corresponding proportionality to the order parameter.

Parameter	**Nomenclature**	**Proportionality**
Elastic Constant	K_{ii}	$\propto S^2$
Birefringence	Δn	$\propto S$
Dielectric Anisotropy	$\Delta\epsilon$	$\propto S$
Magnetic Anisotropy	$\Delta\chi$	$\propto S$
Viscosity Anisotropy	$\Delta\eta$	$\propto S$

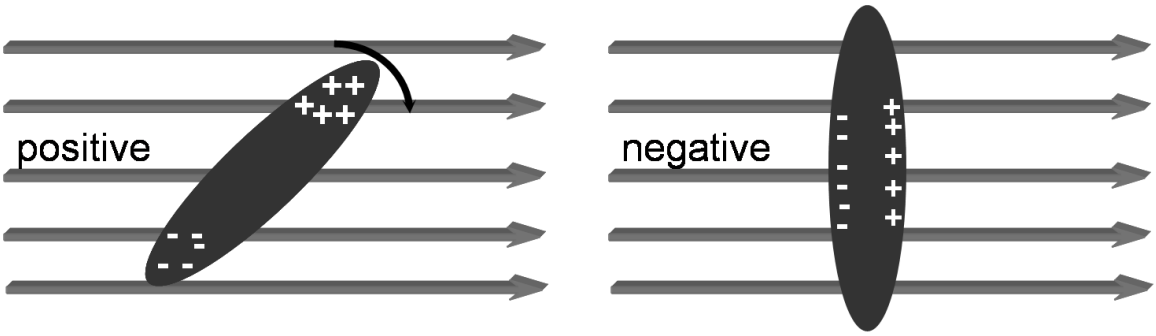

Figure 2.4: Liquid crystal molecules orienting in an applied electric field along the long axis of the molecule. Positive dielectric anisotropy is shown on the left, while a molecule with a negative dielectric anisotropy is shown on the right.

2.2 Properties and Characteristics

The rod-like shape of liquid crystal molecules and their propensity to orient in a specific direction provides many unique characteristics. In an isotropic material, such as a liquid, a property measured along any direction will give the same result. The rod shape of the liquid crystals (specifically the high aspect ratio) create a situation where properties will be measured differently in different directions. This is defined as anisotropy, and liquid crystals are anisotropic molecules. Specific characteristics are observed due to the inherent anisotropy and are discussed in the following sections.

2.2.1 Dielectric Anisotropy

Observations of electric fields applied to liquid crystals have yielded many interesting properties. Liquid crystal molecules have a slight permanent electric dipole, due to the interactions between atoms. Due to this dipole, an applied electric field creates charge separation, causing the molecule to align itself either parallel or perpendicular to the field. The alignment of the molecules is dependent on how the charge separates in the molecule, as shown in Figure 2.4. The molecule will orient with the dipole that is the strongest in the electric field.

2.2.2 Optical Anisotropy

Most applications involving liquid crystals take advantage of their interactions with light. The inherent anisotropy in these molecules affects interactions with light in very obvious, beautiful ways.

The measure of a material's ability to change the propagation of light is expressed through the index of refraction, n. This quantity is defined as

$$n = c/v \tag{2.3}$$

where c is the speed of light in a vacuum, and v is the speed of light through the material. Due to the shape anisotropy of the molecules, liquid crystals have two different indices of refraction. Light propagating through the molecule travels at different speeds through the two different axes. The difference in the indices along these two axes is called birefringence (shown in Figure 2.5), and is defined by

$$\Delta n = n_1 - n_2 \tag{2.4}$$

When viewed under crossed polarizers, any domain in the material that has a nematic director aligned with either the polarizer or analyzer will appear dark. Any molecules that have a director not aligned with either polarizer will transmit light. This unique property is very useful in many applications, including displays and optical sensors.

2.2.3 Elastic Energy

For a nematic liquid crystal, the equilibrium state of the director is constant. In much the same way that changes are measured from the equilibrium state of a spring, deviations in the free energy of the system are measured by taking the square of the derivative of the director. Now the equation becomes much more complicated when it is observed that liquid crystals molecules are free to move in all three spatial directions. The deformation energy of a nematic liquid crystal can be written as

$$F_d = \frac{1}{2}\int_V (K_1 \left[\nabla \cdot \hat{n}\right]^2 + K_2 \left[\hat{n} \cdot (\nabla \times \hat{n})\right]^2 + K_3 \mid \hat{n} \times (\nabla \cdot \hat{n}) \mid^2) dV \tag{2.5}$$

where K_1, K_2, and K_3 are constants, much like the spring constant. These three different constants relate to the three different modes of distortion: splay, twist and bend (Figure 2.6).

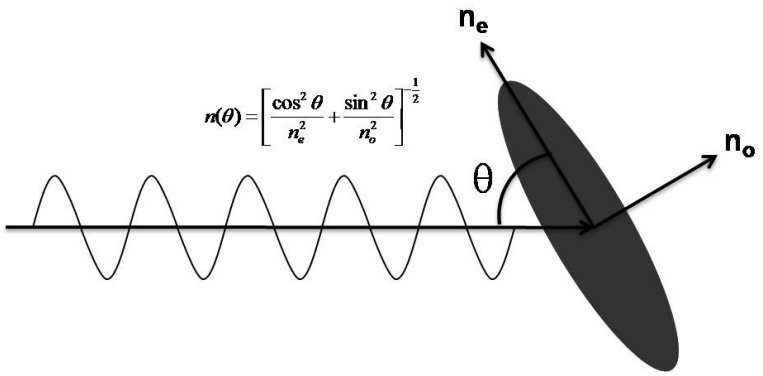

Figure 2.5: The birefringence of a liquid crystal molecule is the difference between the extraordinary, n_e, and ordinary, n_o, indices of refraction.

2.2.4 Surface Alignment

In order to achieve success with many of the current technological applications utilizing liquid crystals, alignment of the molecules in contact with a surface must be controlled. In flat panel displays, for example, both the top and bottom substrates are strongly aligned, forcing a twist in the liquid crystal bulk material. This surface alignment, when paired with a polarizer and analyzer, allows the liquid crystal material to function as a light modulator. In a biological sensor (as in the work described here), a targeted biomolecule creates local changes in the alignment of the liquid crystal, optically indicating its presence. This optical signature is due to a change in the balance of the forces controlling the behavior of the liquid crystal; the natural orientation imposed by the bulk elastic properties is overcome by the change in anchoring energy at the free surface. This change in anchoring energy is correlated with the presence of biomolecules at the interface.

Anchoring Energy

The molecular interactions of liquid crystals in the bulk tend to influence the bulk properties; near the surface, the properties are determined by the interaction of the external surface with the nematic liquid crystal. Surface anchoring is defined as the ability of a surface to cause orientation in a liquid crystal material. The direction or orientation caused by the surface on the liquid crystal is normally referred to as the preferred or easy direction. The amount of energy required to move the molecule away from this preferred direction is called the anchoring energy and is defined by

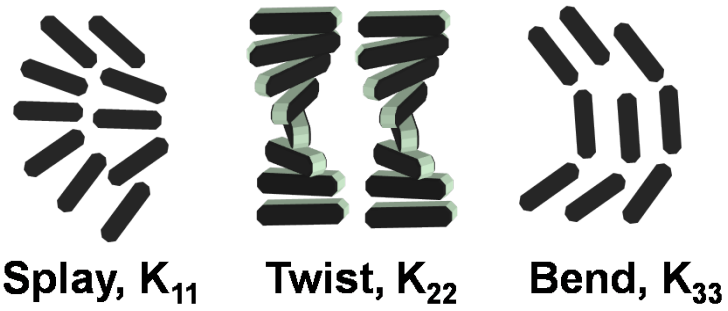

Figure 2.6: The three modes of deformation of liquid crystal molecules.

$$F_s = \frac{1}{2}\int_S W_0 sin^2(\theta - \theta_0) dS \tag{2.6}$$

where $\Delta\theta$ is the change in angle from the easy direction and W_0 is the anchoring energy coefficient. Strong anchoring has a coefficient of approximately $10^{-4}\frac{J}{m^2}$, while weak anchoring coefficients are around $10^{-7}\frac{J}{m^2}$.

Anchoring Transitions

A common method of finding the anchoring strength at a surface is to measure the energy required to move the liquid crystals away from their preferred direction. At a certain point, the applied electric field overcomes the deformation energy imposed by the surface, and the molecules will begin to move. This is the transition (critical) point, and the applied field required to reach that point is known as the threshold voltage. The applied electric field is described by

$$F_e = \frac{1}{2}\int_V \varepsilon_0 \Delta\varepsilon (\bar{E}\cdot\bar{n})^2 dV \tag{2.7}$$

where ε_0 is the permittivity of free space and $\Delta\varepsilon$ is the dielectric anisotropy of the liquid crystal. The total free energy is then represented by

$$F = F_d + F_e = \frac{1}{2}\int_V K_1 \left[\nabla\cdot\hat{n}\right]^2 + \frac{1}{2}K_2\left[\hat{n}\cdot(\nabla\times\hat{n})\right]^2 + \frac{1}{2}K_3 \mid \hat{n}\times(\nabla\cdot\hat{n}) \mid^2 + \varepsilon_0\Delta\varepsilon dV \tag{2.8}$$

The Euler equation is used to minimize the free energy:

$$\frac{\partial F}{\partial \theta} - \frac{d}{dz}\left(\frac{\partial F}{\partial \frac{d\theta}{dz}}\right) = 0 \tag{2.9}$$

This yields a differential equation which can be minimized and solved for the threshold voltage, E_{TH}. The threshold voltage is a function of the deformation energy and dielectric anisotropy of the liquid crystal as well as the spacing between the substrates.

This method of quantifying the anchoring strength is trivial to measure experimentally on a closed cell. A conducting material, such as indium tin oxide, is placed on the substrates, allowing a field to be applied across the liquid crystal. The transition is detected optically, by measuring transmitted light through the cell. This method becomes infinitely more difficult when dealing with anchoring at a free or fluid surface, where the application of a field across the bulk nematic is exceptionally challenging. A further discussion of anchoring transitions and their observation at free and fluid surfaces is presented in Chapter 5.

Homogeneous Alignment

Homeogenous or planar alignment of a liquid crystal material occurs when the long axis is parallel to the substrate, and is shown in Figure 2.7(a). Many commercial applications take advantage of this to exploit the optical properties of liquid crystals. One of the most widely-employed methods for homogeneous alignment the is rubbing method. The surface of a substrate is coated with an alignment material such as a polyimide, and subsequently rubbed in the desired alignment direction with a soft cloth or fabric, creating microgrooves. The liquid crystal molecules, in order to find the lowest energy configuration, align with their long axis in the direction of the grooves. Aligning with the long molecular axis spanning the grooves would create a splay deformation, requiring more energy. When viewed between crossed polarizers, liquid crystals that are aligned in a planar direction transmit light when the long axis of the molecule does not lay in the same plane as either the polarizer or the analyzer.

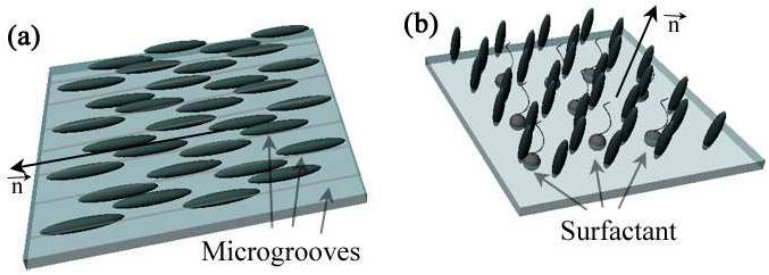

Figure 2.7: Planar liquid crystal alignment using a microgrooved substrate (a) and surfactant induced homeotropic alignment (b).

Homeotropic Alignment

When the long axis of the molecule is perpendicular to the substrate, homeotropic alignment is observed (shown in Figure 2.7(b)). An alignment material (that has a long hydrocarbon tail, such as a polyimide) is used to coat the surface of the substrate. The polar head of the alignment molecule bonds to the substrate and the hydrocarbon tail protrudes into the liquid crystal material. In order to satisfy the lowest energy configuration, the liquid crystal molecules align parallel to the long chains of the polyimide. This kind of alignment avoids all three methods of distortion (splay, twist and bend). The alignment angle can be varied by changing the length of the hydrocarbon tail of the alignment molecule, producing a pre-tilt angle. Liquid crystal that is aligned homeotropically appears dark when viewed between crossed polarizers.

Free surface interactions

Lyotropic and thermotropic liquid crystals and their characteristics and functions have been discussed. The unique electrical and optical properties of these molecules allow for a diverse range of applications. One of the most intriguing and promising applications involves using the optical properties of thermotropics to identify the presence of lyotropic liquid crystals, especially in biological applications. Historically, most applications involving liquid crystals have been based on the interaction between a substrate (typically a glass or polymer) and a thermotropic liquid crystal; flat panel televisions and computer displays are good examples of this. In the extensive study of this interface for the product development of these applications, the response of the thermotropic

liquid crystal to differing boundary conditions at the substrate has been characterized in order to predict and control the orientation of the liquid crystal. Early work included the investigation of anchoring mechanisms by adsorbed CTAB on a surface [70], as well as orientation of nematics by interfaces both near and far from phase transitions [71]. Specifically, alignment at liquid crystal-solid interfaces has been investigated using both the commonly used rubbing method [72, 73], and polyimide alignment layers [74, 75], where the length of the hydrocarbon tail in the polyimide layer has been shown to impact the strength of the alignment and the pre-tilt angle. Clare and colleauges developed a methodology to quantify the anchoring energy of nematic liquid crystal on surfaces treated with gold films [76] and oligopeptides [77]. The Display Laboratory at Brown University has also investigated the alignment of nematics using a variety of techniques, including holographically patterned alignment layers [78] and photonic crystal formation using azo-dye doped liquid crystal material [79].

Research progressed to the investigation of the interaction of the nematic-air interface. Characterization of anchoring at the free surface of liquid crystals is one of the first steps towards understanding the behavior of a liquid crystal based sensor. Slavinec and colleagues [80] studied liquid crystal alignment and anchoring at a curved nematic-air interface using both polarizing optical microscopy and numerical simulations, as shown in Figure 2.8. The structure and anchoring of various liquid crystalline materials at a free surface have also been reported [81–84]. The behavior and mechanisms of the nematic molecules at the free surface is governed by the inherent properties of the liquid crystal.

In the case of liquid crystal sensors, the interface of interest has been shifted from the solid interface to the liquid crystal-aqueous interface. Published literature reporting investigation of this interface is limited. Early research reported on theoretical examinations of orientation at the nematic-isotropic and nematic-vapor interfaces [85]. Biensan and colleagues [86] investigated the orientation of 8CB at the air-water interface using Langmuir films. They reported a first-order phase transition from a monolayer to a trilayer with an increase in surface pressure. Martynski and colleagues [87] also used Langmuir films to study 8CB at the air-water interface.

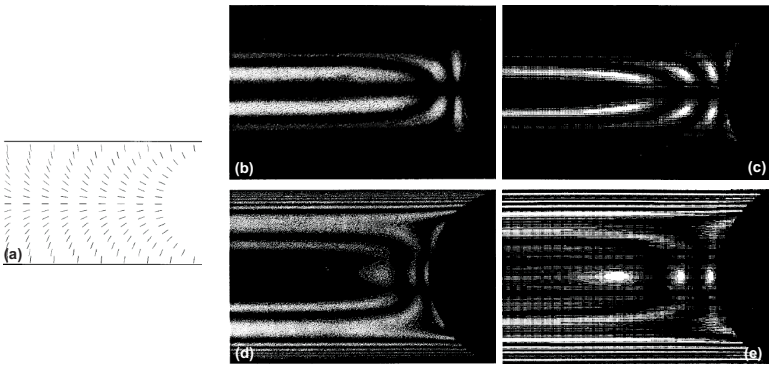

Figure 2.8: Behavior at the interface of a curved nematic and air in a partially filled cylindrical tube enforcing homeotropic anchoring at the walls. Nematic director field (a) with the corresponding measured (b) and (d) and simulated (c) and (e) interference textures. In cases (b) and (c), the polarizer is along the cylinder axis, and in cases (d) and (e) it is rotated by 45°. From [80]

Due to their amphiphilic nature (they contain both a hydrophobic region as well as a hydrophilic region), surfactants form colloids when placed in a bulk solution. Much like the liquid crystal phase is an intermediary state between liquids and crystals, a colloidal solution is an intermediary between a homogeneous mixture and a heterogenous mixture. It was observed that when specific amphiphilic molecules were introduced into a continuous liquid crystal phase, the anchoring at the surface of the droplets was affected [88]. Further investigation, including both molecular simulations and theoretical calculations, was performed in order to accurately model this system for use in biosensor applications [89]. Brake and colleagues have described the anchoring and interactions of liquid crystals at aqueous interfaces, including orientational responses to long chained molecules such as phospholipids [90, 91]. Lockwood and Abbott [92] reported on interactions between surfactants and phospholipids at the aqueous-nematic interface. The chain length and structure of surfactants has been shown to effect the director alignment at liquid crystal-aqueous interfaces.

Confinement of liquid crystals has been studied in droplets [93], cylinders [94], and square wells [95] as well as through optical modeling [96] and anchoring studies [97]. Typically, research has focused on the interaction between liquid crystals and solid surfaces (such as glass, polymer, etc) for applications in the display industry.

Kossyrev and Crawford [98] studied the effects of the confinement of nematic liquid crystals in a square capillary tube. Both homeotropic and planar alignment schemes were calculated, with the

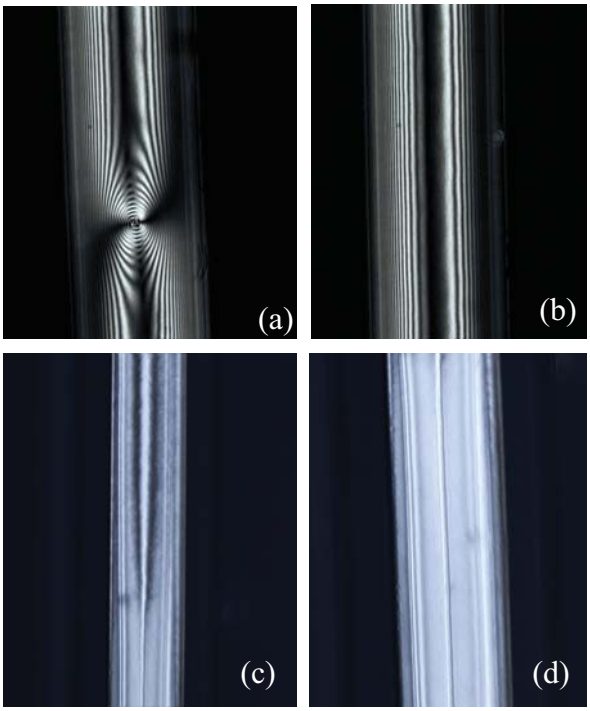

Figure 2.9: Interference pattern of a 50μm square capillary filled with homeotropically aligned nematic liquid crystal with (i) and without (ii) defect; and 80μm square capillary filed with planarly aligned liquid crystal (iii) and (iv). From [98].

resultant escape patterns shown in microscope images (Figure 2.9). One can differentiate between strong anchoring, where the director is fixed by the surface, and weak anchoring, where surface and bulk forces compete. Near the free surface with no chemical bonding, the translational symmetry of the anisotropic molecules is removed, forcing the molecules to find a director, $\hat{n}$, which minimizes the free energy. Interaction with a structureless wall or free surface often induces planar alignment at the boundary. This induced order can penetrate far into the bulk of the nematic.

Polar order should also be considered near the free surface. If a molecule contains a highly polar group on one end, near the free surface this end will tend to orient toward the more polar medium and allow for a range of orientations at the surface based on chemical structure. Hence, a molecular dipole parallel to the long axis of the molecule will induce homeotropic alignment, while a planar boundary condition will be exhibited by molecules with a dipole along the short axis. Other mechanisms which effect anchoring transitions include adsorption effects, electric quadrupolar intermolecular interactions, impurities, liquid crystal mixture concentration homogeneity, and surface topography.

Different orientations of common nematic liquid crystal materials have been observed at free surfaces. 5CB and 8CB molecules tend to align normal to the surface [83], whereas PAA produces a planar alignment [82]. In MBBA and EBBA temperature variation changes the orientation from normal to tilted at a temperature slightly below the nematic isotropic transition [81]. The variations in these alignments provide an interesting range of options for liquid crystal based biosensors.

The unique properties of liquid crystal materials, including birefringence and the ability to control anchoring at surfaces, can be leveraged for use in many applications. Commercialized technologies, such as flat panel televisions and computer displays, as well as emerging technologies like liquid crystal based biosensors, have had great success using a liquid crystal platform. In order to optimize and predict the behavior of this material, it is important to fully understand and characterize their behavior. This chapter has described many unique properties of liquid crystals, and focused mainly on the alignment of nematics at interfaces, especially the ability of free surface interactions to control the alignment using changes in anchoring strength. Chapter 4 describes theoretical simulations and models developed to understand the complex nature of confined nematics in the context of a liquid crystal based biosensor.

Chapter 3

History of Biosensors Using Liquid Crystal Technology

Although promising a very broad and successful future, the current field of liquid crystal based biosensors is still in its infancy. The number of investigators devoting time and resources to this unique application continue to increase; however, currently, there are only a small number of researchers who have published results. Nicholas Abbott and colleagues [90] have produced exciting developments on sub-topics in this field ranging from physical studies of the impact of self-assembled monolayers on the interface between liquid crystals and aqueous solutions to results on the detection of viruses using liquid crystals. Woolverton and colleagues [99] have published results relevant to liquid crystal biosensor research, including the detection of distortions in the bulk of lyotropic liquid crystals due to the presence of immune complexes. Promising results are generating more interest in the field and will ultimately lead to greater collaboration and hopefully the development of a rapid diagnostic based on liquid crystal technology that can be clinically useful in a medical setting. This chapter is devoted to covering the literature on the use of liquid crystals as biosensors, including protein interactions, DNA, viruses and immune complexes. Although the focus remains on identifying techniques which are conducive to the development of a rapid portable diagnostic device, all publications that involve potential liquid crystal biosensors will be discussed.

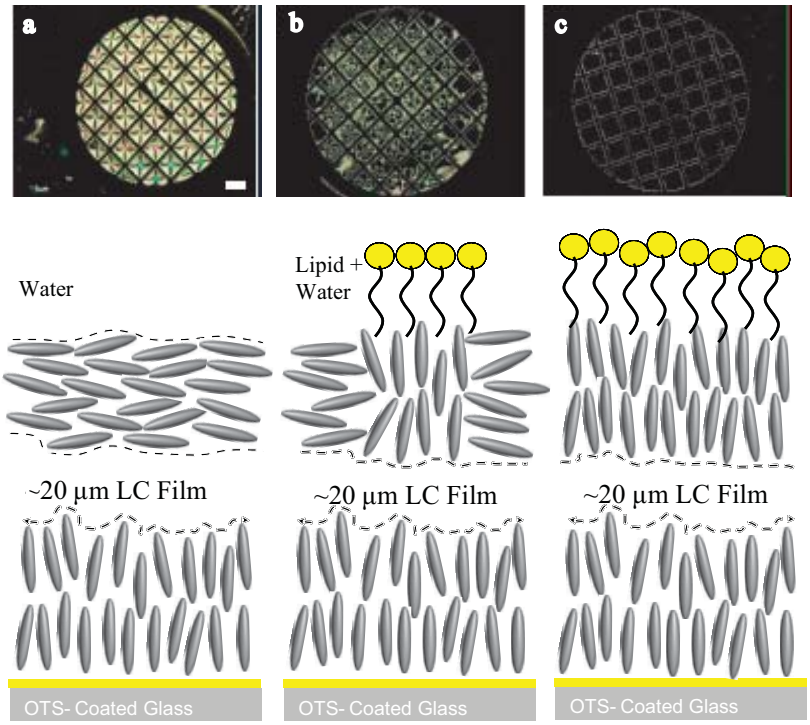

Figure 3.1: A schematic representation of the aqueous liquid crystal interface after injection of phospholipids and accompanying optical images viewed through a polarizing microscope (a) immediately, (b) 10-20 min, and (c) 2 hours after injection. From [90].

3.0.5 Liquid crystal interfaces

The starting point of developing a successful liquid crystal biosensor is the ability to predict, control and manipulate the interface between the liquid crystal and the targeted biological material for detection. Brake and colleagues [90] studied the effects of the assembly of phospholipids at the aqueous liquid crystal interface. Many important biological binding events, such as the entry of protein toxins into cells and the initial stages of viral infections, take place at the biological membrane. Monitoring and reporting these events with a label free method was proposed by observing the orientational changes through polarized light induced in the thermotropic liquid crystal due to the specific binding of the proteins.

More specifically, a layer of phospholipids was introduced to the liquid crystal aqueous interface which induced an alignment change in the liquid crystal (Figure 3.1). Subsequently, phospholipase A_2 (PLA_2), an enzyme that converts phospholipids into fatty acids, was introduced and the changes optically monitored. These results (Figure 3.2) show enzymatic action can be monitored using the

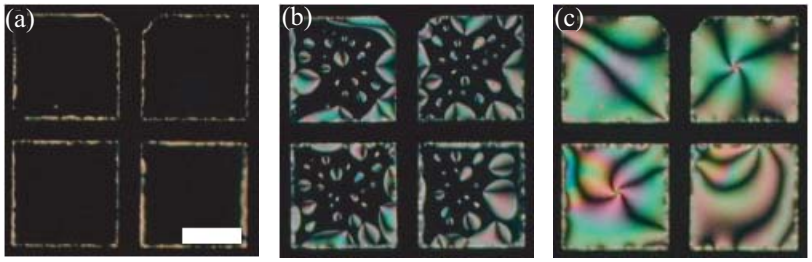

Figure 3.2: Optical images of a common liquid crystal material (5CB) observed between crossed polarizers (a) 0 min (b) 45 min and (c) 90 min after the introduction of phospholipase A_2 into a lipid rich aqueous solution.

phospholipid decorated surface of liquid crystals. Given the reorganization of the liquid crystals is rapid and the reporting of the binding is passive (fluids can continuously flow past the surface), this research opens the door to many promising new technologies.

With the observation that phospholipid rich liquid crystal-aqueous interfaces could be monitored for binding events, it was next proposed that the assembly and properties of these interfaces should be studied in greater detail [100]. A method of controlling the areal densities (surface coverage relative to a bilayer) was developed using mixtures of soluble surfactants and phospholipids, as well as measuring the lateral diffusivity of phospholipids at the interface. A patterned array of differing phospholipid concentrations is possible because of the grid the liquid crystal was deposited in; the grid was created using a detailed and elaborate method. Glass microscope slides were cleaned and functionalized with octadecyltrichlorosilane (OTS) which induces homeotropic surface anchoring. Next, a layer of gold was deposited in a grid formation using an electron beam evaporator. Rectangular wells were created in a 2 mm thick PDMS sheet in which the OTS and gold covered grids were placed. The well was filled with the liquid crystal material (5CB), followed by an aqueous solution. Two needles (inlet and outlet) were inserted through the walls of the PDMS and connected to a pump in order to create a flow chamber. This detailed method allows for the formation and characterization of phospholipids at liquid crystal aqueous interfaces.

Corresponding molecular dynamics simulations were used to explore the interactions between the phospholipid bilayer and some common liquid crystal materials (5CB and 5CF) [101]. Molecular simulations have shown insight into the atomic level processes of these interactions, which are difficult

to study experimentally. The potential mean force (PMF) of a liquid crystal molecule was calculated, and the effect of molecules on the structural properties of membranes was also analyzed. It was found that, at equilibrium, mesogens partition into the membrane and that a molecule's permeation into the membrane is controlled by its solubility in water. Also, the elastic properties of the membrane change with the introduction of mesogens. The introduction of a protein into the membrane causes the membrane to adjust to match the hydrophobic length of that protein. It was noted in the study that much larger simulations would be needed in order to fully understand the elastic interactions. These results provide insightful information for the development of biosensors, given the delicate nature of the balance controlling the alignment of liquid crystals at interfaces.

A number of other investigations were conducted by Abbott and colleagues. The first of these concerned the development of a simple experimental system to investigate the self-assembly of surfactants and phospholipids at interfaces [92]. Optical observation of the ordering of liquid crystals was made easier using a simple geometry (Figure 3.3). In a second study, the influence of surfactant tail branching and organization was studied [102], with interesting correlations to biological membranes. As expected, the orientation of the liquid crystal material was dictated by interactions with the aliphatic tails of surfactants. Much as a biological membrane's permeability is determined by branching in the lipid bilayer, surfactant tail branching also impacts the orientation of the liquid crystal due to poorer packing. Chemical compositions of liquid crystals also have an impact on their orientations when in contact with surfactants. The impact on liquid crystal materials of polyelectrolyte multilayer films (PEM) [103] was also observed. The formation of these films was found to be coupled with the orientational order of the liquid crystal material.

As previously mentioned, the ability of biomolecular interactions, at a liquid crystal interface, to change the long term orientation of the bulk liquid crystal provides the basis for liquid crystal biosensors. Understanding the ways in which different biomolecules affect the orientation of these liquid crystal molecules is crucial to the functionality of a LC based diagnostic tool.

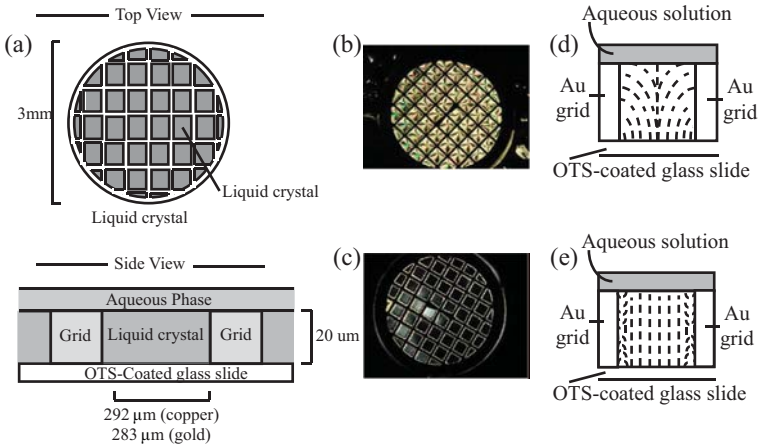

Figure 3.3: Geometry created to study the interfaces of thermotropic liquid crystals and aqueous phases. (a) Optical images between crossed polarizers of 5CB in a nematic grid immersed under water (b) or an aqueous solution of surfactant (c). Director profiles of planar alignment of the liquid crystal at the interface (d) and homeotropic alignment (e). From [92].

3.0.6 Liquid crystal biocompatibility and liquid crystal substrates

In order to successfully replace the glass substrates commonly used for display applications with a liquid crystal interface for biomaterials, the interaction between thermotropic liquid crystals and mammalian cells must be characterized. Given the recent interest in the development of a rapid biosensor which detects alignment changes in a nematic liquid crystal, Luk and colleagues [104] studied the effects of thermotropic liquid crystals on mammalian cells. Eight mixtures of liquid crystals with different functional groups were studied against two cell lines: connective tissue (3T3 fibroblasts) and SV-40 transformed epithelial cells (HCECs). The 'A' series contained the ether functional group; the 'B' series contained ether and ester functional groups; the 'C' series contained fluorophenyl groups; and the 'E' series contained no functional groups. To measure cell viability and liquid crystal toxicity, cell lines were plated and allowed to proliferate. Upon removal of the medium, either liquid crystal, cell culture medium or phosphate buffered saline (PBS) was added and incubated for 4 hours. After rinsing, fluorescence was measured. To measure cell proliferation in the presence of the 'C' series of liquid crystals, the SV-40 HCECs were plated and left overnight, followed by incubation for 4 hours in either liquid crystal, cell culture medium or PBS. After rinsing, the cells incubated for five days and the number of cells was counted using fluorescence. Based on these assays, it was determined that 'E', 'A', and 'B' series liquid crystals, 5CB and E7 are toxic to

living cells; yet, the authors state the mechanism by which these materials cause toxicity is not yet fully understood. The 'C' series and TL205 were found to be non-toxic to cells during the course of a four hour incubation. A correlation was discovered between the chemical functionality of liquid crystals and their toxicity to cells.

The focus of this chapter is background and previous work in the development of a liquid crystal biosensing technique for use in the diagnosis of infectious disease. Many of the detection schemes described in this section utilize identification of binding events based on the reorganization of the bulk of the liquid crystal. In essence, the liquid crystal acts as a magnifying glass to amplify these binding events, leading to optical detection. In order for this detection scheme to be successful, the liquid crystal medium must be compatible with the targeted microbe. Structural instability or lysis would cause degradation of the sensor's effectiveness. Woolverton and colleages [105] hypothesized lyotropic chromonic liquid crystals are less toxic to bacteria than either surfactant based lyotropic liquid crystals or thermotropic liquid crystals. In order to assess the validity of these statements, two different assays were used to evaluate the effect of eight liquid crystal materials (6 lyotropic and 2 thermotropic) on the bacteria *Staphylococcus aureus*, *Escherichia coli*, and *Bacillus atrophaeus*. After suspending the bacteria in liquid crystal (or control) for 15 minutes, bacterial colonies were counted. The second assay determined the permeability of the cell membrane by the liquid crystal using fluorescence methods. As suggested by the authors, lyotropic chromonic liquid crystals were not toxic to *S. aureus*, *E. coli* or the spore form of *B. atrophaeus*. The other lyotropic liquid crystals tested (surfactant based CPCl and CsPFO) were toxic to vegetative cells, but not the bacterial spores; the opposite was true for the thermotropic liquid crystals (5CB and E7).

With the emerging field of biosensors based on liquid crystal technology drawing research interest and funding, studies such as the two most recently discussed will prove critical for the development of a clinically relevant tool. In addition to understanding how biomolecules reorient liquid crystals for detection, the characterization and understanding of the effects of liquid crystals on biomolecules must also be understood.

One of the first steps in determining the suitability of liquid crystals for biological detection is

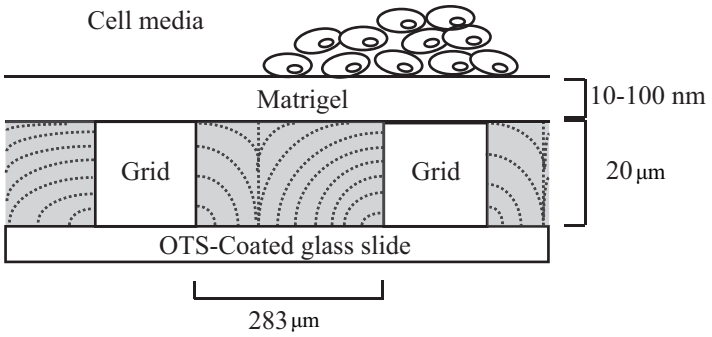

Figure 3.4: Schematic illustration of the experimental setup used to study the interactions of liquid crystals, mammalian cells and extracellular matrix.

to characterize the orientational response to an introduced substance. Guzman and colleagues [106] used simulations to observe the reactions of a liquid crystal material to nanoparticles adsorbed at the walls of a sensor. Different patterns were studied, including random and periodic adsorption, as well as the effects of both large and small concentrations. It was found that, for random adsorption systems, the disorganization of the alignment of the liquid crystal is gradual and based on the addition of particles. In contrast, for periodic adsorption along the walls, the stability of the system is based on the lag between the periods on opposing walls. The authors made several conclusions based on the simulations. The critical amount of particles required to create an instability in the liquid crystal material cannot be predicted based on surface coverage alone. Secondly, the sensor was more sensitive if the particles adsorbed individually rather than in clusters. Lastly, a parameter known as the critical concentration, c_c, can be used to describe the concentration of particles needed for the liquid crystal to display multiple domains. Research such as this begins to define the detection limits for a liquid crystal based biosensor.

Another interesting application of liquid crystals in biology is the utilization of liquid crystal materials as a substrate and culture medium. Lockwood and colleagues [107] investigated a thermotropic liquid crystal (TL205) as a culture medium for human embryonic stem cells (hESCs). A thin film of Matrigel, an extracellular matrix which provides support and anchorage for cells, was placed on top of a grid containing the liquid crystal (3.4). Experiments were run to determine both cell viability as well as the response of the orientational order of the liquid crystal material. The cells survived for up to 12 days, and the alignment of the TL205 was found to be coupled to the

presence of the Matrigel. This study has confirmed the successful culture of cells using liquid crystal material, and allows for imaging of interactions between the liquid crystal and extra cellular matrix.

Surface preparation for the alignment layer in a substrate for a liquid crystal based biosensor can often be time consuming and costly. Methods have been researched to find a biocompatible and efficient means of manipulating surfaces. Currently, surface alignment is induced either by mechanical means (such as surface rubbing) or chemical modifications, including self assembled monolayers. To replace traditional rubbing methods, Hoogboom and colleagues [108] used directional drying of a low-salt buffer to induce alignment. The buffer was dried on a polyimide coated indium tin oxide (ITO) layer. An optical cell was created using the dried buffer substrates and filled with a nematic liquid crystal material (5CB). Although domains of oriented liquid crystals were visible, the material was not as ordered as cells created using traditional alignment methods. A twisted nematic (TN) cell was formed, but showed no TN effect on the substrates. This result implies the anchoring energy of the rubbed PI plate was much higher than the plate containing the dried buffer. DNA was combined with the buffer and dried directionally across a substrate. A cholesteric phase was seen in the corresponding optical cell, implying a chiral confirmation of the liquid crystal. Although this technique combines the preparation and the analyte steps, the stability of the cell was limited. The optical cells lost their chiral phases within several days, and also suffered from thermal degradation.

Another possible substrate for a liquid crystal based biological assay was proposed by Kim and colleagues [109]. Films of a protein (bovine serum albumin, BSA) were immobilized on glass slides and then rubbed unidirectionally with a cloth. Liquid crystals were found to align parallel to the rubbed direction, and retained this alignment when contacted with solutions containing BSA, fibrinogen, lysozyme, and non-specific antibodies. However, upon contact with a solution containing anti-BSA IgG, the liquid crystal material assumed a non-uniform orientation. The ability of rubbed films of BSA to orient liquid crystals, resist the nonspecific adsorption of other proteins in aqueous solutions and allow reorientation in the presence of specific binding offers a possible substrate for liquid crystal based biosensors.

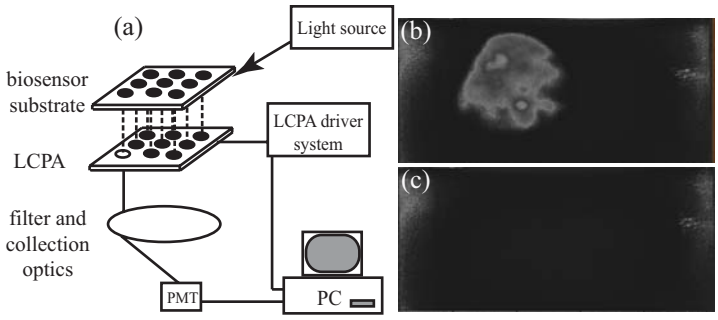

Figure 3.5: A schematic of a setup utilizing a liquid crystal pixel array for use in a biosensor array (a). Fluorescence images of the liquid crystal pixel array sensor in the transparent (b) and the dark (c) states. Images from [110].

3.0.7 Other techniques for liquid crystal biosensors

Lundgren and colleagues [110] developed a liquid crystal pixel array (LCPA) to discriminate fluorescence signals on a biosensor array. The advantages of an array format for biosensing are numerous and include high throughput, low cost per reaction, and a high number of targeted analytes. One of the limitations of more traditional techniques is the number of biosensing elements required. The researchers here incorporated all of the biosensing elements into a single platform, which reduces the cost associated with the assay. A schematic of the setup and the operational procedure is shown in Figure 3.5. Fluorescence based detection is still utilized by the biosensor; however, this study proposes a new imaging system based on a liquid crystal pixel array. Each pixel in the system can be selectively operated to either transmit signals (transparent state) or block the signal (dark state). In this way, a single optical fiber can be used to deliver the optical signals from the sensors to the analysis software. These experiments show a LCPA can be used successfully to facilitate a single detection channel biosensor array. The authors have also demonstrated the use of a single excitation device, as well as running multiple assays simultaneously.

Gel electrophoresis is a powerful tool used in molecular biology to separate proteins and DNA based on differences in charge, mass and size. Araki and Tanaka [111] proposed replacing the typically used solvent or gel with a nematic liquid crystal. Typically, in gel electrophoresis, the differences in particle mass or charge cause separation in the gel. In the model using liquid crystals as a solvent, defects caused by the presence of the particles in the liquid crystal influence the motion

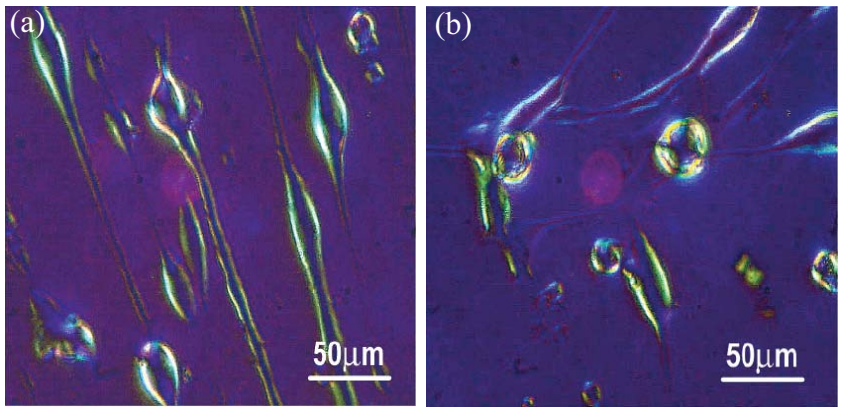

Figure 3.6: Optical images taken between crossed polarizers of muscle cells (a) and fat cells (b) below a layer of nematic liquid crystal. From [112].

of the particles. These changes in movement based on induced defects are a function of the surface characteristics of the particle and provide a basis for particle separation. The authors developed a simulation method to predict a moving particle in liquid crystal that includes the hydrodynamic, surface anchoring and elastic effects.

Although spectroscopy and imaging techniques have not been discussed here in depth, the work of Fang and colleagues [112] is worth noting. Liquid crystals were used as a medium to image muscle cells, fat cells, and neurons. Given the delicate nature of the orientation of liquid crystals, any topological defect or nonuniformity of the surface in contact with the liquid crystals can lead to changes in the order around that location. These changes in orientation based on morphological features have allowed for the imaging of cells as shown in Figure 3.6. Theoretical discussions of continuum elastic theory are used to explain the realignment of the nematic director at local features of the cells. Using this theory it was estimated that the optical resolution of this technique is the optical wavelength used divided by twice the birefringence of the liquid crystal.

3.0.8 Imaging protein immobilization

Using the results from studies on the interactions at a liquid crystal aqueous interface and the compatibility of liquid crystals with biological materials, protein binding events can be detected. Proteins are complex organic compounds consisting of amino acids linked by peptide bonds; they are essential to cellular functions including enzymatic activity, structural and mechanical activities

(such as scaffolding), the immune response and cell signaling. The ability to amplify and transduce protein binding events using liquid crystals is a critical step in the development of a liquid crystal biosensor.

Luk and colleagues [113] used a common nematic liquid crystal material (5CB) to image the binding of proteins onto receptors, and to determine whether the orientation of the receptor affected the overall binding ability. Maximizing the binding ability of proteins will increase the sensitivity of detection devices, allowing a greater density of desired analytes, which is critical for optical detection. Several factors can decrease the binding ability of a protein, such as conformational changes induced by immobilization and the inaccessibility of the binding site due to an inopportune immobilization geometry. The experimental system developed to test the impact of immobilization orientations on binding ability prevented nonspecific binding, provided a constant areal density, and included identical interfacial microenvironments for both random and controlled protein orientations. Self-assembled monolayers (SAMs) of alkanethiols were formed on evaporated films of gold. Measurements were taken to determine the azimuthal anchoring energy and the orientations of liquid crystals in contact with these self assembled monolayers [76]. The receptor molecule, ribonuclease A (RNase A) was immobilized to this surface of monolayers in either a preferred direction or a random orientation using different two different schemes. The targeted protein (ribonuclease inhibitor (RI)) was bound to the RNase A and the thickness of the bound protein layer was measured using ellipsometry and the changes in the orientations of the liquid crystals reported the protein binding events.

The key aspect in using liquid crystals to detect protein binding events is the disruption of surface alignment due to the immobilization of proteins on the surface (Figure 3.7). An optical cell was created by sandwiching two surfaces which contained either random or controlled orientations of immobilized proteins with an interior spacing of 13 μm. liquid crystal was drawn into the cell by capillary action and was viewed using polarizing microscopy. Figure 3.8 shows the optical images of liquid crystal used to detect the binding of RI to RNase A immobilized on SAMs with both preferential and random orientations, as well as a schematic of the protein orientations. This data

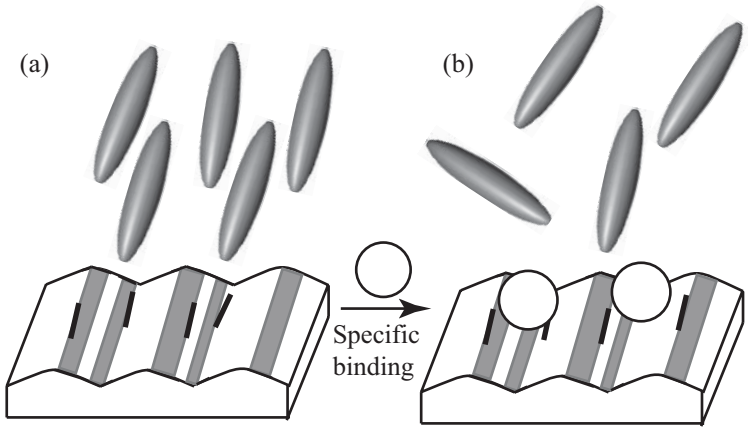

Figure 3.7: Schematic of the alignment of liquid crystal material due to surface topography of the substrate (a). Disruption of the alignment due to protein binding events on the surface (b).

clearly shows that immobilizing proteins with a preferential orientation increases the binding ability; the study reports a random orientation binds only 25% of the ligands that a controlled orientation does. The increase in binding capacity makes this an attractive technique for a rapid biosensor to detect protein binding events on surfaces, as the amplification of the binding due to the large optical change in the liquid crystal alignment is easily detected. These results strongly emphasize the importance of a controlled binding environment.

Another similar study reports on the orientational changes of liquid crystals due to covalently immobilized peptides on surfaces [114]. Peptides are amino acids without secondary structure; in general, peptides are shorter proteins and are used in the study of protein structure and function. This study used a peptide sequence for the Src protein kinase, which is associated with forms of colon and breast cancers. Methods were developed to control the areal density of the immobilized peptides in order to find an optimal density for reporting using liquid crystals. To determine the optimal areal density, cells were created by sandwiching a liquid crystal material (5CB) between two substrates with varying densities. For the low areal density (1% peptides), immediately after preparation line defects were seen due to the disruption caused by the peptides on the alignment of the liquid crystal. After annealing to 36°C and cooling, the line defects disappeared and the samples assumed a preferred planar orientation. This effect was not observed for high areal densities ($5 - 100\%$ peptides), even after 100 hours of observation. These results suggest a time dependence

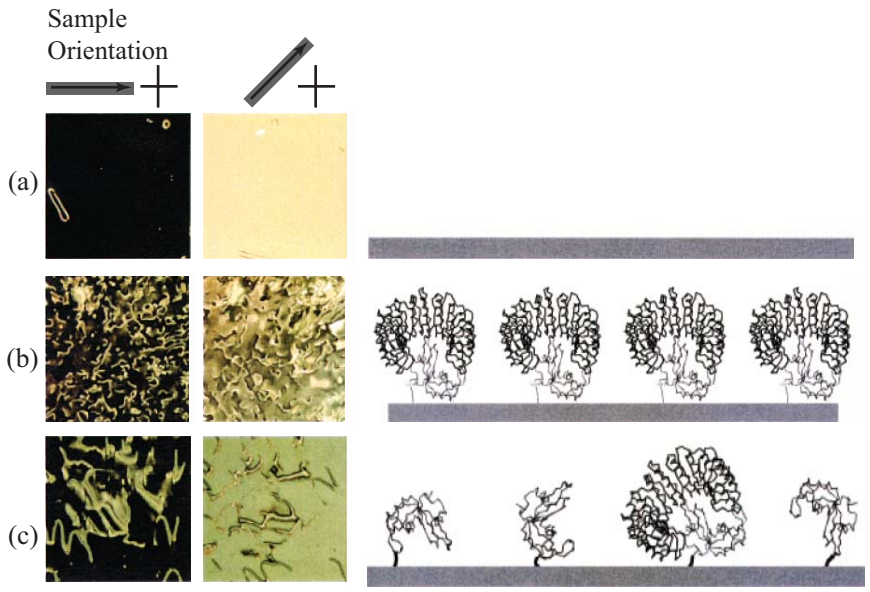

Figure 3.8: Optical images of nematic liquid crystal material (5CB) sandwiched between two substrates and viewed between crossed polarizers: Self assembled monolayers only (control) (a), preferentially oriented RNase A with bound RI (b), and randomly oriented RNase A with bound RI (c). From [113].

of the reorganization of 5CB with the density of immobilized peptides.

Another experiment conducted using liquid crystals as a method to detect peptide-protein binding events was based on the principal that the interference of bound protein affects the relaxation of the defect found in low areal density peptide bound substrates. Specific peptide-protein binding events were successfully observed using liquid crystals after a 17 hour annealing process at 36 °C. Spatially resolved peptide arrays were also successfully imaged using liquid crystals, which have applications including a biosensor array. One of the main and most relevant conclusions (to liquid crystal biosensor applications) is that the time required for the orientational order of the liquid crystal to respond to the presence of bound peptides on a surface depends on the areal density of the peptides, providing a characterization of the time response for a liquid crystal based biosensor.

In both of the previous studies discussed, liquid crystals were applied to the surface containing the binding events after binding occurred. Luk and colleagues [115] proposed a study to determine which lyotropic liquid crystals would facilitate binding events within the liquid crystal material itself. A few properties were determined necessary in a lyotropic liquid crystal to permit binding. Proteins spontaneously fold in such a way as to enclose their hydrophobic elements deep inside their

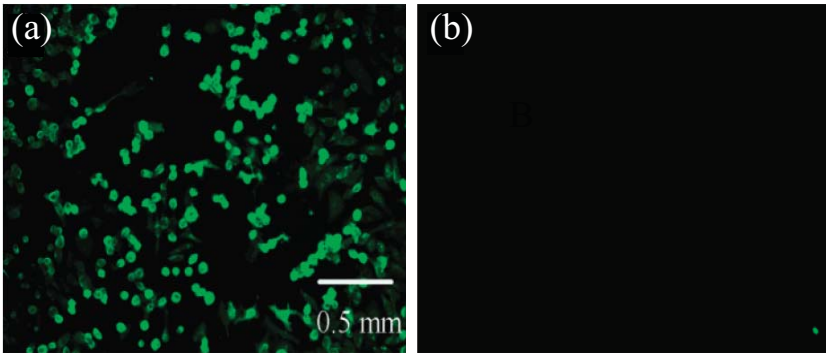

Figure 3.9: Fluorescence images of anti VSV antibody bound to surface bound antigens on mammalian cells in lyotropic liquid crystal (a) and antibiotin IgG (control) (b). From [115].

structure and allow the hydrophillic elements to remain on the perimeter. This process determines which binding sites will be accessible and allows specific binding. If a protein undergoes external stress or is an environment that causes it to unfold (a process called denaturing), a loss of binding ability occurs and the protein can no longer carry out its function. A lyotropic liquid crystal, which is to allow binding activities, cannot be allowed to denature the targeted proteins within it. Additionally, the mesogens of the lyotropic liquid crystal cannot associate with the binding sites on the protein in such a way as to hinder the interaction with the targeted molecule. Lastly, the lyotropic liquid crystal cannot be so viscous that it prevents movement and diffusion of the proteins. The proteins must be able to diffuse into close proximity with each other to allow binding to occur.

Five classes of lyotropic liquid crystals, based on anionic, nonionic, cationic, and zwitterionic surfactants and chromonic lyotropes were tested for their ability to facilitate protein binding events. Two separate sets of experiments were run to test the binding ability of each lyotropic liquid crystal material. In the first set of experiments, human IgG was immobilized on a surface and the lyotropic liquid crystal solution containing antibodies was applied to the surface and allowed to remain for four hours. The slide was rinsed, and the bound antibody was imaged using fluorescence microscopy. The second set of experiments involved applying a drop of the lyotropic liquid crystal-antibody mixture on the surface containing bound antigen and then covering with a microscope slide. Again, fluorescence microscopy was used to image binding of the labeled antibodies to the human IgG. The ten lyotropic liquid crystals screened in this study for their ability to facilitate binding within the liquid crystal

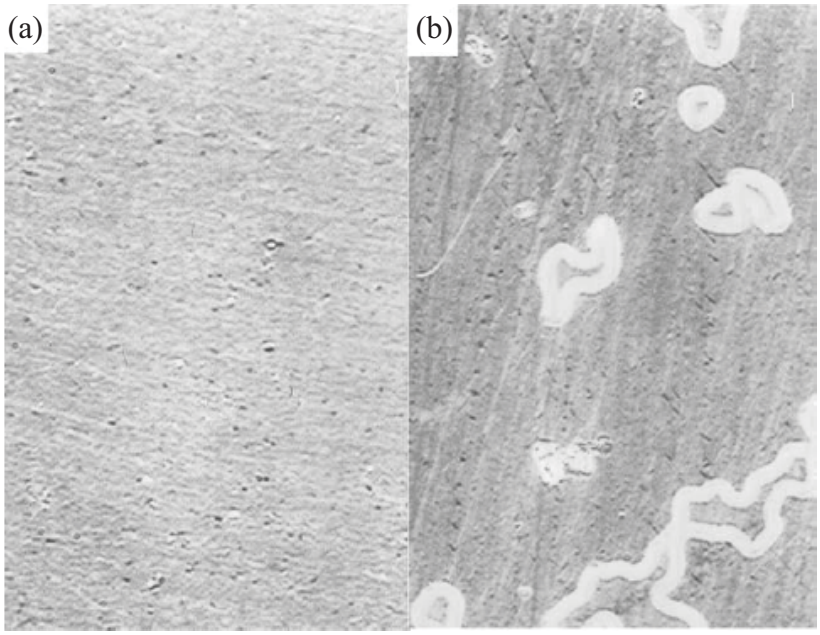

Figure 3.10: Optical images taken from a polarizing microscope of the alignment layer (a) with polarizers at 0° and the same alignment layer viewed between polarizers at 45° after exposure to lipase (b). From [116].

suggest the molecular structure of the lyotrope is a controlling factor. Three of the ten tested liquid crystals allowed specific binding of antibody to the surface bound antigen: cetylpyridinium choloride (CPC1), tetradecyldimethylamineoxide (C14AO) and disodium cromoglycate (DSCG). Because of its high birefringence and low viscosity, DSCG proves promising for biosensor applications.

Particularly relevant for a rapid infectious disease diagnostic was the final experiment run in this study. Antibodies directed to viral antigens on the surface of cells immersed in liquid crystal were imaged. Mammalian cells (human epitheloid cervical carcinoma - HeLa) were inoculated with vesicular stomatitis virus (VSV) and then incubated in the liquid crystal (DSCG). An anti-VSV antibody was prepared in DSCG and incubated on the cells for 1 hour. The results, shown in Figure 3.9, prove the binding of antibody to surface bound viral antigens is both facilitated by the liquid crystal and is highly specific. The application of this technology as a basis for a rapid point-of-care infectious disease diagnostic is promising.

Enzymes are another specific group of proteins which accelerate, or catalyze, chemical reactions. A lipase is a water soluble enzyme which catalyzes the hydrolysis of ester bonds in lipid substrates. Hoogboom and colleagues [116] developed a liquid crystal based sensor to detect the enzymatic

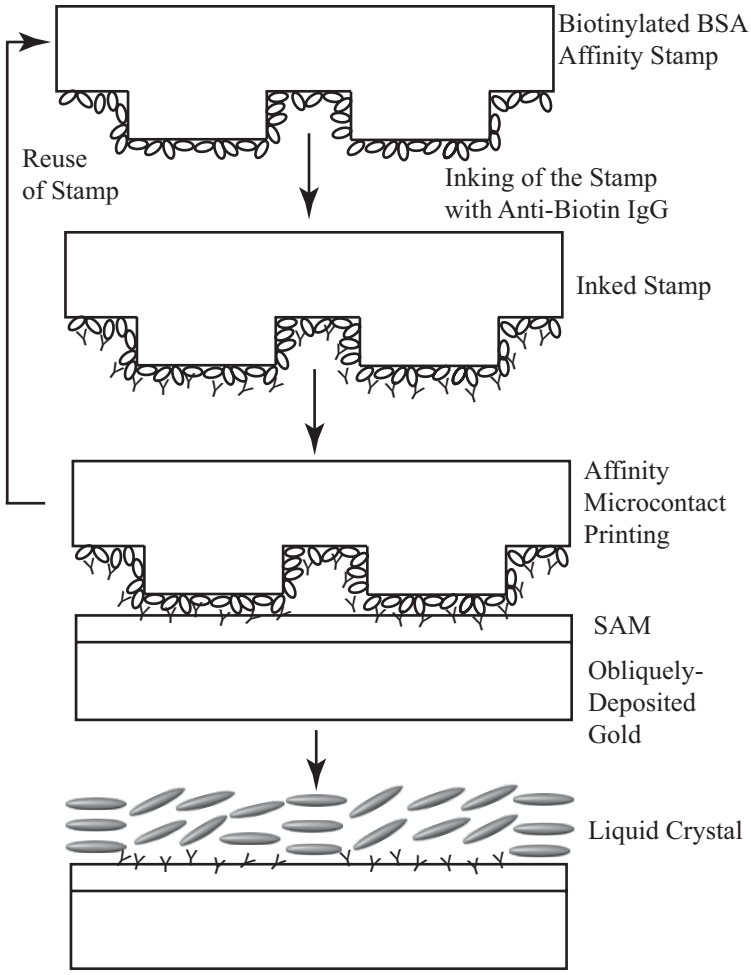

Figure 3.11: Schematic diagram of process used to image microprinted proteins using affinity stamping.

action of a lipase (lipase B from *Candida antarctica*, CALB) by incorporating an ester containing group in the alignment layer. The hydrolysis of the layer disrupts the alignment of the liquid crystal (5CB), which was viewed under polarizing microscopy. Disruptions of approximately 100 μm were observed, whereas in the control, the largest area of disruption was 10 μm (Figure 3.10). The surface chemistry changes caused by the enzymatic action of the lipase account for polarity changes in the alignment layer, which in turn reorient the mesogens. This reorientation is transferred into the bulk, amplifying the changes such that they can be viewed by the naked eye. Further planned experiments include investigating different alignment layers for the detection of other classes of enzymes.

A different direction in the amplification of protein binding events using liquid crystals involves affinity microprinting. In order to detect more than one analyte for increased efficiency during

detection, the idea of elastomeric stamps has been introduced [117]. A grid of 300 μm $\times$ 300 μm squares was cast in a PDMS stamp and covalently functionalized with bovine serum albumin (BSA). The stamp was then 'inked' by incubation in a solution with the targeted antibody. Contact was then applied to the surface of a substrate containing self assembled monolayers (SAMS). The inking process is shown schematically in Figure 3.11. The substrate was then covered with a thin film of liquid crystal and imaged using polarized microscopy. Three properties for the contact surface were targeted as essential for the process to be successful. The surfaces had to be hydrophilic, in order to facilitate a maximum transfer of proteins from the stamp to the detection surface. In order to prevent desorption of the target proteins during contact with the aqueous solution or liquid crystal, the chemical functionality of the surface was altered. Also, the surfaces had to allow for the imaging of the captured proteins using the inherent birefringence of liquid crystals. Uniform alignment of the liquid crystal on the surface prior to stamping allows easier detection of the targeted analyte by providing a higher contrast. It was determined that amine-terminated monolayers supported on obliquely deposited gold films uniformly align a nematic liquid crystal (5CB). Immediately after application of the liquid crystal to the surface, planar alignment is observed; however, after an incubation period of 8 hours at higher temperatures, a transition to homeotropic alignment was seen.

Results of the microprinting experiments are promising for a biological sensor targeting multiple analytes. After inking of the PDMS stamps by either anti-biotin IgG (target) or anti-goat IgG (goat), they were brought into contact with the amine-terminated monolayers. Optical cells were formed using a stamped substrate on one side and an OTS treated glass side (inducing homeotropic alignment) on the other. The cell was filled with liquid crystal using capillary action. Optical images were taken using polarized microscopy and the results are shown in Figure 3.12. The figure shows the targeted surface and the control both 1 and 8 hours after stamping under crossed polarizers. A schematic depicting the orientation of the liquid crystal is shown beneath each image. Earlier experiments determined that the SAMs forced a transition of the liquid crystal from planar to homeotropic during the annealing process. The binding of the proteins to the surface inhibits that

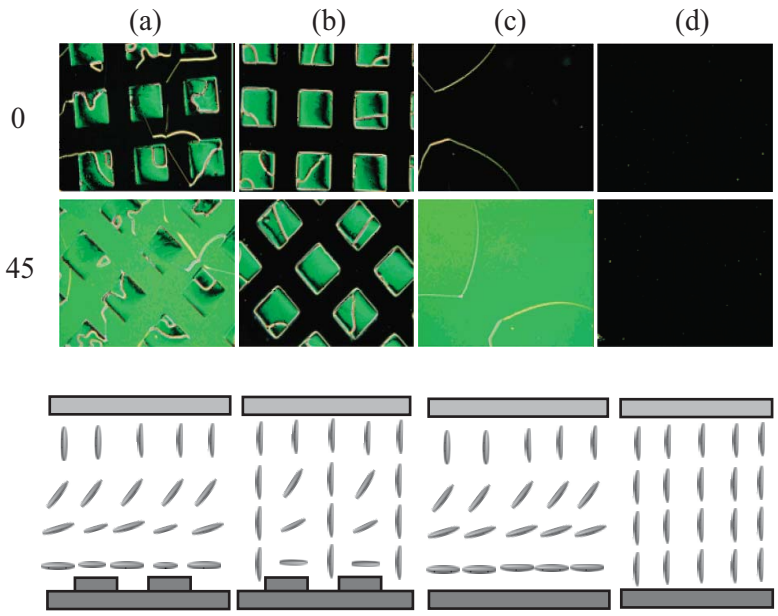

Figure 3.12: Optical images through crossed polarizers of a nematic liquid crystal material (5CB) sandwiched between an alignment layer of amine terminated SAMs and an OTS treated glass slide: Anti-biotin IgG (target molecule) 1 hour after contact (a); after 8 hours of annealing (b); the control (Anti-goat IgG) 1 hour after contact (c); and after 8 hours of annealing (d). From [117].

process, as shown by the dark regions not supporting proteins at all sample orientations between crossed polarizers. This result was confirmed using conoscopy. The tilt angle was calculated through 10 hours of incubation using the change in the birefringence of the liquid crystal. After 10 hours, the orientation was observed to be uniformly homeotropic.

It was hypothesized that affinity microcontact printing could be used to detect proteins on surfaces other than obliquely deposited gold. Proteins were stamped onto glass surfaces and optical cells were created and viewed using polarizing microscopy. For times under 20 hours no noticeable difference was observed between areas that did and did not support proteins. Areas not supporting protein did eventually transition to homeotropic alignment, although the transition was much slower than on gold surfaces. The glass slides produced reorientation in approximately 8 days, as opposed to 8 hours for the gold substrates, which has implications in a rapid point of care device. Prior studies led to the investigation of the reuse of the affinity stamps. Stamps were used three times and the thickness of the transferred protein was measured using ellipsometry. Variations in thickness ranged from 10.8 to 8.5 to 8.3 nm through the three stampings.

It was successfully proven in this study that amine terminated monolayers induced homeotropic alignment in a nematic liquid crystal (5CB). Microprinting of proteins blocks the transition from planar to homeotropic alignment after incubation for several hours, reporting the presence of proteins on the surface in a microprinted pattern. The ability of this technology to be used in an array format is a definite advantage for a rapid point of care diagnostic for multiple pathogen screening.

Further investigation into microcontact affinity printing was performed using transmembrane proteins. Transmembrane proteins span the lipid bilayer in which they are embedded, containing a hydrophobic domain in the interior of the membrane and hydrophillic domains both inside and outside the cell or compartment. Jang and colleagues [118] detected a transmembrane glycoprotein, epidermal growth factor receptor (EGFR), which has been linked to lung, ovary, and colon cancers. Based on the results of the previous study [117], where amine terminated SAMs were found to orient nematic liquid crystal material, antibodies to EGFR were immobilized on the surface of an elastomeric stamp. Before the stamp was contacted with the monolayer covered gold film, drops of cell membrane were incubated on the surface of the stamp. After contact, an optical cell was created using a top substrate coated with OTS and filled with 5CB. Optical images taken between crossed polarizers again showed that areas stamped with EGFR suppressed the transition of 5CB from planar to homeotropic alignment. A difference in contrast between the target and the control was detectable after 1 hour; however, after 12 hours of annealing a high contrast became visible. Transmitted light intensity was measured; the cells containing EGFR transmitted more than 5 times the light. The estimated areal density of the EGFR molecules in this study was calculated to be approximately 10^3 molecules/μm^2. Cell membrane extracts and crude cell lysates were successfully used to detect the presence of transmembrane protein using a visualization of the disruption of liquid crystal orientation.

Many of the experimental designs used to detect protein binding events contain complex surface preparation methods. In order to facilitate the development of a biosensor which is easily fabricated, Choi and colleagues [119] demonstrated a novel technique for the alignment of liquid crystal and

immobilization of the bioreceptors. To avoid complex microfabrication techniques, the receptors (D-biotins) and the homeotropic alignment material were mixed and then spin-coated onto the substrate. The substrate was then thermally treated prior to exposure to the targeted proteins (avidin in PBS). It was subsequently rinsed, dried, and formed into an optical cell. Non-specific binding was tested to ensure that neither the liquid crystal molecules nor the buffered saline interfered with the protein binding. Planar alignment was seen in the cell containing the bound protein, whereas the control cell displayed homeotropic alignment when viewed between crossed polarizers. This study offers a promising technique to reduce the cost of liquid crystal based biosensors by decreasing the complexity of the surface alignment techniques.

The research discussed here concerning the optical detection of protein binding events based on the anchoring transitions of liquid crystals at nematic surfaces provides a promising direction in biosensor development. However, there are a few limitations of these methods. As discussed earlier, some liquid crystal materials (including the thermotropic liquid crystal 5CB) are toxic to certain biological materials. Also, aligning the liquid crystal at the substrate surface is difficult. The receptors bound to the surface serve a dual purpose; they must not only function as specific binding sites, but they must also be capable of aligning the liquid crystal. Given these limitations, Shiyanovckii and colleagues [99] investigated the detection of immune complexes in a bulk liquid crystal as opposed to at a surface. Both the receptors and the specific antibodies were free to move about within the bulk liquid crystal; in this experiment, lyotropic chromonic liquid crystals (water-based and non-toxic) were used. Theoretical calculations of the director distortions around a spherical particle and the transmission of light through crossed polarizers based on those distortions were calculated. An experimental assay was run to determine the toxicity of the lyotropic chromic liquid crystal; it was found that the exposure of *E. coli* to the liquid crystal had no effect on its viability.

Latex beads (diameter ~ 0.56 μm) were used to simulate a microbe in the experimental investigation. The beads were coated with an antigen (streptavidin) and added to the liquid crystal. A fluorescently labeled specific antibody (anti-streptavidin) was also added to allow for the formation

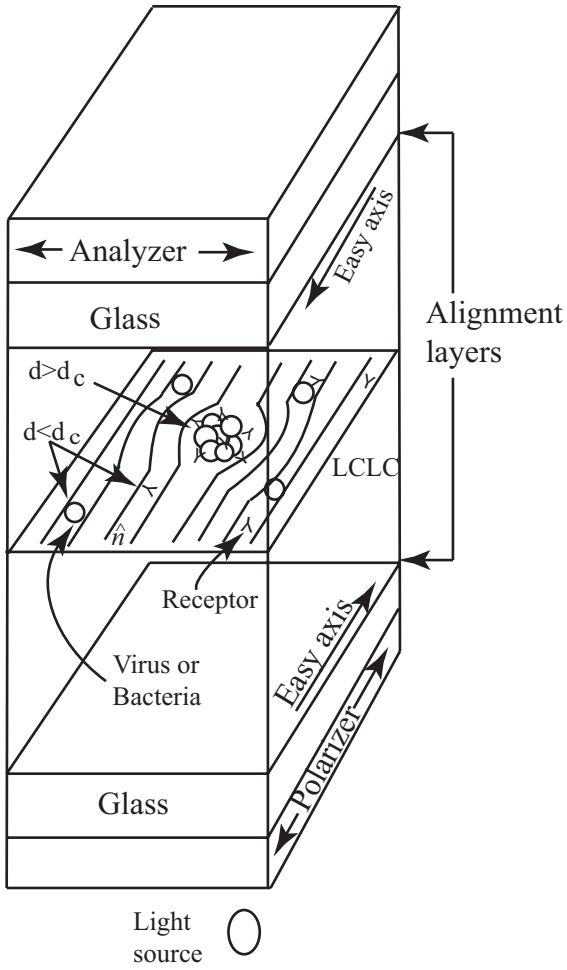

Figure 3.13: Schematic illustration of the setup used to detect immune complexes in the bulk of a lyotropic chromonic liquid crystal (LCLC). d_c is the critical size over which distortions appear in the liquid crystal.

of immune complexes. An optical cell was created using two glass substrates, coated and rubbed with polyimide to induce planar alignment, as shown in Figure 3.13. The liquid crystal/antigen/antibody mixture was allowed to capillary fill the cells, which were subsequently sealed with epoxy. Thirty minutes after exposure, the samples were evaluated using both fluorescence as well as polarizing microscopy. It was found that only complexes greater than 2 μm in size allowed light transmission through the polarizers. This data suggests that once the complexes reach 1 μm in size, the intensity of transmitted light increases with the radius of the complex. This led to the proposal of the critical size, d_c, which is dependent on material properties and the cell thickness. It was proposed that, although the current experiment found d_c to be around 2 μm, this critical size was tunable based

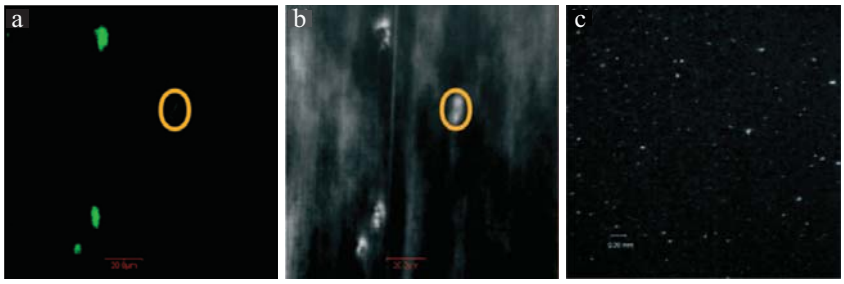

Figure 3.14: Fluorescence (a) and birefringent (b) images due to immune complexes formed from *Bacillus atrophaeus* spores and specific antibody. A low magnification view of the complexes viewed between crossed polarizers (c) is also shown. Immune complexes identified between crossed polarizers but not identified in fluorescent images are circled in images (a) and (b). From [120].

on the anchoring length of the liquid crystal. This method provides many advantages, including very specific interactions of antigen-antibody binding, the rapid formation of immune complexes (allowing very near real time detection) and the lack of complicated alignment techniques.

Given the promising results found by the authors on antigen coated latex beads, another study was performed [120] to detect the presence of bacterial spores. *Bacillus aatrophaeus* (BA), a non pathogenic surrogate for *Bacillus anthracis* was used as the targeted pathogen. Optical cells were created using rubbed polyimide slides, and the liquid crystal mixture containing both the bacterial spores as well as fluorescently labeled anti-BA antibody was allowed to flow into the gap. BA/anti-BA immune complexes were visualized with both fluorescence as well as polarizing microscopy (Figure 3.14). Complexes were detected using both optical methods; however, the birefringent polarizing microscopy method identified spores not detected by fluorescence. The control (anti-streptavidin) did not form complexes with the bacterial spores, and the spores themselves did not show up in either the fluorescence or the polarizing microscopy images.

This technique offers many advantages. The alignment method used on the glass substrates has been refined by the display industry and is widely used and understood. Also, this technique takes advantage of the presence of pathogens using the magnification of the liquid crystal distortions on all surfaces of the complex.

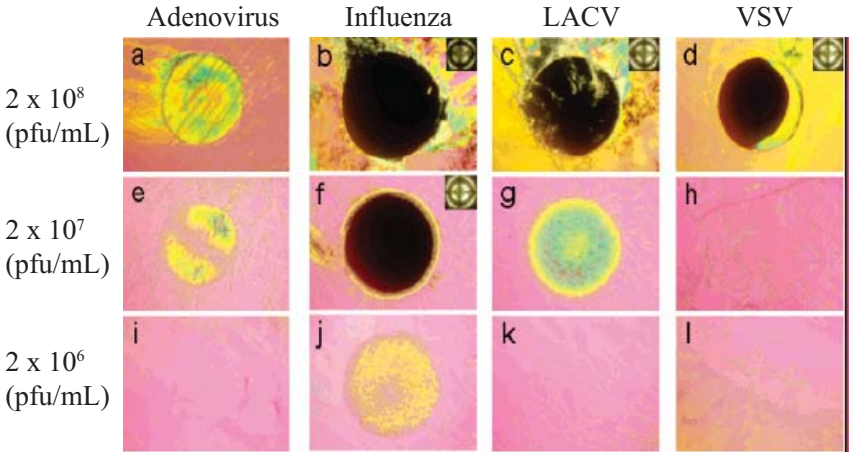

Figure 3.15: Optical cell imaged between crossed polarizers containing 5CB and differing concentrations of virus. The samples are oriented such that the direction of gold film deposition was oriented at an angle of 45° from one of the polarizers. The insets in images (b)-(d) and (f) are conoscopic images of the same samples. From [122].

3.0.9 Virus detection using liquid crystals

Viruses are assemblies of proteins and nucleic acids, and as such (given the aforementioned research into detection of proteins and immune complexes) are a logical next step for liquid crystal based infectious disease diagnostics. The first step in detection is to identify and understand the orientation of liquid crystals to surface bound virions. Tercero Espinoza and colleagues [121] characterized the orientation of 5CB on vesicular stomatitis virus (VSV) bound to cationic, anionic, and neutral surfaces. Their goal was to characterize the orientations of nematic liquid crystals due to surface bound virus; hence, the specific capture of the virus from mixtures was not addressed. Experiments showed cationic surfaces initially induce planar alignment, but, within five days produce homeotropic alignment of the liquid crystal. In contrast, when cationic surfaces were incubated with solutions of VSV and then contacted with 5CB, homeotropic alignment was immediately seen. This observation is promising as the underlying detection technique for a viral diagnostic.

Using these results, Jang and colleagues [122] hypothesized the external structure of viruses could be identified and possibly differentiated based on induced alignment changes of liquid crystal. Four different viruses, all of roughly the same dimension, were studied; three of these are enveloped in a lipid bilayer, and three different structures were presented (spherical, bullet shaped, and an icosahedron). Cationic surfaces were formed by depositing poly-L-lysine on obliquely deposited

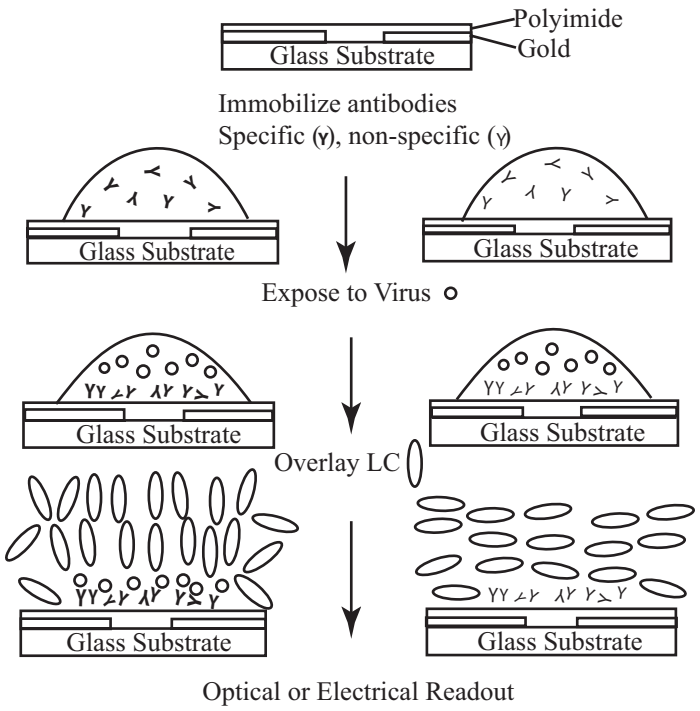

Figure 3.16: Illustration of the procedure used to detect the presence of enveloped viruses both optically and electrically.

gold films, to which purified viruses were immobilized using electrostatic interactions. Fluorescence imaging was performed to confirm the presence of the bound virus as compared to a control. To study the effect of the virus bound surface on the orientational behavior of 5CB, a drop of virus solution was placed on the surface and allowed to remain for two hours. After rinsing, an optical cell was formed using the virus contacted surface as a bottom substrate and an OTS coated (homeotropic alignment) top surface. The liquid crystal (5CB) was drawn into the cell and optical images were taken using polarizing microscopy. The three enveloped viruses presented homeotropic alignment, confirmed using conoscopy, suggesting the interaction between the lipid bilayer of the virus and the liquid crystal molecules is responsible for this orientation. The effect of differing concentrations of virus on liquid crystal orientation was also studied to find an estimate of the minimum density of the virus responsible for homeotropic alignment. Decreasing the concentration of the virus changed the resulting orientation of the liquid crystal, as shown in Figure 3.15. From these experiments, it was estimated the upper limit of the density of virions to induce homeotropic alignment is approximately 1 virion/100 μm^2, making this an extremely sensitive technique for the detection of enveloped viruses.

The detection of enveloped viruses was refined by Acharya and colleagues [123]. A glass substrate containing microelectrodes was coated with a thin film of polyimide. Specific targeted antibodies were immobilized on the surface by incubation, prior to exposure of the sample to the solution containing the virus (Figure 3.16). An optical cell was created, and the orientation of the liquid crystal was determined using polarizing microscopy (optical detection) or by measuring the change in capacitance (electrical detection). Specific binding of the targeted virus was confirmed by immobilizing four different antibodies on the surface. Homeotropic alignment was viewed only on the region containing the specific antibody. Quantitative detection of the bound virus was achieved using both the optical and electrical methods. Also, the accelerated transport of the virus onto the surface was accomplished using AC electrokinetic effects.

3.0.10 The future of liquid crystal sensors

Research leading to the development of liquid crystal based biosensors has been discussed. Competing diagnostic techniques, including microfluidics, molecular methods and optical techniques have been outlined as current and competitive technologies. Current infectious disease diagnostic methods, such as lab culture, microscopy and immune response were discussed along with their benefits and limitations. Techniques for alternative sensor substrates, liquid crystal alignment, and imaging and pixel arrays utilizing liquid crystal technology have been introduced as possible developmental tools for a biosensor. Research reviewed on the imaging of protein immobilization on substrates included the effects of protein folding on ligand binding, peptide-protein binding events, and protein interactions imaged in the bulk of the liquid crystal material. Affinity microcontact printing was reviewed as an alternative technique for monitoring protein binding. Characterization of liquid crystal anchoring changes due to bound virus was also examined, along with induced orientational alignment from virus envelopes.

As evidenced by the aforementioned discussion, liquid crystal sensor technology has a number of potentially important applications in the realm of infectious diseases and public health. Despite myriad advances in the treatment and prevention of communicable diseases, in many circumstances

the rapid diagnosis of specific causal pathogens continues to elude clinical medicine. Rapid diagnosis is important as morbidity and mortality from infectious diseases are frequently directly correlated with the time to initiation of appropriate therapy. On an individual case-by-case basis, a rapid and reliable bedside diagnostic assay to identify specific infectious agents would be a great advance and would likely result in improved patient outcomes. Sporadic, yet common infectious diseases such as meningitis, sepsis, and pneumonia may be caused by a variety of different organisms and represent obvious targets for this technology.

On a broader scale the application of liquid crystal sensors as rapid diagnostic tools may be especially promising in the arena of biodefense and globally emerging infectious diseases. Bioterrorism remains a clear and present global threat; early detection is essential to not only recognize covert attacks but to manage casualties and protect the public health by interrupting the chain of contagion transmission [124]. Rapid diagnostic platforms, such as liquid crystal sensors, could prove useful in healthcare settings, such as hospitals and clinics, as well as in monitoring of environments at risk for bioterrorism. Similarly, as emerging infectious diseases, such as SARS, monkeypox, avian influenza and the associated specter of pandemic influenza persistently threaten the global community, a rapid and reliable diagnostic assay would permit real-time epidemiologic surveillance of animals, humans and environs, thus facilitating epidemic tracking, the first stage in responding to public health threats. The development of liquid crystals as biological sensors, with their potential as a low cost, portable, sensitive and specific, point-of-care diagnostic platform, offers promise as a high-value technology that can be readily adapted to both healthcare settings and field use and serve as a critical component in our armamentarium against infectious diseases.

Chapter 4

Modeling of Liquid Crystal Anchoring at Free and Fluid Surfaces

Given the extremely complex nature of confined nematics and the delicate interactions with biomolecules expected in a biosensor, it is important to fully understand the behavior of the liquid crystal material. To this end, a collaboration was formed with theoretical liquid crystal researchers at the University of Ljubljana, in Slovenia. Through this collaboration, models and simulations were developed to mirror the experimental parameters. Without these models and their corresponding predictions, the iterative process of refining experimental parameters and retesting them in order to target the desired biomarker would be tedious at best. Using the theoretical predictions, variations in the sensor well size, depth, and aspect ratio were optimized, as well as the liquid crystal material and sidewall anchoring strengths. Changes in the structure of confined liquid crystal are observed with variations in surface anchoring strength; this correlation is important for use in a biosensor. This chapter discusses the theory behind the simulations and models, as well as pertinent results obtained for various applied parameters.

4.1 Development of Theoretical Simulations

The vectorial order parameter field, referred to as the director $\vec{n}$, characterizes the average orientation of the molecules with the orientations $\vec{n}$ and $-\vec{n}$ equivalent in non-polar materials (as in the case of 5CB). In confined geometries, the director is generalized into the order parameter tensor Q_{ij} to account for possible formation of defect structures, as the inherent nematic symmetry ($\vec{n} \rightarrow -\vec{n}$) makes use of the director difficult. The director $\vec{n}$ and the order parameter tensor Q_{ij} are related through the following relation:

$$Q_{ij} = \frac{S}{2}(3n_i n_j - \delta_{ij}) + \frac{P}{2}(e_i^{(1)} e_j^{(1)} - e_i^{(2)} e_j^{(2)}) \tag{4.1}$$

where S is the degree of the nematic order, P is the biaxiality and $e_i^{(m)}$ are the secondary nematic directors. Using Q_{ij}, tensorial invariants are constructed to build the free energy functional of a distorted nematic liquid crystal. A delicate interplay between nematic surface interaction, nematic elasticity and defect formation occurs at the interface of our nematic sensor. To model the response of the nematic to the changes at the sensorial interface we employ the Landau-de Gennes free energy minimization approach [125], which is an established phenomenological method in different confined liquid crystal systems. It attributes to each phenomenon different free energy density terms and sums them together in the total free energy functional F. When the total free energy (F) is minimized, the equilibrium nematic profile is obtained. The total free energy within the Landau-de Gennes framework can be written as: [126]

$$F = \int_{LC} f_{el} dV + \int_{LC} f_{ord} dV + \int_{surf} f_{surf} dS \tag{4.2}$$

where f_{el} is the elastic free energy density, f_{ord} is the free energy density ascribed to the nematic degree of order, and f_{surf} is the surface interaction. The free energy densities are given by the

following relations:

$$
\begin{aligned}
f_{el} &= \frac{1}{2}L_1\frac{\partial Q_{ij}}{\partial x_k}\frac{\partial Q_{ij}}{\partial x_k} + \frac{1}{2}L_2\frac{\partial Q_{ik}}{\partial x_i}\frac{\partial Q_{jk}}{\partial x_j} + \frac{1}{2}L_3 Q_{ij}\frac{\partial Q_{lk}}{\partial x_i}\frac{\partial Q_{lk}}{\partial x_j}, \\
f_{ord} &= \frac{1}{2}AQ_{ij}Q_{ji} + \frac{1}{2}BQ_{ij}Q_{jk}Q_{ki} + \frac{1}{4}C(Q_{ij}Q_{ji})^2, \\
f_{surf}^{HOM} &= \frac{1}{2}W_H(Q_{ij} - Q_{ij}^0)^2, \\
f_{surf}^{PLAN} &= W_P(\tilde{Q}_{ij} - \tilde{Q}_{ij}^{\perp})^2
\end{aligned}
\tag{4.3}
$$

where L_1, L_2, L_3 are three elastic constants, A, B, C are nematic material constants, W_H and W_P are homeotropic and planar anchoring strengths, Q_{ij}^0 is the preferential order parameter tensor in the homeotropic regime, and modified order parameter tensors $\tilde{Q}_{ij}$ and $\tilde{Q}_{ij}^{\perp}$ are defined according to Fournier and Galatola [127] to give degenerate (non-uniform) planar anchoring. The following material properties for the liquid crystal 5CB are used [128]: L_1=5.1583pN, L_2=5.0610pN, L_3=3.6663pN, A=-0.086 $\frac{MJ}{m^3}$, B=-2.12 $\frac{MJ}{m^3}$, and C=1.73 $\frac{MJ}{m^3}$. Equilibrium nematic configurations are obtained numerically by minimizing the total free energy F using an explicit relaxation algorithm on a cubic mesh with a x=5nm resolution [129]. Since the operation of the sensor is based on surface effects and not just the bulk response of the liquid crystal, multiple Euler-Lagrange equations are used for the different surfaces in the well. A visual representation of this is given in Figure 4.1 (right frame), where different colors are attributed to different types of mesh points. The top surface varies between f_{surf}^{HOM} and f_{surf}^{PLAN} , depending on the type of anchoring regime being modeled. The side walls and bottom of the well only use f_{surf}^{HOM}, with the anchoring strength W_H chosen to match the experimental parameters.

Our sensor platform is tetragonal with rectangular edges, where either planar-homeotropic or homeotropic-homeotropic surfaces meet. A planar-homeotropic edge prefers local uniform alignment, whereas a homeotropic-homeotropic edge generates a core of a circular +1 or a hyperbolic -1 disclination line exactly at the edge. In our tetragonal sensor geometry, the different edge defects can position themselves many different ways in respect to one another, which results in the formation of a number of potentially stable or metastable configurations in the nematic bulk. Interestingly,

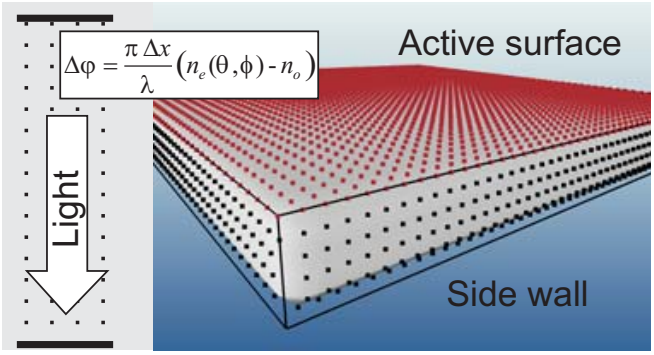

Figure 4.1: A schematic presentation of the simulation box. The nematic bulk region is shown in white, the side and bottom surface mesh points (with fixed anchoring strength) are presented in black, and the active top surface mesh points, which impose differing strengths of either homeotropic or degenerate (non-uniform) planar anchoring, are represented by red. The left frame (in grayscale) indicates that the polarization micrographs are calculated by considering only the phase shift between the ordinary and extraordinary polarization; n_o is the ordinary refractive index, whereas n_e is the extraordinary refractive index dependent on the local orientation of the director given by θ and ϕ.

for particular symmetric configurations of the edge defects, additional +1 hedgehog or -1 hyperbolic point defects can form in the center of the wells or at the top surface. It should be noted that the relative energy balance between different bulk nematic structures depends strongly on the anchoring strength at the well surfaces, and therefore small changes in surface properties can trigger structural transitions of the liquid crystal. This strong dependence can be exploited for use in a biosensor; small changes in surface anchoring strength can induce orientational transitions in the liquid crystal. In order to have control of the structure formation in numerical calculations, proper initial conditions for the order parameter tensor (or its director projection) are chosen. The director projection of the order parameter tensor, mimicking an escaped structure, is used for the sensor operation regime with a homeotropic top surface:

$$\vec{n}_H^{init} = \frac{(\vec{r} - 2d\hat{e}_z)}{|(\vec{r} - 2d\hat{e}_z)|} \tag{4.4}$$

where $\vec{n}_H^{init}$ is the position vector from the coordinate origin chosen in the center of the well, d is the well depth and $\hat{e}_z$ is a unit vector pointing out from the surface of the well. For the sensor regime with the top planar surface we use the initial director projection $\vec{n}_P^{init}$ with a +1 hedgehog defect at the top surface :

$$\vec{n}_P^{init} = \frac{\frac{(\vec{r} - 2d\hat{e}_z)}{2}}{\frac{|(\vec{r} - 2d\hat{e}_z)|}{2}} \tag{4.5}$$

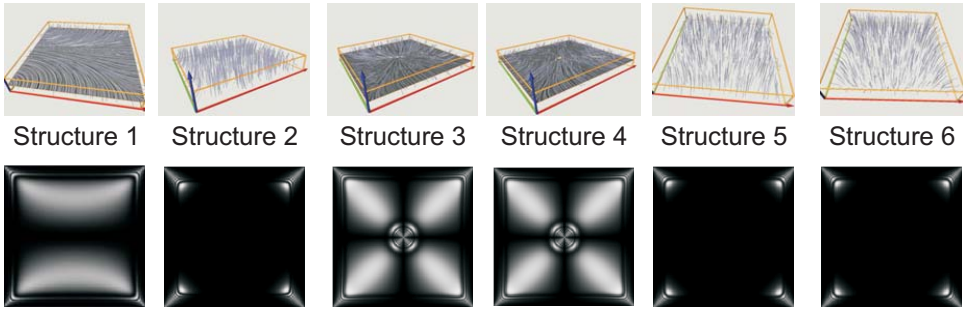

Figure 4.2: Six possible director field configurations for a homeotropic upper surface. Corresponding simulated optical micrographs are shown under each structure.

The simulation volume accessible by numerical calculations using the order parameter tensor is limited by the internal nematic length scale - nematic correlation length, as it sets the scale for the spatial resolution of the mesh to be at the order of a few nm (5 nm). Since there is also a limit on the number of numerical mesh points ($\sim 10^7$) that can be used, our simulation wells are rescaled by a factor of $\alpha = 100$, yielding 2.5x2.5x0.25 μm wells. A scaling approximation can be used for nematic field configurations at the micrometer scale, where the total free energy is governed primarily by the elastic director field deformations, and less by variations in the scalar nematic order (which occur on the nanometer scale.) Geometrical dimensions of the well and wavelength of the transmitted light scale linearly with α, which requires the model calculation anchoring parameters W_P and W_H to be rescaled by α^{-1}. For the sidewalls and floor of the wells, the fixed anchoring 10^3 $\frac{J}{m^2}$ was used to match experimental parameters. Validation of theoretically predicted nematic configurations in sensor wells is accomplished by a qualitative comparison of polarization micrographs with experimental results. In order to generate the polarization micrographs, the Jones 2 x 2 algorithm extended by Ondris-Crawford et al [130] for applications in liquid crystals is used. This approach cuts the LC sample into a square grid of columns through which independent plane waves are propagated (see left frame in Figure 4.1). Director structure within a given column gives the relative phase shifts of the transmitted polarization. Phase shifts are calculated by 2x2 matrix multiplication.

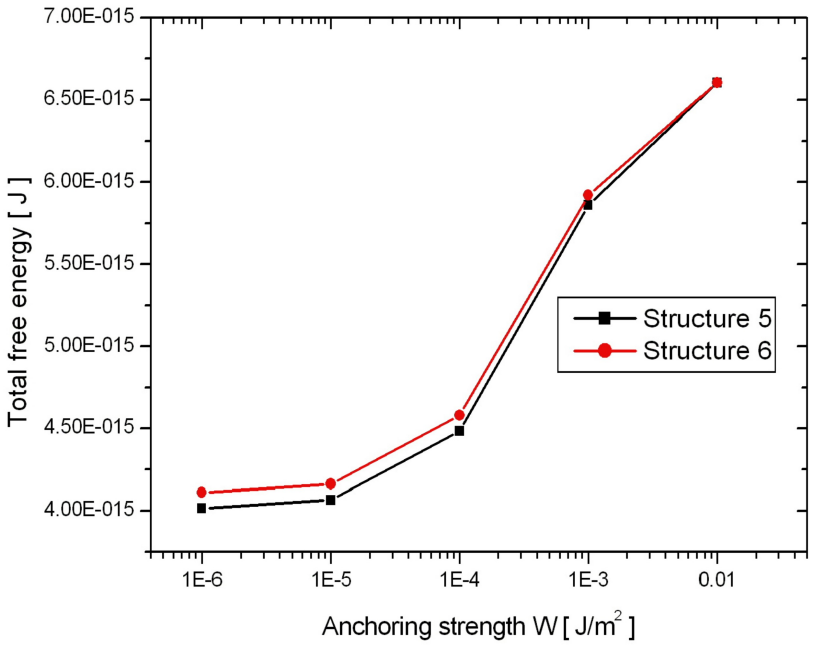

Figure 4.3: The total free energy as a function of the upper surface anchoring strength for potential homeotropic structures 5 and 6.

4.2 Theoretical Results and Predictions

Using the methodology described above, structures and simulated optical micrographs were generated for the first iteration of experimental sensors. The first round of sensor wells had physical dimensions of 260x260x40μm, and were exposed to air to simulate a homeotropic environment, and water to initiate a planar one. The bottom and sidewalls of the well were constrained in the simulations to strong homeotropic anchoring, in order to mirror experimental parameters.

4.2.1 Equilibrium States

If the upper surface (or the open "active" surface) anchoring is homeotropic, as is the case for 5CB [84], six different director field configurations are possible. All six of these structures, shown in Figure 4.2, are stable and can appear in the sensor wells. Structure 1 is a"finger-like" structure, with a splay deformation in the XY plane and bend in the Z direction, while Structure 2 shows a diagonal alignment. Structures 3 and 4 contain point defects in the center of the well, with the

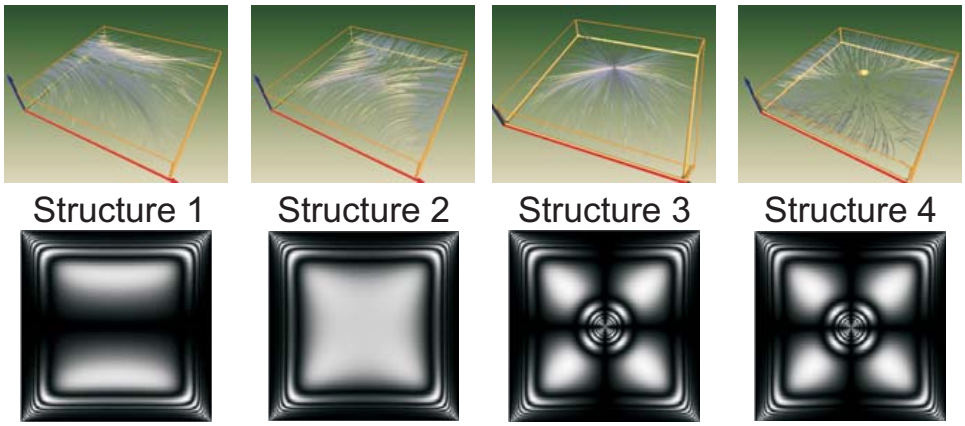

Figure 4.4: Four potential structures for a confined nematic well with imposed planar upper anchoring.

former displaying a radial and the latter showing a hyperbolic defect. Escape structures are observed in Structures 5 and 6, with radial and hyperbolic point defects, respectively, escaping up along the Z direction. A cursory comparison of the simulated micrographs with the experimental optical microscopy results easily narrows the possible observed structures to 2, 5 or 6. By closely observing the symmetry and intensity distribution of the white stripes at the border with the dark region, and the rotation of the "dark arms" in the corners of the cell, it is observed that Structure 2 is not the structure observed in the experiments. So both escaped structures, 5 and 6, remain as viable candidates. Delineating the structure which most closely matches the experiments proves difficult. Both structures display polarization micrographs (for strong upper surface anchoring) which are within a one constant approximation identical, no matter how the crossed polarizers are rotated.

One solution is to calculate the total elastic free energy of both structures and then compare them, since the structure with the lowest free energy should be the equilibrium one. Figure 4.3 gives the total free energy as a function of the upper surface anchoring strengths for structures 5 and 6. Interestingly, the relative ratio between the upper surface anchoring and sidewall surface anchoring proves to be important, since if the side (and bottom) surfaces are stronger than the upper surface, then the director escapes in one direction (Structure 5); otherwise, it escapes in another direction (Structure 6). Based on this calculation and comparison with experimental results for 5CB in air, it is assumed the escaped radial configuration (Structure 5) is the equilibrium state present in the

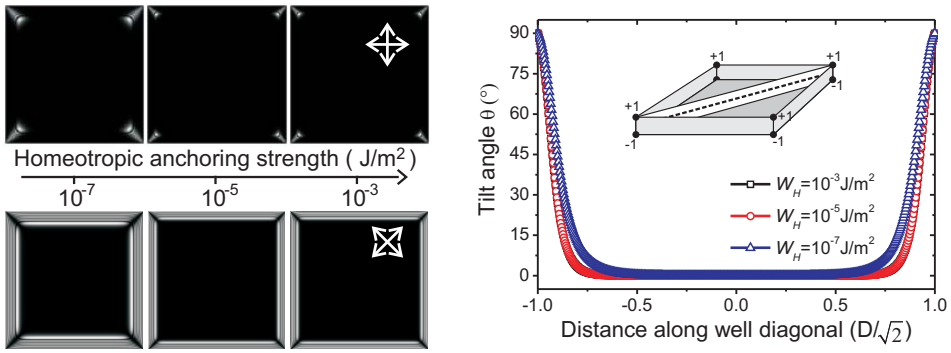

Figure 4.5: Simulated results for a liquid crystal sensor in the homeotropic regime. The image on the left shows simulated micrographs (0° in the upper row and 45° in the lower) for three different values of the upper anchoring strength. The length of the light "tails" is shown in the graph on the right by measuring the director tilt angle along the well diagonal.

sensor wells.

When the upper surface exhibits planar degenerate anchoring, the theory predicts the existence of four possible structures (Figure 4.4.) Structures 1 and 2 show splay in the XY plane and a bend deformation in the Z direction. Radial and hyperbolic point defect structures are observed in Structures 3 and 4. As with the homeotropic upper surface, simulations were compared with experimental results, and Structures 3 and 4 both had simulated micrographs that were viable matches with experiments. Symmetry and positioning of edge disclination lines show that either a +1 radial hedgehog or a -1 hyperbolic defect form in the center of the top planar surface, as expected. The two defect configurations can be discriminated by observing the twist in polarization micrograph patterns, as the twist is seen only for -1 defects which relax their elastic bend deformation through this mechanism. Uniform planar anchoring was also studied, and results are discussed in Chapter 5.

4.2.2 Sensing in the Homeotropic Regime

The homeotropic regime, where liquid crystal molecules are parallel to the sidwalls of the well at the upper surface, offers a platform for a detection scheme. The wells appear dark in the center when viewed with optical microscopy, indicating homeotropic anchoring, which was confirmed through a full rotation between crossed polarizers. Strong homeotropic anchoring on the floor and sidewalls of the wells contribute edge effects, leading to the light "tails" and defects observed in the corners and

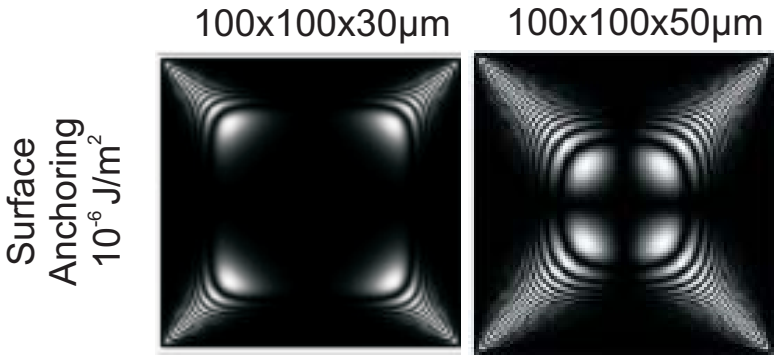

Figure 4.6: Changes in the simulated polarizing micrographs of homeotropic sensor wells with variations in aspect ratio. Both wells have well side lengths of 100μm and identical anchoring conditions; the well on the left is 30μm and the right image is 50μm.

along the walls. The length of the tails is dependent on several variables, including the aspect ratio of the well, the upper anchoring strength, and the anchoring strength at the floor and sides. As the upper anchoring strength is decreased, the contribution from the floor and sides increases and the tails are extended, as seen in Figure 4.5. This change can be measured and quantified, generating a platform for a sensor in the homeotropic regime. In order to quantify this effect as a function of the upper homeotropic anchoring strength for sensor applications, the director tilt angle with respect to the z-axis (pointing out of the wells) is measured, along the well diagonal (as shown in the right pane of Figure 4.5). In the center of the wells, the nematic is uniformly highly ordered, whereas in the corners the tilted "tails" penetrate in the wells for at most 20% of the diagonal.

In order to investigate the impact of changing various parameters without the cumbersome and tedious process of iterating each parameter experimentally, simulations of various changes were performed. First, the aspect ratio of the wells was changed in order to observe any change in impact of the bottom and sidewall anchoring on the bulk nematic. Figure 4.6 shows two different wells, with identical anchoring conditions on all sides. Both wells are 100μm on a side, with one having a depth of 30μm and the other 50μm. The shallower the well, the higher the contribution of the floor (strongly homeotropic), producing a larger dark area in the center of the optical micrograph. As the depth of the well is increased, the contribution from the bottom of the well decreases while the sidewalls have more of an impact. This produces stronger edge effects, as seen in the micrographs.

Another parameter that has potential to impact the length of the "tails" in a homeotropic sensing

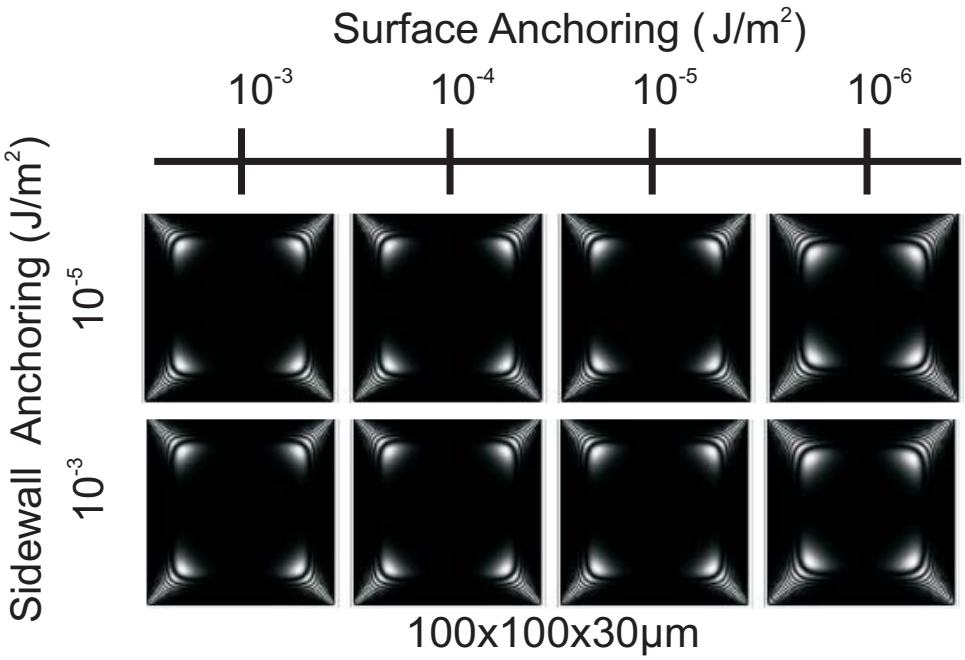

Figure 4.7: Effects of variations in sidewall anchoring in the homeotropic regime for a 100x100x30μm well.

regime is the anchoring strength on the sidewalls and floor of the sensor. Figure 4.7 shows simulated optical micrographs for two different anchoring strengths, 10^{-5} $\frac{J}{m^2}$ in the top row, and 10^{-3} $\frac{J}{m^2}$ in the bottom row. As the anchoring on the active (upper) surface is varied, changes in the micrographs are monitored. Although very slight changes in the intensity of the tails can be differentiated, no major differences between the two can be seen. There are differences in the appearance of the sensors between very weak and very strong upper surface anchoring, and as previously mentioned, the length of the white "tails" could be measured and used as a platform for a homeotropic sensor.

Although the homeotropic regime holds promise as a sensor, and has been proven viable by both simulations as well as experimental results, further progress was not pursued in the research presented here. The goal of this dissertation and the corresponding research was the development of a liquid crystal based sensor for the clinical detection of disease. Although a sensor in the homeotropic regime may be useful for some applications, due to the need to detect small optical changes it was not pursued as a clinical device for biomedical applications in this research.

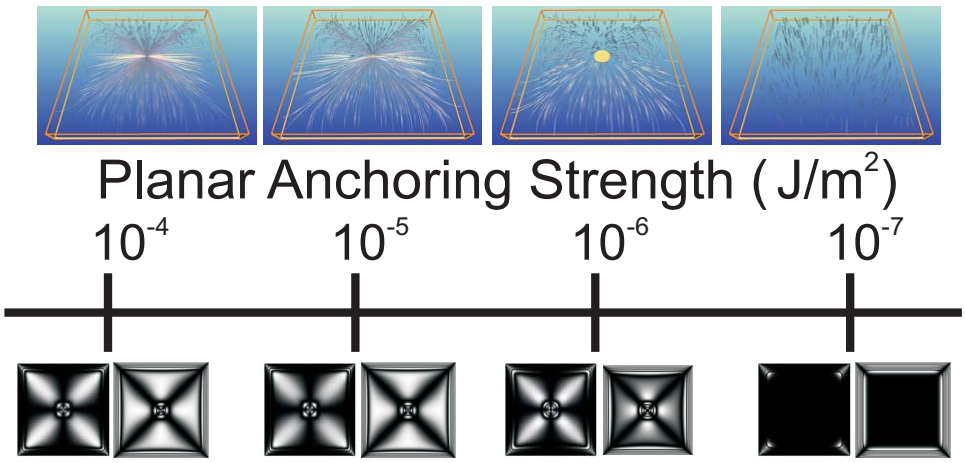

Figure 4.8: Nematic structures observed in a 260x260x25μm well with variations in planar upper anchoring strength. Simulated optical micrographs at 0° and 45° are shown for each value of the upper anchoring strength. As the upper surface becomes weaker, the contribution of the lower surface increases and drives the structure from a defect to an escape configuration.

4.2.3 Planar Regime Sensor

After investigating the potential for a sensor in the homeotropic regime, the focus in research was shifted to a planar upper surface. This models the behavior of nematic liquid crystal materials (particularly 5CB) in contact with an aqueous solution. Given that biomarkers are generally detected in a fluid, this specific setup was particularly interesting for a liquid crystal based biosensor application.

In Figure 4.8, director configurations for different anchoring strengths at the top planar surface are shown. Corresponding simulated micrographs for both 0° and 45° are shown for each value of the upper anchoring strength. The cross structure that appears in the micrographs with the central +1 defect at the top surface is stable over a wide range of anchoring strengths, but becomes unstable at lower planar anchoring strengths. At these lower anchoring strengths, the structure transforms to the escaped radial structure previously observed for a homeotropic top surface. This structural transition is due to the interplay between the planar top surface and the homeotropic bottom surfaces. With strong upper anchoring at the planar surface, the contributions of the homeotropic bottom surface are overcome, and the defect structure which displays the cross pattern is observed. As the upper anchoring strength is decreased, the bottom surface becomes strong enough to drive the structure with a defect into an escaped structure. Hence, we see a transition in the optical micrographs from

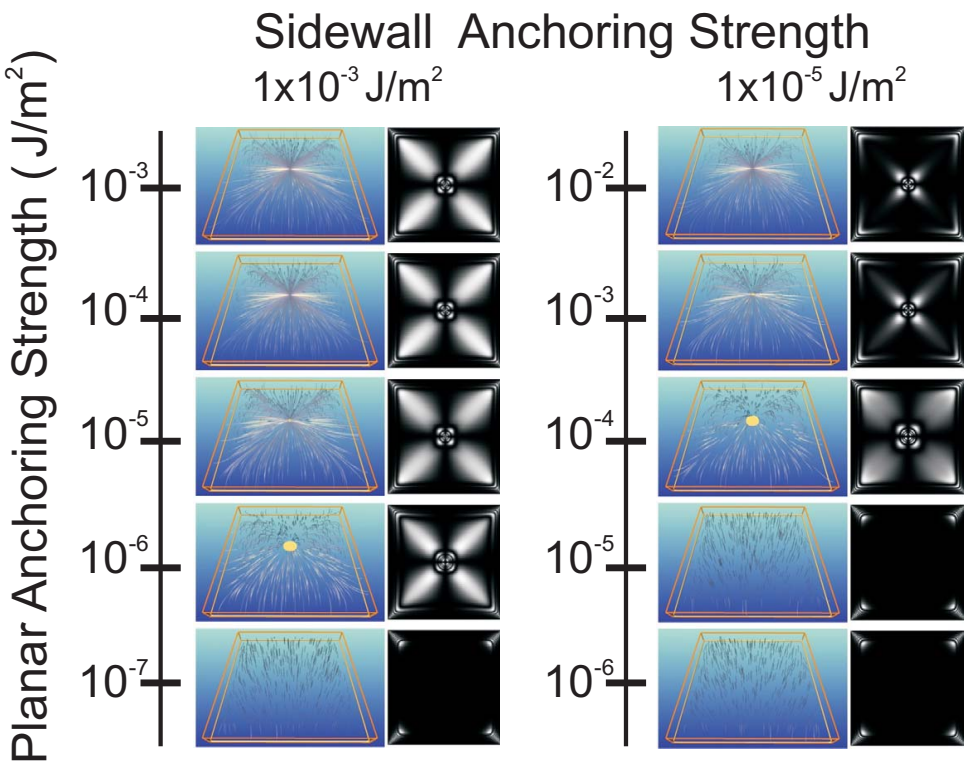

Figure 4.9: The effects of sidewall anchoring strength variation on wells with dimensions of 260x260x25μm. Images on the left show very strong sidewall anchoring(10^{-3} $\frac{J}{m^2}$), while the right column shows weaker anchoring (10^{-5} $\frac{J}{m^2}$). Changes in the nematic structure are shown for a range of upper surface anchoring strengths.

the planar cross structure to the dark homeotropic configuration. These very significant optical differences in the polarization micrographs identify a very interesting regime for the operation of a planar sensor.

This important result identifies an opportunity for a sensing application. A decrease in the planar anchoring strength drives the transition of the sensor from a planar defect structure to a homeotropic escape structure. This transition can be correlated with increasing concentration of a surfactant or biomolecule. The large optical differences in appearance of these two structures provides an attractive option for planar sensing.

After identifying the existence of a strong optical transition point in the planar regime, the possibility of "tuning" the sensor using parameters was investigated. Because the impact of the sidewall and bottom anchoring strength was found to be significant, changes in the magnitude of this anchoring strength was studied. The wells shown in Figure 4.9 had dimensions of 260x260x25μm.

The images in the column on the left had very strong sidewall anchoring (10^{-3} $\frac{J}{m^2}$), which in the wells on the left the strength was lowered to 10^{-5} $\frac{J}{m^2}$. As previously discussed, when the upper anchoring was decreased, the influence of the bottom anchoring was magnified. The prediction for this set of simulations was that decreasing the bottom and sidewall anchoring strength would increase the anchoring strength at which the transition from the planar defect structure to the escape structure occurs. Figure 4.9 proves that prediction correct, as it shows a stronger upper anchoring strength is required to force the transition. This provides a potential parameter to tune the transition of the sensor if needed.

This chapter has discussed the methodology and results of theoretical simulations and models of a nematic liquid crystal sensor. Changes in various parameters including surface anchoring, sidewall and bottom anchoring strength and aspect ratio were studied. These simulations and predictions offer insight into the complex behavior and structures observed in the confined liquid crystal wells, and provide methods in which to refine a potential sensor applications. These results based on theoretical models open the possibility for a sensor to detect changes in concentration based on a correlation with changes in anchoring strength at the fluid interface. Experimental results as well as biological aspects will be discussed in forthcoming chapters.

Chapter 5

Experimental Results: Anchoring and Structural Transition

5.1 Sensor Fabrication

Basic liquid crystal physics, surface interactions and anchoring, and theory and modeling methods have been discussed. This chapter presents experimental methods and results for the creation of micro-wells filled with aligned nematic liquid crystal. In order to create an environment which both confines the liquid crystal material as well as leverages the delicate nature of the forces controlling their alignment at surfaces, micro grids were fabricated. Different techniques and equipment were used for the manufacture of these grids and their subsequent filling with liquid crystal, and the methods and selection of the optimal processes are described below.

5.1.1 Photolithography

Due to its widespread availability and low cost, glass was chosen as a substrate for the sensor. Glass slides (Fisher Scientific, Pittsburgh PA) were cut into one inch square substrates, and subsequently cleaned using a piranha etching method. Sensor grids were fabricated using a standard photolithographic process. The negative photoresist SU8 (Microchem Corp, Newton MA) was spin-coated onto

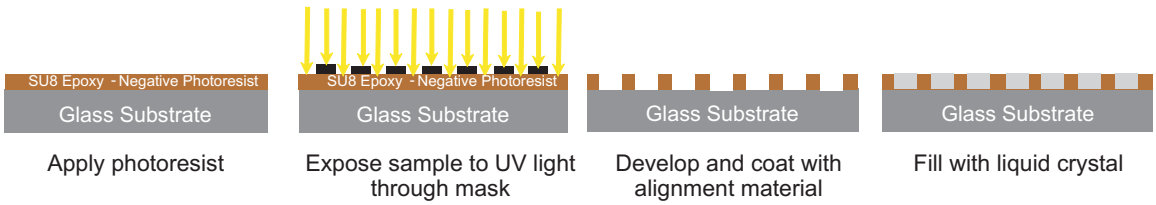

Figure 5.1: A schematic depicting the photolithographic process used to create the sensors. Negative photoresist was spin-coated onto the glass substrate. After exposure to UV light, the sensors are developed and subsequently coated with an alignment material before being filled with liquid crystal material.

the glass substrate for a desired thickness according to published literature from the manufacturer. In negative photolithography, a photo-sensitive epoxy resist is exposed to UV light using a mask to define the pattern. Areas that are to remain after the develop phase are exposed to the light, while sections that are to be washed away are not exposed (shown in Figure 5.1). The areas that receive the UV light cross-link into polymer chains, making them resistant to the developer. Areas not exposed are rinsed away during the development step. After exposure, a post-expose bake step is completed, in order to further cross-link the exposed areas. Once the sample has been allowed to cool to room temperature, it is placed in the developer in order to rinse away unexposed material. The sample must be aggressively rinsed so that all excess material, including the 90° corners, are washed away. After development, the sample is rinsed in isopropanol to halt the development, and then dried thoroughly with with a stream of nitrogen.

During the course of this research, adhesion of the negative photoresist to the glass substrate was found to be a significant problem. Through the course of the development or the rinse stages of the process, the material would lift off of the glass substrate and either entirely separate or create air pockets underneath the grid. In order to combat this, multiple steps were added to the process. To guarantee that no moisture was on the surface prior to application of the photoresist, the glass substrates were dehydrated by baking in an oven or on a hot plate at 200°C for five minutes. In addition, a filter (365nm I-line) was added between the source and the sample. Initially, a UV box as well as a UV source were used for exposures; however, it was found that regulated power and intensity (along with the collimated light) from a mask aligning system (Suss MicroTec, Waterbury Center CT) produced superior results. An adhesion promoter, OmniCoat (Microchem Corp, Newton MA),

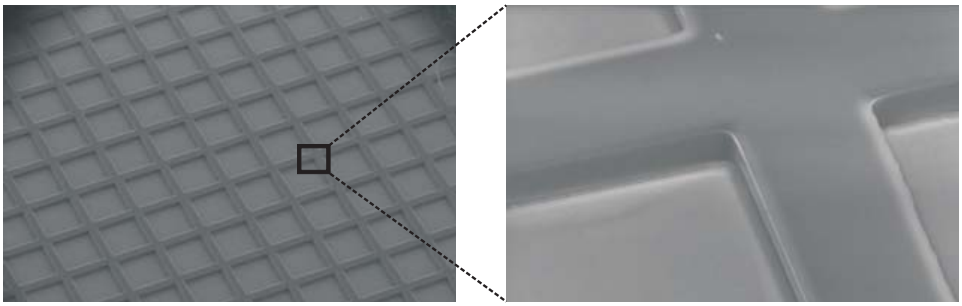

Figure 5.2: Scanning electron microscope images of the sensor wells, prior to alignment layer coating and fill with liquid crystal.

manufactured by the same company as the SU8 photoresist, was used between the glass substrate and the photoresist layer, but negligible improvements were observed.

Other parameters, listed in Table 5.1, required extensive optimization during the process to ensure consistent replication of the wells. In addition to optimization of photolithographic steps such as pre-bake, exposure, post-bake, and development times, other parameters need to be corrected for. To ensure square sidewalls of the grid, the mask must be in very close contact with the sample. If there is any gap between the mask and the sample, UV light seeps out from under the mask and permeates the sample for a certain radius. One cause of this lack of contact of the mask is build up of the photoresist at the edge of the sample. During the spin coating process, photoresist naturally builds up at the edge of the glass on all sides. This edge can be removed using the commercially available Edge Bead Remover from MicroChem Corp. Another preventative step used is to coat the opposite side of the glass that it is scored on. Using materials past their expiration date was found to diminish the reproducibility of the process.

Table 5.1: Experimental parameters of the photolithographic process.

Parameter	**Purpose**	**Outcomes of sub-optimal values**
Pre-exposure bake	Bake off solvent	Premature polymerization
Exposure duration	Cross-link exposed material	Underexposing produces incomplete structures; overexposing leaves excess material
Post-exposure bake	Further cross-link material	Incomplete structures
Development time	Remove excess material	Rounded corners, extraneous material
Cure	Thermal resistance	Permeation by solvents

5.1.2 Experimental Material Properties

In order to ensure the integrity of the photoresist material, thermal investigations were performed to ensure the material remained stable throughout the course of the experiment. Thermogravimetric analysis (Model 951, TA Instruments) was used to test the sensor's thermal stability over the range of temperatures to which it would be exposed. During TGA, the weight loss is monitored as the sample is heated at a constant rate in an inert ambient. TGA results for SU8 showed a less than 2% change in mass from room temperature (25°C) up to 125°C, which easily covers the experimental range the sensor will be operating in.

Theoretical models predict the surface profile of the liquid crystal in the sensor wells has an impact on the behavior of the nematic. In order to accurately model the surface, the contact angle between the nematic liquid crystal and the polyimide coated nematic should be determined. A contact angle goniometer was used to measure the angle of a single drop of liquid crystal on a flat glass substrate coated with SU8 and the aligning polyimide. Using optical methods, the contact angle was determined to be approximately 32° with respect to the coated substrate.

5.1.3 Nematic Alignment Layer

The response of an open surface sensor and the understanding of its behavior is dependent upon the ability to control the boundary conditions. In a square shaped well containing liquid crystal, the anchoring at the sidewalls and bottom of the well is very important to the behavior of the bulk material. Common alignment methods, such as rubbing and the use of polyimides, were discussed previously. Since the geometry of the wells make the rubbing process extremely difficult, a homeotropic alignment material(SE-1211, Nissan Chemical, Japan), which produces strong anchoring, was spin-coated onto the wells. The polyimide was suspended in a solvent in order to improve the coating process, and was subsequently baked off by placing the sample in an oven at high temperatures (180°C) for 30 minutes. The process of baking off the solvent was found to degrade the integrity of the polymer wells. It was hypothesized that this degradation was due to the permeation of the polyimide and/or solvent into the incompletely cured photoresist material. An additional

curing step for the photoresist was added after the development and rinse. This additional step, which was held at a higher temperature than the sample would reach when coated with the polyimide and solvent (200°C for 30 minutes), significantly improved the sample quality after coating with the alignment layer. An important result of the spin coating process is that all of the well walls, including the sides, are coated with the polyimide alignment material. This proves important when interpreting the experimental results.

5.1.4 Liquid Crystal Fill Techniques

One of the most important variables in creating a repeatable and predictable sensor is the method in which the wells are filled with the liquid crystal material. For the sensor results presented here, the liquid crystal material 4'-pentyl-4-cyanobiphenyl (5CB, commercially available as K15, EMD Industries, Germany) was used. Results on variations in liquid crystal material will be reported in later chapters. In order to accurately model the behavior of the nematic, the depth of the liquid crystal in each sensor must be measured, and it must remain consistent from batch to batch. The behavior and response of a well with dimensions of 100x100x25μm filled to a 10μm depth will differ greatly from one filled to 20μm. This proved to be a very difficult task, requiring the investigation of multiple fill techniques. The liquid crystal fill depth was measured in the wells using a white light interferometer (Zygo Corporation, Middlefield, CT). Through these measurements, the fill depth as well as the surface profile of the liquid crystal, as shown in Figure 5.3, was obtained. Figure 5.3(a) shows the measurements of sensor wells that do not contain any liquid crystal material.

First, the traditional method of spin-coating the liquid crystal onto the sensor was tested. It was observed that although spin-coating filled all of the sensor wells, small pools or puddles of material remained in certain areas, similar to the results seen in Figure 5.3(b). A modification to this method was attempted, in order to help disperse the material. Prior to the spin, the liquid crystal material was spread over the sensor using a glass capillary tube. This modification improved the results only marginally, and alternative methods were sought. A Meyer rod was fixed a set distance above a translating stage. The sensor was fixed onto the stage, and a drop of the nematic material was

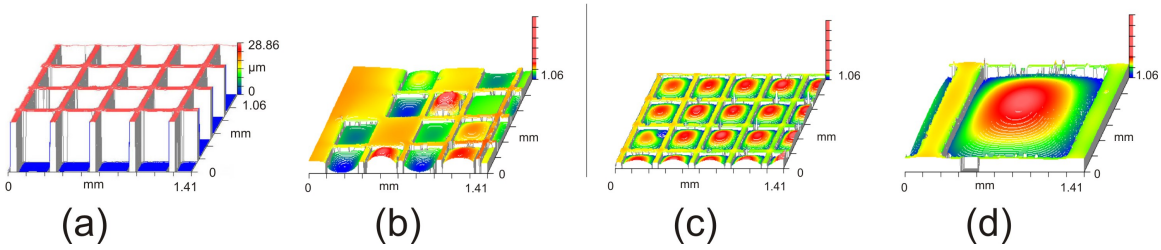

Figure 5.3: Sensor well characterization using a light white interferometer. (a) Square well before addition of liquid crystal material. (b) Poor fill technique, showing pools and incomplete filling. (c) Capillary fill technique using surface tension, producing a more consistent filling of the grids. (d) A close up showing the surface profile of the confined liquid crystal in the well.

applied. The stage was then moved under the rod, in effect spreading the material over the sensor. No pooling was observed; however, there was uneven distribution over the width of the sensor, with variations in depth up to 50%.

The final method explored was the exploitation of the high surface tension of the liquid crystal material, using capillary tubes. A controlled volume of material was dropped onto an area of the sensor. Micro-capillary tubes, with an inner diameter of 300μm, were used to contact the droplet. Excess material was drawn into the droplet, leaving a small volume of material on the sensor. This method was more successful than previous methods, but still had a variation of 25%. In order to reduce this variation, the droplet was "pulled" across the wells using the end of a small capillary tube. As the droplet of material moves across the sensor, wells are filled evenly as the surface tension forces a fairly consistent volume of material to remain in each well. These results are shown in Figure 5.3(c), with an expanded view in Figure 5.3(d).

5.2 Experimental Setup and Characterization

The fabrication methods for a liquid crystal sensor with square shaped wells have been described. The characterization of these wells, along with the experimental methods used to test their response to various stimuli, are described here.

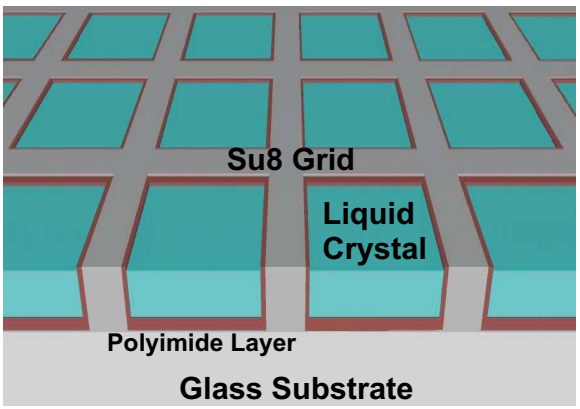

Figure 5.4: A schematic depicting the completed sensors. Microwells are fabricated on a glass substrate using photolithography and coated with an aligment material. The wells are then filled with the liquid crystal material, leaving an open (active) upper surface.

5.2.1 Polarizing Microscopy

Completed sensors (schematic shown in Figure 5.4) were investigated using polarizing microscopy. Polarizing microscopy operates similarly to a compound microscope, with the addition of a polarizer and an analyzer above and below the microscope stage. The stage is also allowed to rotate in order to alter the orientation of the specimen with respect to the polarization direction. For all of the experimental results presented in this research, the polarizer and analyzer are aligned at a 90° angle to each other (referred to as crossed polarizers). For this research an Olympus BX-60 (Olympus, Center Valley PA) microscope was used, with 5x, 20x and 50x objectives. Sensors were explored between crossed polarizers, using only the 435nm emission line from a mercury arc lamp. This narrow emission line allowed for the generation of more accurate simulated optical micrographs through theoretical modeling. Figure 5.5 shows an image of the experimental setup, including the camera mounted above the microscope to capture digital images of the samples.

5.2.2 Experimental Methods

The investigation of the sensor using polarizing microscopy involved two main configurations. The first was the interface of the free surface of the sensor and air. In this situation, the sensor was placed on the microscope stage and images were taken while the sample was rotated. The next setup investigated was the sensor-fluid interface. Two different methods were used for this regime in

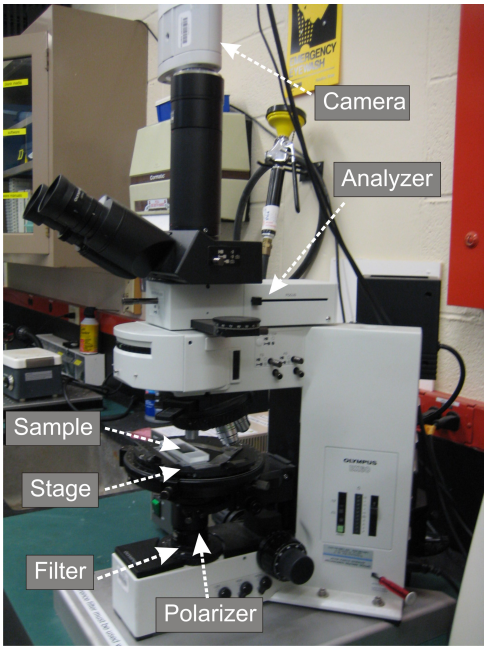

Figure 5.5: An image of the polarizing microscope setup used to obtain experimental data. The sample is placed on the rotating stage and viewed between crossed polarizers. A camera is mounted above to collect date, and a filter allows only the 435nm emission line from the mercury arc lamp to be transmitted.

order to investigate the local nematic alignment. In the first method, controlled volumes of aqueous solutions were pipetted into a Petri dish into which sensors were quenched after being heated above the clearing point. This method provided a very consistent interface and was viable for an extended period of time. In the second method, drops of fluid (approximately a 10μL volume) were applied to the active surface of the sensor while on the microscope stage. This method allowed for a very controlled location on the sensor to be investigated; however, after approximately 20-25 minutes, the drop began to evaporate due to the heat from the light source and the ambient environment. Uniform planar aligned was explored, and for this regime, a very viscous fluid (glycerol) was placed on the sensor and a cover slip was applied on the top to enforce anchoring.

One of the key challenges in the experimental investigation of the sensors was maintaining a consistent experimental location. Initially, the entire surface of the sensor was filled with liquid crystal, providing a large working area. Due to experimental inconsistences, small changes and imperfections exist in the sensor. These are due to defects such as dust and other particles, or small errors in the process. When the entire substrate is covered with the experimental fluid being

investigated, locating the exact same wells in the field of view proved difficult, leading to a lack of homogeneity from data point to data point. To combat this problem, distinct domains were created when the sensor was filled with liquid crystal. Each domain was numbered, and the edge of each domain was observed in the field of view of the microscope. This removed some of the experimental error and inconsistencies.

5.3 Results

The experimental results presented here will focus on two main anchoring regimes: homeotropic and planar degenerate, which are most suited for use in an active response liquid crystal sensor. Planar degenerate most closely models the desired condition of an upper free surface exposed to an aqueous solution of interest. Uniform planar alignment at the upper surface was also explored and the results are presented; however, due to the limited potential for application in a sensor, more attention is focused on homeotropic and planar degenerate configurations.

The first regime studied was the free surface of the sensor in air. As mentioned previously, nematic 5CB has been shown to adopt a strongly homeotropic orientation at the LC-air interface [84]. Figure 5.6 shows experimental results of the sensor wells filled with LC and observed using polarizing optical microscopy. The large image on the left shows the field of view as seen in the microscope, showing consistent alignment over a large sensor area. The images on the right show the progression of one well as it is rotated between crossed polarizers. Dark regions in the center of the sample represent homeotropic alignment of the molecules, and the light areas at the edges and corners represent the contribution in the horizontal plane, due to the homeotropic anchoring at the sidewalls. The length of the tails is dependent on several variables, including the aspect ratio of the well, the upper anchoring strength, and the anchoring strength at the floor and sides. The structure observed in this wells was very stable over a large time period (the same structure was observed when the samples were viewed again a number of months later). The samples were also submitted to thermal cycling, repeatedly heating the material above the nematic-isotropic transition and then cooling. The structures were very stable, continually returning to the homeotropic state.

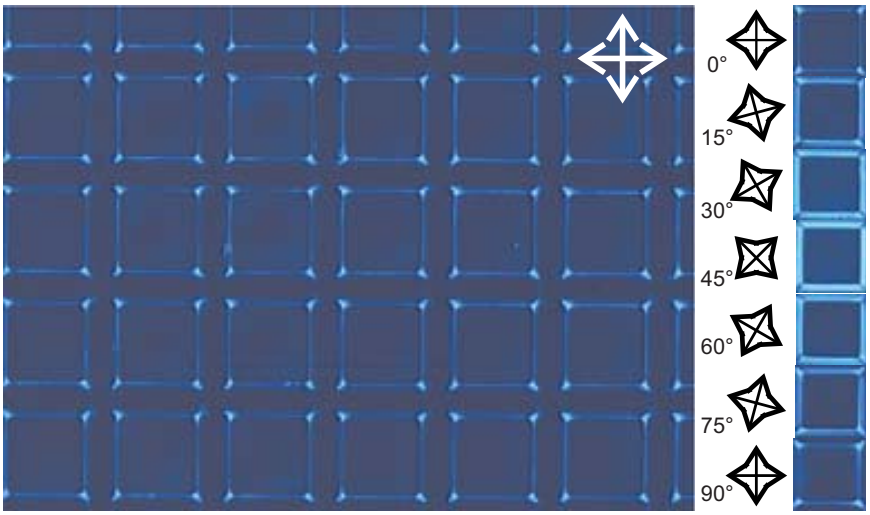

Figure 5.6: Experimental optical micrographs showing strong homeotropic anchoring at the upper surface of the sensor wells. The image evolution on the right shows the sensor rotated between crossed polarizers.

Uniform anchoring at the top surface was also studied (Figure 5.7). In these experiments, a cleaned and dehydrated glass substrate was treated with a polyimide and rubbed to induce planar alignment in a controlled direction. This substrate was then brought into contact with the active surface of the sensor, creating an optical cell, which was then capillary filled with 5CB. Figure 5.7(a) shows a polarizing micrograph with the rubbing direction of the upper substrate parallel to the edge of the sensor (rubbing direction shown in the center), and Figure 5.7(b) shows the substrate oriented with the rubbing direction at 45°. These configurations are referred to as bent 0°and bent 45°; both samples were viewed between crossed polarizers at 0°. Simulated director field configurations with their associated micrographs that correspond to the experimentally formed structures are presented in Figures 5.7(c) and (d). The bent 0° has director distortions mostly concentrated close to the two opposite side surfaces, while the bent 45° has director distortions close to all four side surfaces. These two structures are similar to those found in Tsakonas et al [95] for a two-dimensional case; however, they are additionally bent in the Z direction of the wells.

Following observations of the sensor response in air, an aqueous environment was explored. After being heated beyond the isotropic transition temperature, the sensor grid was submerged in de-ionized water and changes in the sensor observed between crossed polarizers. Upon contact with

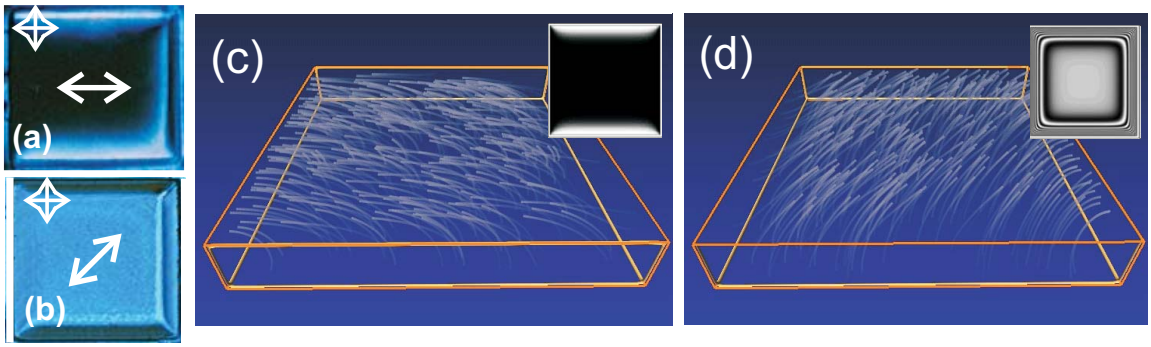

Figure 5.7: Uniform planar anchoring enforced at the top surface viewed between crossed polarizers at 0°, with the rubbing direction of the top surface (a) parallel to the substrate edge and (b) at a 45°angle. Simulated equilibrium director field profiles with insets representing the corresponding simulated optical micrographs for (c) parallel and (d) 45° rubbing direction.

the aqueous solution (water), the wells transitioned to a planar alignment on the upper surface, as shown in Figure 5.8. Each grid displays a defect, which in the majority of samples appears in the center of the well. In a small percentage of samples, the defect is pinned to a side or a corner of the well. These pinned defects are most likely remnants of the method in which the solution is applied to the well, as all of the pinned defects appear on the same side of the well. The dark regions form a cross-type structure, which follows the rotation of crossed polarizers. The distinct cross structure seen in the micrographs are fingerprints of point defect formation in the center of the wells.

5.4 Structural Transition

The goal of this research is the ability to detect a targeted biomolecule by optically observing changes in the surface alignment of a liquid crystal based biosensor. It has been shown by theoretical simulations earlier in this work that changes in the upper surface anchoring strength can induce structural transitions in the bulk nematic. It was believed that these structural transitions could be correlated to the concentration of a surfactant added to the fluid at the interface. To simulate the behavior of the molecule and the response of the sensor, a well known surfactant was chosen as a model for the targeted biomolecule. Sodium dodecyl sulfate (SDS, Sigma-Aldrich, St. Louis, MO) is a classical anionic surfactant having one hydrophilic headgroup (sulfate) and one hydrophobic tail (dodecyl chain), which is commercially used as a detergent. The hydrophobic hydrocarbon tail

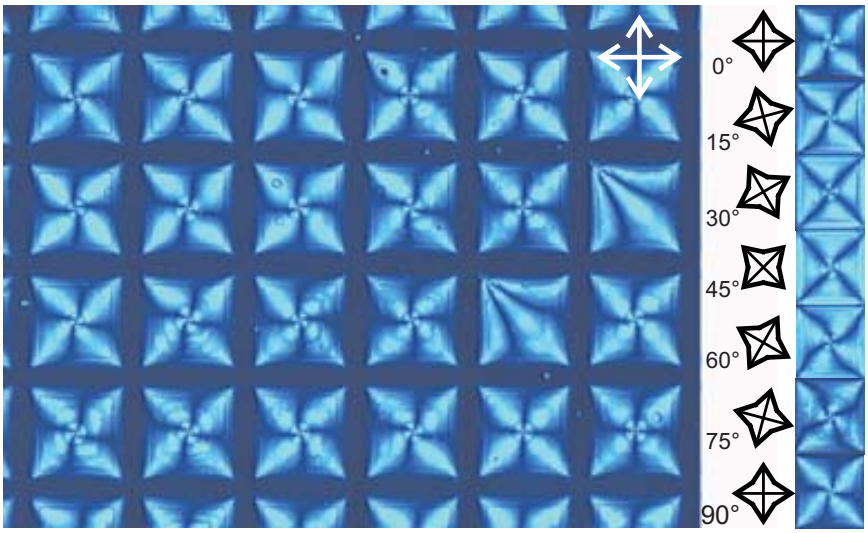

Figure 5.8: Planar upper surface produced by the introduction of an aqueous solution to the top of the sensor. Experimental micrographs show the 'cross structure' at 0°and through crossed polarizers (sequence of images on right).

replicates many molecules found in biological membranes. The chemical structure of SDS is shown in Figure 5.9. In order to study structural transitions of liquid crystal in contact with this surfactant, SDS was dispersed into de-ionized water and vortexed thoroughly to ensure an even distribution. Before each application of SDS to a sensor, the solution was vortexed rigorously for a minimum of 15 minutes in order to break up any micelle formation. Based on theoretical predictions, it is hypothesized that at a critical concentration of the surfactant, the planar upper surface anchoring will weaken enough to allow the defect structure to transition to an escape structure. The concentration of surfactant therefore has an inverse correlation with the anchoring strength; with the increase in surfactant, the planar anchoring strength decreases, eventually causing an orientational transition in the sensor.

Figure 5.10 shows a sensor initially exposed to water and then subsequent concentrations of SDS. Each titration was allowed to equilibrate, and the same wells were observed at each concentration to ensure continuity through the experiment. Figure 5.10(a) demonstrates the typical cross structure observed for planar orientation of the free surface. As SDS is added to the solution, the defects, which previously were stable in the middle of the well, tend to migrate outward. There is also an observed rotation in many of the wells. As the strength of the planar anchoring decreases on the

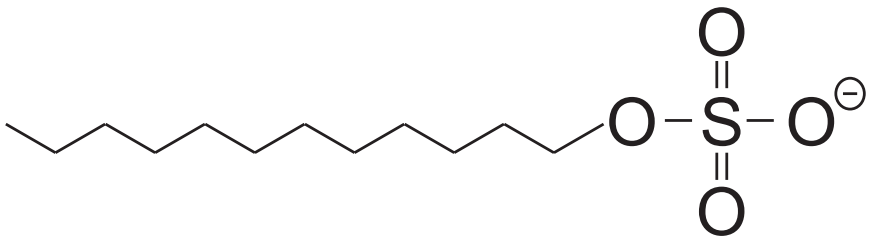

Figure 5.9: The chemical structure of sodium dodecyl sulfate, a homeotropic surfactant used to study anchoring transitions at the open surface of the liquid crystal sensor.

open surface and the orientation moves towards a weaker planar regime, a slight tilt is most likely induced in the molecules at the interface. This leads to the appearance of a rotational pattern in the optical micrographs. As the concentration is increased (Figure 5.10(c)), almost all of the wells show a disruption in the planar pattern, displaying a twist. At a concentration of 1.1mM SDS, all of the wells immediately display a homeotropic pattern upon contact with the SDS solution (Figure 5.10(d)). The transition is observed over a small range of concentrations (1.0mM - 1.1mM), and the same homeotropic pattern is observed for any concentration above the transition point. This pattern remained stable for more than 40 minutes (at which point the dilutions were initiated), and is almost identical to the strong homeotropic anchoring at the top surface observed when the upper surface of the sensor is exposed to air. These experimental results confirm theoretical predictions that the concentration of surfactant at the upper surface influences orientational anchoring by changing the planar surface anchoring strength. This transition was observed in models by decreasing the planar anchoring strength at the free surface.

After observing the transition from strong planar to homeotropic, water was added to the SDS solution to test the reversibility of the transition. As the concentration of the surfactant was decreased (and consequently the planar upper surface anchoring was increased, Figures 5.10(e) and (f)), the strong homeotropic pattern was replaced by a pattern of planar origin which displays defects pinned to the sides of the wells. The formation of the defects in the regions of the top surface closer to the side walls and their pinning can be qualitatively explained by the effect of homeotropic side walls. The homeotropic anchoring on these walls helps to stabilize the planar orientation in the side regions of the top surface, thus making these regions more energetically favorable for defects.

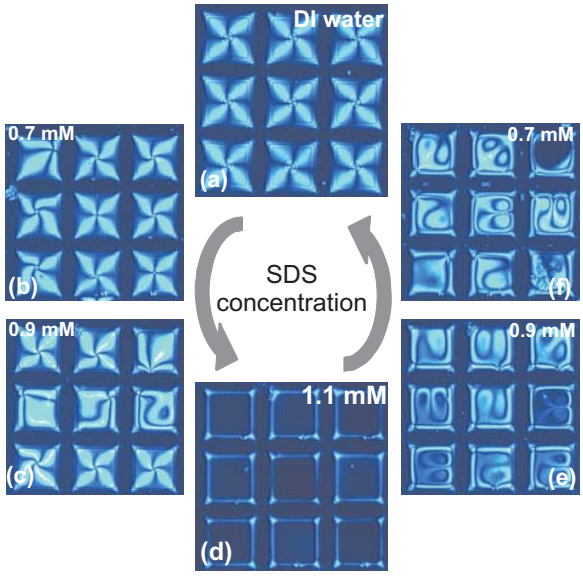

Figure 5.10: Structural transitions of the liquid crystal orientation through the introduction of SDS, a homeotropic surfactant. Varying concentrations of the surfactant solution were added, while the transition from planar to homeotropic was observed for both increasing and decreasing concentrations of solvent. (a) DI water (b) 0.7mM SDS (c) 0.9mM SDS (d) 1.1mM SDS (e) 0.9mM SDS (f) 0.7mM SDS

These results reinforce the correlation between the surfactant concentration and the upper surface anchoring strength.

The transition observed with the addition of a surfactant, as predicted in the theoretical simulations, provides a very significant optical change which can be used in sensor applications. This transformation was observed to have a threshold value, as opposed to a very slow progressional transition. Small changes in the structure are observed as the concentration of the surfactant is increased, but the largest optical change occurs as the concentration surpasses the threshold value.

For potential sensor applications, control of the range of the sensor (in essence, "tuning" the window in which the structural transition is detected by varying the anchoring strength) would be significant. To investigate this possibility with our liquid crystal based sensor, wells were fabricated at one-fifth the scale of the original sensors. By keeping the aspect ratio the same while decreasing the overall dimensions of the wells, the nematic profile is roughly retained, but the surface anchoring strengths were effectively re-scaled. The same nematic profile at different scales requires $W_p d \approx const$, which shows that by scaling down the size, effectively, the anchoring strength increases.

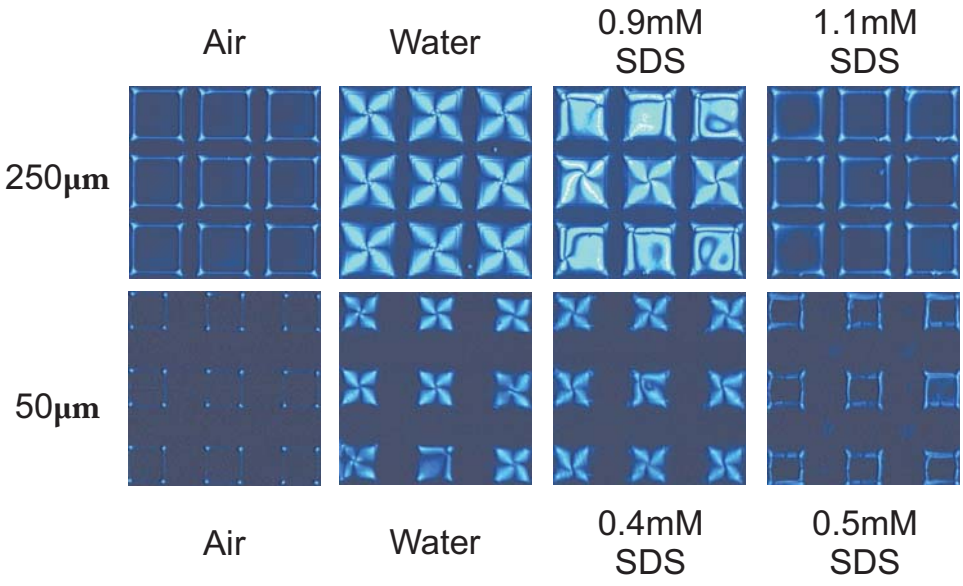

Figure 5.11: The structural transition of the nematic liquid crystal for two different sized sensor wells: 250x250x25μm, shown in the top row, and 50x50x5μm, shown in the bottom row. The concentrations of SDS at which the nematic transitions from a planar alignment to homeotropic decreases with a decrease in well depth.

Changes at the side walls and bottom of the wells are small, since the surfaces are within the limit of strong anchoring. The top surface, which undergoes the transition, is now at a smaller scale and therefore has a larger anchoring strength. In terms of surfactant concentrations, anchoring strength at the upper surface increases for lower concentrations of the perturbing homeotropic surfactant. Figure 5.11 shows a series of experiments with both the larger (250x250x25m, shown in the top row) and smaller (50x50x5m, bottom row) sensor wells, exposed to air, water, and varying concentrations of homeotropic surfactant (SDS). As demonstrated previously, strong homeotropic alignment was observed in air, and strong planar observed when the surface was contacted with water. Increasing amounts of SDS were added until the homeotropic transition was observed. This transition took place at 1.1mM SDS for the larger wells, and as hypothesized, at a lower concentration, 0.5mM SDS, for the smaller wells. It is expected that further variations in the geometry of the sensor wells would lead to increased control of the sensor response. The ideal operational range of the sensor is dependent upon the targeted detection molecule and other experimental parameters such as the desired time of response.

The observation and control of a transition in the structural alignment of confined liquid crystal

provides a platform for the detection of biomolecules which interact with the surface nematic. The introduction of surfactant molecules decreases the anchoring strength at the upper surface, which exhibits a planar defect structure, allowing the transition to a homeotropic escape structure. This transition, due to the changes in the anchoring strength, is correlated with the concentration of the surfactant at the surface. This chapter has discussed the design, fabrication and characterization of a sensor substrate which is filled with aligned liquid crystal. Experimental results for three different regimes were presented; homeotropic, planar uniform, and planar degenerate. Chapter 6 will discuss the application of these results to the detection of a biomarker for the diagnosis of disease.

Chapter 6

Endotoxin Detection using a Liquid Crystal Based Biosensor

Through a collaboration forged with infectious disease specialists, the research presented here is directed towards the detection of endotoxin using a liquid crystal biosensor. Several criteria were used in identifying a microbial target for sensor development. First, it was important to choose a clinically important and relevant syndrome as well as one in which their is a void in diagnostic capabilities. Syndromes were avoided for which sufficient rapid diagnostic techniques are currently available, or would not provide an immediate impact. Second, taking into account the expertise of the physicians in the collaboration, an area of infectious disease research was targeted in which not only is there widely recognized expertise and knowledge, but the materials and targeted pathogens are readily available. Lastly, a toxin was identified that contains a structure similar to those whose interactions with liquid crystals have been investigated.

Background on the physics of liquid crystals, theoretical modeling of confined nematics, and experimental results of the detection of a homeotropic surfactant used to model endotoxin have been presented in earlier chapters. A correlation between the introduction (as well as concentration) of surfactant molecules and the upper surface anchoring has been established, identifying a structural transition which can be used as a platform in a biosensor. This background work was extensive, and

has laid a solid foundation for the experiments presented here. An introduction and background of infectious disease was introduced in Chapter 1, and so will be only briefly mentioned here. Endotoxin structure and function are presented along with a brief introduction to sepsis, the infectious disease which is a direct result of the expression of endotoxin by microorganisms. Experimental methodologies for the detection of endotoxin and results are discussed.

6.1 Biological Background and Lipopolysaccharide

An infectious disease results from the presence of a pathogenic microorganism, such as bacteria, viruses, fungi, protozoa, parasites and prions. These organisms can be transmitted from person to person, and in certain settings cause disease. The body contains large numbers of commensal organisms that are part of the normal flora frequently found on or in the body of healthy people, and do not cause disease under usual conditions. If the normal balance of these commensal organisms is disrupted, or an external pathogen is introduced that the immune system can not adequately respond to, disease results.

Bacteria, which will be used as a platform for detection in this research, represent a large group of prokaryotes. These single-celled microorganisms do not contain a nucleus and are found in every environment on earth. On the human body, they are typically found on the skin, in the respiratory, digestive and urinary tracts, and in the genital system in high concentrations. The most widely used classification system of bacteria uses the Gram stain, and separates bacteria into two large groups based on the composition of their outer membranes. Gram-positive bacteria contain peptidoglycan in the cell wall, which retains the initial stain, appearing purple under a microscope. Gram-negative bacteria do not absorb this dye and are counter-stained, appearing pink.

A main theme of biological cells is compartmentalization; compartments are separate from one another and develop in an aqueous environment. Lyotropic liquid crystal membranes form around these compartments in order to keep the aqueous environments separate from one another and to preserve individual functions. Without the presence of these membranes, many of the necessary functions of the cell would be, at the very least, much more inefficient than they currently are. In

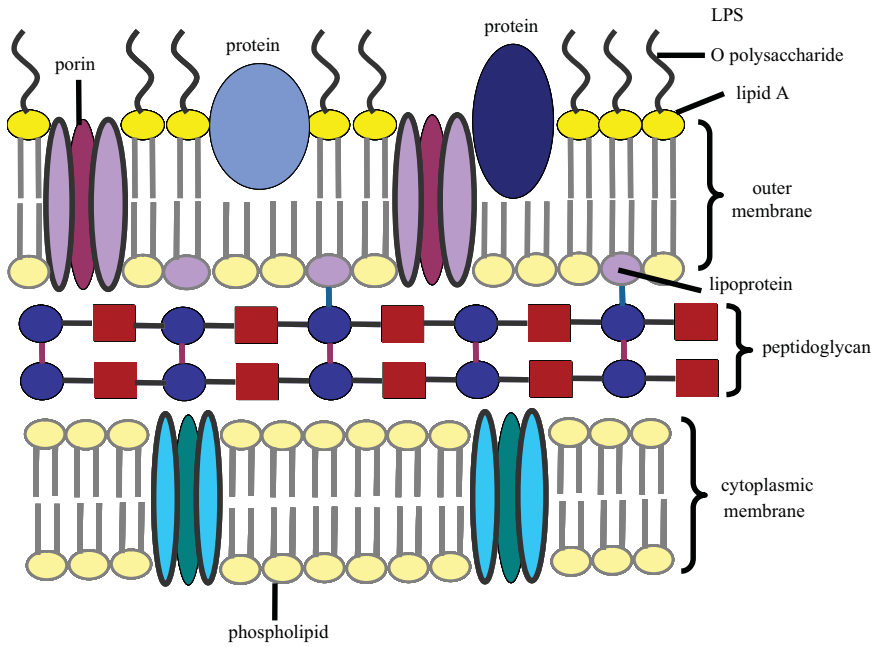

Figure 6.1: The cell membrane of a Gram-negative bacterium. The phospholipids form a lyotropic liquid crystal layer which is permeable to only certain sized molecules.

the case of bacteria, membranes separate the organisms from their external environment.

Phospholipids, molecules with a hydrophillic head group and a hydrophobic hydrocarbon tail, form a bilayer which regulates permeability. Figure 6.1 shows a lipid bilayer from a Gram-negative bacterial cell membrane. Proteins embedded in the membrane act as a filter, only allowing certain molecules to permeate. Changes in the structure of the membrane regulate the molecules that are allowed to pass through. A double bond in the hydrocarbon chain creates a less densely packed bilayer which increases its permeability, allowing larger molecules to pass through. A main component in the bacterial membrane is lipopolysaccharide (LPS) molecules. It has been estimated that one bacterial cell contains approximately 3.5 x 10^6 LPS molecules, and that roughly three-quarters of the bacterial surface consists of LPS [131].

Approximately 35 years ago, while observing the interaction of bacteria and the immune system, Lewis Thomas wrote "It is the information carried by the bacteria that we cannot abide. The gram-negative bacteria are the best examples of this. They display lipopolysaccharide endotoxin in their walls, and these macromolecules are read by our tissues as the very worse of bad news. When we sense lipopolysaccharide, we are likely to turn on every defense at our disposal... [132]" LPS

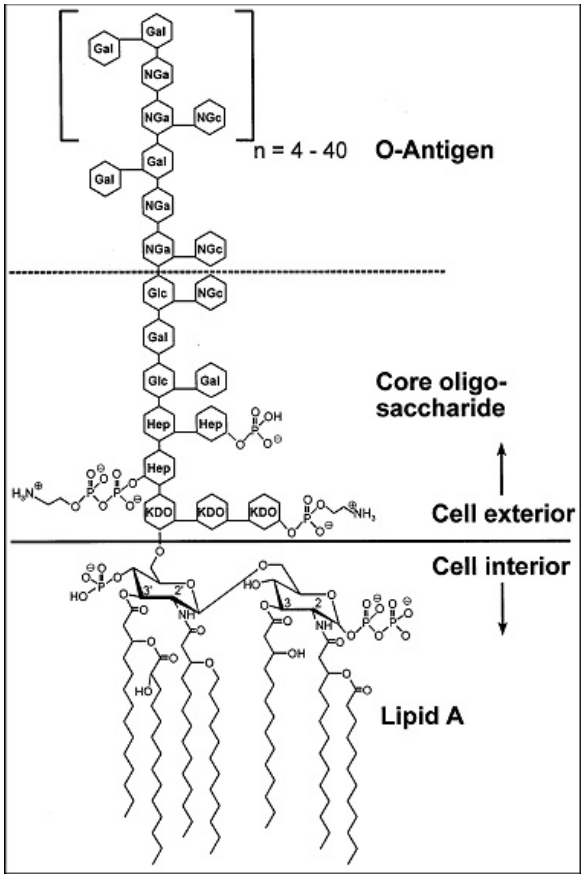

Figure 6.2: A lipopolysaccharide (LPS) molecule from *E. coli* O111:B4. The three main components, Lipid A, core oligosaccharide and the O-antigen are shown. From [135].

molecules have two main functions in the bacterial membrane: structural integrity and resistance to chemical degradation. This complex molecule consists of three main components. Lipid A is a glycolipid which anchors the LPS in the outer leaflet of the membrane, and it is the most highly conserved component. Lipid A has been found to be responsible for the toxicity of the molecule [133]. The central core is nearly the same in most Gram-negative bacteria, and consists of a short series of sugars which can be divided into an inner and outer portion. The O-antigen is a long carbohydrate chain made up of repeating sugar subunits, which differ from strain to strain. This component exhibits structural variability, functioning as an important surface antigen. The variability of this oligosaccharide chain causes the molar mass of an endotoxin monomer to vary from 10 to 20kDa [134].

Given the ability of bacteria to survive in a multitude of conditions, LPS molecules are ubiquitous in the environment. The lipid A portion of endotoxin is linked into the bacterial cell wall,

but is continually released to the environment during cell death and replication. Due to its amphiphilic nature, in an aqueous environment LPS molecules have been found to act as a detergent and aggregate into micelles [136]. The critical micelle concentration at which this occurs was found to be between 1.3 and 1.6μM for *E. coli* O111:B4, and the aggregation number was between 43-49 molecules per micelle at a concentration of 2μM LPS.

6.2 Sepsis

6.2.1 Pathology

The immune system and its response to the presence of microorganisms is an extremely complex process. The human body consists of both an internal,normally sterile, and external environment. The nasal and oral cavities, respiratory system, digestive tract and the urogenital organs are all connected to the external environment and are home to many different bacteria that do not cause disease. When a commensal or pathogenic bacteria crosses the barrier between the internal and external environments, an immune response is evoked. Typically, the bacteria is recognized as being foreign and is targeted by the immune system, which then proceeds to kill the bacteria and repair any damage. This response includes both humoral components as well as inflammatory cells, activating a large array of mediators [137]. During sepsis, the damage to the body is caused not by the pathogenic organism, but by the body's own immune response to the presence of the organism. Many cases of sepsis begin with a localized infection by endogenous bacterial flora. This local infection then becomes systemic, invoking a massive immune response, causing damage and destruction to the body. In healthy individuals, there is a baseline level of endotoxin present in order to challenge the immune system, keeping it primed to act against pathogenic bacteria.

The term "sepsis" has become a physiologic as well as a clinical term. An expert committee comprised of members of the American College of Chest Physicians and the Society of Critical Care Medicine developed a set of definitions for sepsis, severe sepsis and septic shock [138], shown in Table 6.1. Bacteremia is considered present in association with positive blood cultures. Sepsis is

Table 6.1: Widely used definitions of terms used to describe the body's systemic response to infection. From [1].

Term	**Definition**
Infection	Presence of organisms in a normally sterile site
Bacteremia	Cultivatable bacteria in the blood stream
Systemic inflammatory response syndrome (SIRS)	The systemic response to a wide range of stresses. Two or more of the following: Temperature >38°C or <36°C Heart rate >90 beats per min Respiratory rate >20 breaths per min WBC>12,000 cells per mm^3 or <4000 cells per mm^3
Sepsis	The systemic response to an infection. If associated with proven or clinically suspected infection, SIRS is called "sepsis."
Hypotension	A systolic blood pressure of <90mm Hg, MAP <70mm Hg, or a reduction of >40mm Hg from baseline.
Severe sepsis	Sepsis associated with dysfunction of organ(s) distant from the site of infection, hypoperfusion, or hypotension.
Septic shock	Sepsis with hypotension that, despite adequate fluid resuscitation, requires pressor therapy.

defined as the combination of pathologic infection and physiological changes, including tachypnea, tachycardia, hyperthermia or hypothermia; when organ dysfunction distant from the site of infection, hypoperfusion (shock) or hypotension (low blood pressure) are also observed, the condition is deemed severe sepsis. Septic shock is defined as sepsis with hypotension that requires vasopressor therapy.

6.2.2 Causes and Epidemiology

Sepsis and septic shock can be caused by bacteria, viruses, fungi and parasites, although ninety percent of cases are caused by bacteria; Gram-negative bacteria account for 37.6% of total cases of sepsis. Patients presenting with elevated temperature, heart rate, respiratory rate and/or white blood cell count are suspected of harboring sepsis and represent a common proximate reason for patients entering a hospital setting. As medical advances and treatments are increasing the lifespan of the average human, the burden of both hospitalizations as well as medical procedures are increasing. This has led to an increased elderly population and an increase in patients receiving immunosuppression treatments. The number of invasive procedures, such as the insertion of catheters, allowing for

the introduction of commensal bacteria to the internal environment and potential infection continues to grow. Occurrences of nosocomial sepsis, which is a septic process acquired while in a hospital setting, have increased with the increase in hospitalized patients [21]. These immuno-compromised groups and those hospitalized remain at a higher risk for infection, leading to a higher risk of sepsis. Although the attack rate of sepsis for infants is very high (greater than 500 cases in 100,000 per year), the median age for patients with a hospital diagnosis of sepsis is approximately 60 years.

Although instances of sepsis, severe sepsis and septic shock are hard to estimate due to the lack of studies performed since the standardized definitions, the frequency appears quite high. In 2000, there were nearly 660,000 cases of sepsis in the US alone, with an in-hospital mortality rate of 17.9% [139]. Sepsis is the 10th leading cause of death overall in the United States and care of patients with this syndrome costs in excess of $50,000 per patient [140]. It has also been shown that sepsis substantially reduces the quality of life of those who survive [141].

6.2.3 Current Clinical Diagnostic Methods

Due to its complex nature and physiological manifestations, sepsis is difficult to clinically detect. According to Mandell and colleagues [1], "No bedside or laboratory test provides a definitive diagnosis (for sepsis)." Because sepsis is the body's systemic response to infection, there is considerable variability from person to person, as well as temporal variability. This makes a clinical diagnostic difficult to develop and calibrate. Blood cultures can be useful in determining the likely microbial pathogen, although they are somewhat time-intensive, requiring a minimum of 24 hours. Research towards establishing a correlation between cytokine levels in patients who are infected and those who exhibit systemic response to other stimuli, has thus far been unsuccessful. This dearth of consistent, reproducible diagnostic techniques for septic infection suggests that endotoxin detection may be a beneficial strategy.

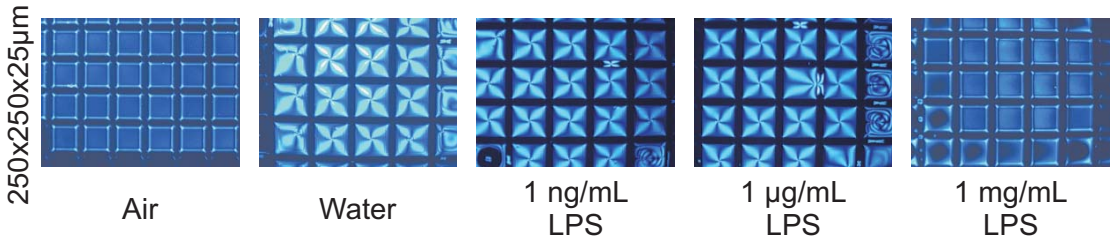

Figure 6.3: Initial experimental results for a 250x250x25μm sensor filled with 5CB in contact with lipopolysaccharide (LPS). The sensor response to air as well as water is shown as a baseline control for comparison. A transition from the planar state to the equilibrium state is observed at roughly a concentration of 1mg/mL LPS. Polarizing optical images were taken with the polarizer at a 90° angle to the analyzer.

6.2.4 Research into Endotoxin Detection

Significant research has been devoted to the study and detection of LPS interactions [142, 143]. De Haas and colleagues [144] used a biosensor chip (coated with streptavidin, which binds strongly to biotinylated LPS) to study interactions of LPS with various proteins and peptides. Other detection methods such as fluorescence based biosensors have been constructed to detect the presence of bacterial endotoxin [145, 146]; evanescent wave fiberoptics [147] and quartz crystal biosensors [148] have also been studied.

6.3 Experimental Detection of LPS

The goal of this research is to leverage existing knowledge and experience gained through the commercialization of liquid crystal devices for the detection of a biomarker for sepsis. Previous chapters have presented background on liquid crystal physics as well as existing work in liquid crystal sensors. Theoretical simulations and models have been created to more fully understand the complex behavior of the confined liquid crystal in contact with various environments. A surfactant, sodium dodecyl sulfate (SDS), was used to simulate the biosensor's response to LPS in a model system. It was observed that as the concentration of SDS was increased, the planar anchoring strength at the upper surface decreased, allowing for an optically detectable structural transition. Experimental results of the biosensor in contact with LPS are presented here, according to the experimental procedure introduced in Chapter 5.

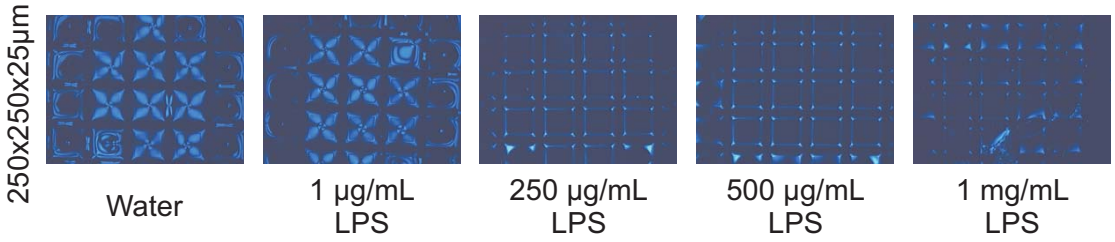

Figure 6.4: Further experimental differentiation of the transition point for a 250x250x25μm sensor. The structure of the liquid crystal transitions somewhere between 1 and 250μg/mL. Each sensor was allowed to equilibrate, and images were taken after approximately 10 minutes.

The first experiment designed and run was to observe the general behavior of the sensor in contact with LPS in aqueous solution, in order to compare the results with theoretical predictions. Figure 6.3 gives results for concentrations of LPS from 1ng/mL to 1mg/mL, a clinically relevant range, for 250x250x25μm sensor wells. A drop of each solution was applied to a distinct domain of the sensor, which was viewed between crossed polarizers. Each domain was allowed to equilibrate, and was observed for approximately 30 minutes. As predicted by theory, when the concentration of a surfactant at the upper surface increases (decreasing the planar anchoring strength at the top surface), the sensor undergoes a transition. This structural transition, marked by the optical change from a planar to homeotropic regime, was observed to occur with the presence of LPS. Here, this transition occurs in the range of 1μg/mL to 1mg/mL. Optical images of the sensor exposed to air and water (as a control) are presented for comparison. The equilibrium states compare very favorable with the simulated optical images predicted by theoretical modeling. The homeotropic regime, observed with the sensor exposed to air and to 1mg/mL LPS, is somewhat brighter than previous results. The images were slightly overexposed during the data collection in order to fully view the defects and structures present.

After the equilibrium states were observed and the occurrence of a transition between the structures was confirmed with the presence of LPS, another experiment was run to further narrow down the concentration at which the transition appears. Figure 6.4 shows 250x250x25μm sensor wells exposed to 3 concentrations of LPS between 1μg/mL and 1mg/mL. The transition appears between concentrations of 1 and 250μg/mL of LPS, and was confirmed with multiple repetitions of the experiment. Concentrations of 250, 500 and 750μg/mL all evoked a transition to the homeotropic

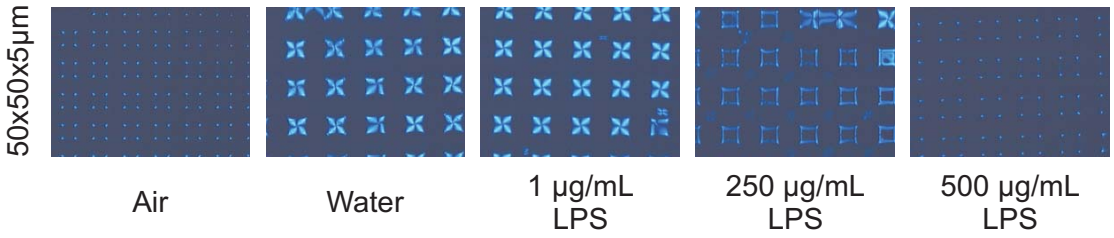

Figure 6.5: Polarizing optical images showing the structural transition of a 50x50x5μm sensor. The depth was decreased in the sensor to increase the contribution of the sidewall anchoring, yet the aspect ratio of the well was held constant. The transition appears to remain between 1 and 250μg/mL.

structure, as is clearly displayed in the Figure. Water, as the control, and the lowest concentration (1μg/mL) of LPS both display the cross structure which is evidence of the defect configuration in the well. As predicted, an increase in LPS concentration causes an increase in the upper anchoring strength, transitioning from a strong defect structure to a weaker defect or an escape structure (as evidenced by the dark appearance of the wells).

As discussed previously, a collaboration was formed between engineers in the Display and Photonics Laboratory at Brown University and infectious disease experts at Memorial Hospital of Rhode Island. After the initial targeting of LPS as a biomarker, the physicians also provided information as to the behavior and structure of the molecule, as well as a clinically useful target concentration to detect. Concentrations of 1mg/mL would prove fatal in a patient, and were thus not clinically relevant for a detection device. The target goal for the sensor was a detection concentration of approximately 100ng/mL, which would require at least a three order of magnitude reduction in the current detection concentration. The simulation and modeling work presented earlier, along with the experimental system using a model surfactant, showed the ability to control the sensor response by varying experimental parameters of the sensor. The sidewall anchoring strength was investigated theoretically, and was found to increase the concentration needed to induce a transition. Since this moves the sensor detection in the wrong direction, it was not explored experimentally with LPS. Variations in the well depth, aspect ratio and liquid crystal material were considered, and the results are presented here.

The first parameter studied was variation in the well depth. As explained in Chapter 5, reducing

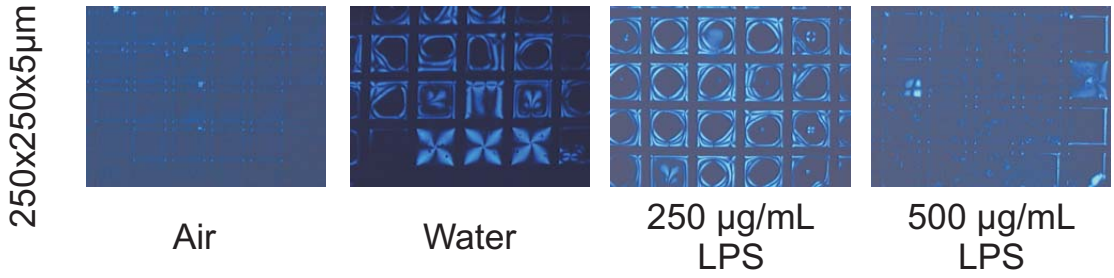

Figure 6.6: Variation in aspect ratio shown for a sensor well filled with 5CB. The 250x250x5μm well displayed some variability in the equilibrium states, but completely transitioned to a homeotropic structure around 500μg/mL.

the overall dimensions of the sensor well while holding the aspect ratio constant effectively re-scales the anchoring strength, yet keeps roughly the same nematic profile. The same nematic profile at different scales requires $W_p d \approx const$, which shows that by scaling down the size, effectively, the anchoring strength increases. This effect was explored experimentally, with results shown in Figure 6.5. A 50x50x5μm well was fabricated, coated with a nematic alignment material, and filled with 5CB. The equilibrium states for air and water remain the same, and a structural transition is observed for increased levels of LPS. Concentrations of 250 and 500μg/mL invoke an immediate transition to the escape structure, while 1μg/mL concentrations still show the defect structure. It is hypothesized that the transition for these wells occurs at a lower level than for the larger wells (closer to 1μg/mL than 250μg/mL), but since the detection concentration remains much too high to be clinically relevant, other methods were explored.

Variations in aspect ratio were also explored experimentally with LPS. Using the initial well side length of 250μm, but decreasing the depth to 5μm essentially increased the aspect ratio from 10:1 to 50:1. It was hypothesized that this change would decrease the impact of the sidewalls while enhancing the contribution from the strong homeotropic anchoring on the floor of the well. Experimental results are given in Figure 6.6. The equilibrium structure observed in air is easily recognized as the escape structure seen previously for homeotropic upper anchoring, but the equilibrium structure for water varies between the cross structure (predicted by theoretical models) and a different structure not previously observed. By decreasing the aspect ratio, it is hypothesized that the planar upper surface anchoring induced by the water is no longer strong enough to overcome the very strong homeotropic

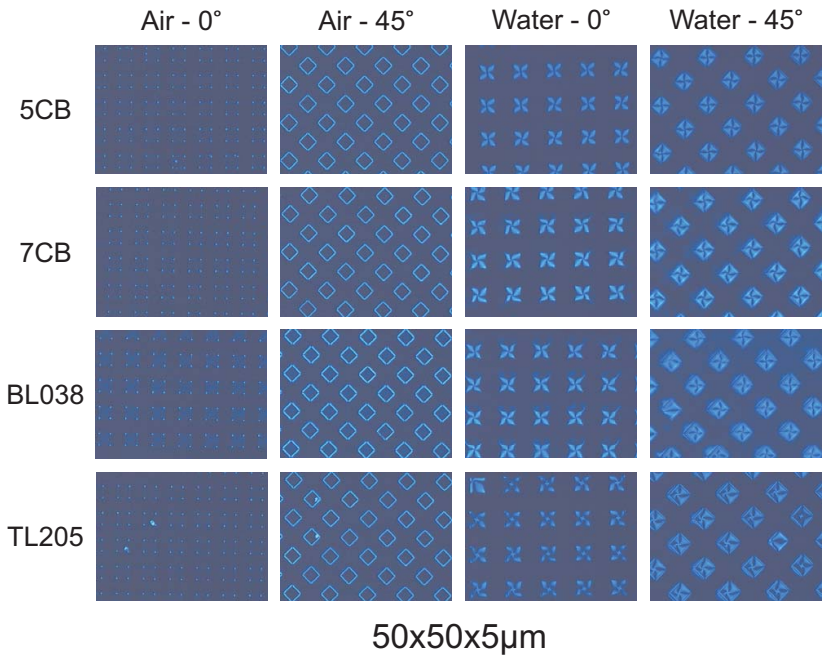

Figure 6.7: Equilibrium states for 50x50x5μm sensor wells filled with four common nematic liquid crystal materials: 5CB, 7CB, BL038, and TL205. Polarizing optical micrographs are shown for the upper surface exposed to air and to water at both 0° and 45° with respect to the polarizer. The equilibrium states show similar structures, although with some variations in the center defect.

anchoring contributions from the lower surface. Because these two surfaces are now in such close proximity, the impact of the lower surface drives the structure to a weak defect structure (optically appearing dark in the center), with some impact of the sidewall anchoring seen in the light areas. The mode of distortion experience by the liquid crystal in these wells is bend as they move from homeotropic lower surface anchoring to planar on the upper surface. Material properties of the liquid crystal, such as its elastic constants, impact this behavior, and so the next variation studied was a change in the liquid crystal material itself.

The commonly used nematic liquid crystal material, 5CB, was chosen for the vast amount of knowledge concerning its properties and behavior. 5CB has been widely studied, as well as used extensively in the Display and Photonics Laboratory. As previously mentioned, the nematic material goes through a bend distortion in the sensor wells in the planar, or defect, structure. In order to harness the structural transition to homeotropic (the escape structure) for use in a biosensor, the wells must display a defect structure in the equilibrium planar state. If the transition to homeotropic has already begun, the sensor loses its attractiveness as an optical detection device, since the optical

signal is not nearly as quantifiable. Given this criteria, the ideal liquid crystal material would have a high elastic constant for bend deformation, yet still exhibit the defect structure in a planar state. Theoretical analysis confirms this and predicts that a higher elastic constant liquid crystal material would increase the sensitivity of the structural transition.

Equilibrium states for multiple nematic liquid crystal materials in air and when exposed to water were investigated. Figure 6.7 shows results for two cyanobiphenyls, 5CB and 7CB, as well as two commercially available nematic mixtures, BL038 and TL205. In order to closely examine the optical appearances of these materials under polarizing microscopy, the sensor wells are shown at both 0° and 45° with respect to the polarizer. Since it has been studied extensively both theoretically and experimentally in this research, 5CB is shown in the top row for comparison. Another cyanobiphenyl which has two more carbons in its aliphatic tail, 7CB, is shown in the second row. 7CB behaves similarly to 5CB, displaying the escape structure in air and the defect structure when exposed to aqueous solution. The commercial mixtures BL038 and TL205 are shown in the bottom two rows, and although the optical image is similar to the equilibrium structures of the cyanobiphenyls, some degradation of the structure is observed. In particular, TL205 optically displays the early stages of a transition to an escape structure. These materials were all tested with LPS solutions to discover their suitability for an optical biosensor.

Figure 6.8 displays the response of the two nematic mixtures upon introduction of LPS solution. Air and water were used as controls, and concentrations that had consistently produced a transition in 5CB filled wells (250 and 500μg/mL) were applied. A smaller microscope objective was used in these cases to observe a larger field of view. The TL205 induced a transition at 500μg/mL, but both materials failed to produce a transition to homeotropic at 250μg/mL. For this reason, the responses of these materials were not studied further.

Properties and characteristics of cyanobiphenyls, a commonly used nematic liquid crystal group, are listed in Table 2.1. Each of these materials has a rigid biphenyl core structure and an aliphatic hydrocarbon tail. The differences in the materials lies in the number of carbons in tail; for instance, 5CB contains five hydrocarbons, 6CB contains six, etc. Increasing the tail length increases the

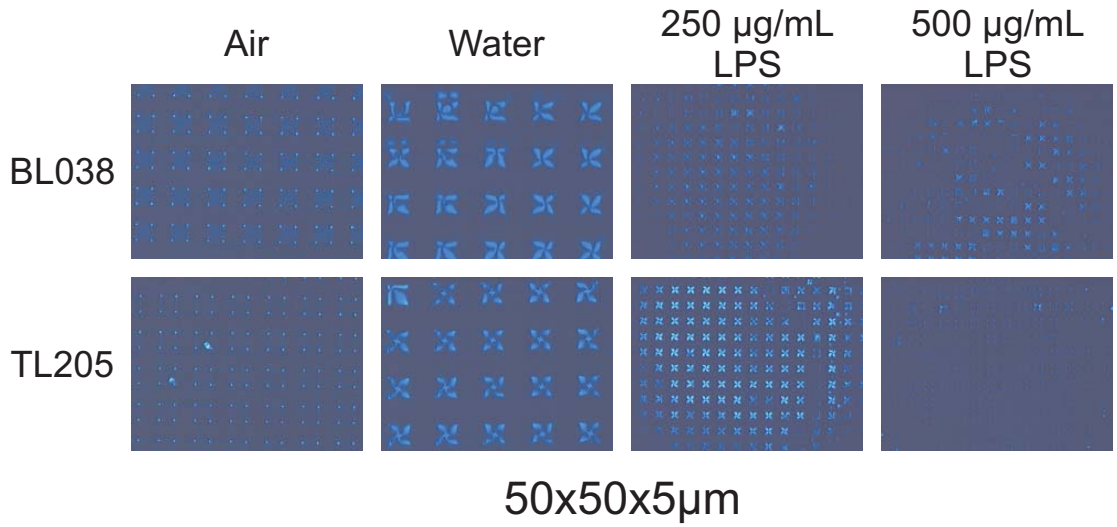

Figure 6.8: Optical response of two commercial nematic mixtures, BL038 and TL205, to the presence of LPS in solution. Although both appear to transition, the concentration at which this occurs is higher than for the cyanobiphenyls.

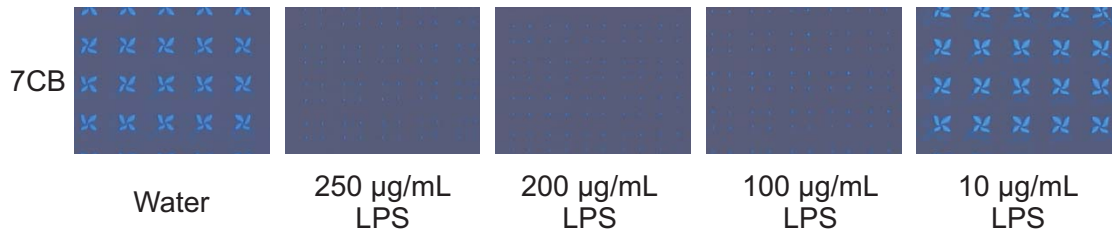

Figure 6.9: The structural transition of 7CB in the presence of LPS. The 50x50x5μm sensor wells transition from a planar structure to homeotropic between 10 and 100μg/mL LPS, which is a lower concentration than observed with any other liquid crystal material and geometry.

elastic constants for the material, including the bend deformation constant, K_{33}. The greater bend constant could make the liquid crystal material in the well more likely to transition to a homeotropic upper surface at a lower surfactant concentration, as discussed earlier, due to the correlation between concentration and surface anchoring strength. Figure 6.9 shows the results of LPS concentrations ranging from 250μg/mL to 10μg/mL applied to a sensor filled with 7CB. Previously, using 5CB, the lowest concentration used that induced a transition was approximately 250μg/mL. Here, a transition is observed somewhere between 100μg/mL and 10μg/mL, providing a promising direction for increased biosensor sensitivity.

This chapter has discussed the background of LPS molecules, as well as detailed experimental results using LPS in aqueous solutions. Given the goal of decreasing the concentration at which a

transition is observed, multiple experimental parameters were varied. Sensor responses were noted, providing valuable input for continued research into this topic.

Chapter 7

Conclusions

7.1 Thesis Summary

The research presented in this thesis covers the development of a biosensor containing confined nematic for the optical detection of a targeted pathogen. Collaborations were formed with Memorial Hospital of Rhode Island as well as the University of Ljubljana for medical expertise and theoretical modeling, respectively. A targeted pathogen associated alarm molecule and general inflammatory mediator (bacterial lipopolysaccharide) was identified based on expertise and potential success with optical detection. Chapter 1 outlines the need for science and engineering technology in the development of medical diagnostics, along with existing technologies and medical diagnostic protocol. Basic liquid crystal properties and phenomena are given in Chapter 2, with a particular attention paid to surface interactions and anchoring at free and fluid surfaces. Chapter 3 gives previous work in the area of liquid crystal biosensors.

7.1.1 Modeling and Simulations

The behavior of confined nematics in square microwells is complex due to the number of forces, such as surface effects, bulk properties and applied fields, acting upon them. In order to better understand and predict their behavior, theoretical simulations and models were developed. Minimizations of the

free energy, combined with experimental boundary conditions, were used to numerically generate a nematic profile of the liquid crystal sensor well. From these profiles, simulated optical micrographs were created in order to compare theoretical results to experimental ones. Chapter 4 describes this process in detail.

From these studies, equilibrium states for the sensor in air and water were developed. The variation of experimental parameters were tested using the models, predicting control of the sensor response. As the anchoring strength on the upper surface is decreased, the contribution of the side and bottom surface anchoring overcomes the bulk elasticity and drives a transition to an escape structure. Changes in the depth, aspect ratio, and sidewall anchoring strength were varied and the response of the sensor characterized. This information was utilized in the optimization of the sensor for detection of endotoxin.

7.1.2 Experimental Results

A sensor containing microwells was fabricated using standard photolithographic processes and was filled with aligned nematic liquid crystal material. The equilibrium states of the sensor when exposed to air and water (homeotropic and planar upper anchoring, respectively) were observed and compared with theoretical results. A model surfactant, sodium dodecyl sulfate or SDS, was used to characterize the sensor response to an applied homeotropic surfactant. At a critical concentration, a transition from the planar anchoring to the homeotropic regime was observed; Chapter 5 reviews these results. This transition is easy to detect optically, as well as consistent, creating potential for a liquid crystal biosensor.

Sepsis, a major clinical syndrome, is the 10^{th} leading cause of death in the United States. Infectious disease specialists at Memorial Hospital of Rhode Island and the Center for Biodefense and Emerging Pathogens have done extensive work on the role of LPS, or endotoxin, in sepsis. LPS in aqueous solution was introduced to the sensor in clinically relevant concentrations to determine if its presence would induce a structural transition in the liquid crystal similar to that of SDS. A transition was observed at approximately 250μg/mL, with the sensor transitioning immediately upon contact

with the LPS solution.

In order to reduce the concentration of LPS required to trigger a transition (effectively decreasing the upper anchoring strength), various experimental parameters were modified. The aspect ratio, depth and liquid crystal material used in the sensor were all varied, with the end result being a transition concentration of 10μg/mL, as described in Chapter 6.

7.2 Concluding Remarks

The motivation and goal of this work was the design of a device which utilized current liquid crystal technology to improve public health. Instead of performing basic science and searching for an application, an application was identified at the beginning of the work and guided the direction of the research. This top down approach to translational research promises great scientific and technical contributions to medicine in a wide variety of fields, including imaging techniques, diagnostic devices and implant technology. In addition to biomedical applications, this work has contributed to the study of liquid crystals in contact with aqueous solutions, and the orientational response of a confined nematic in contact with surfactants.

Although control of the sensitivity of the biosensor was demonstrated, there is still great potential for further investigation into this field. Although it is hypothesized that detecting concentrations of endotoxin on the order of 10ng/mL will be difficult with this technology, this platform can still be leveraged for use in a detection device. As a method for optical detection of endotoxin, it holds many advantages over competing technologies. The transition upon contact with LPS is immediate; it requires no wait time for results. The work presented here outlines a fabrication method that is both inexpensive and well suited to mass production. The sensor platform is robust, with the liquid crystal sensors maintaining their integrity over a wide range of conditions and temperatures. No complex equipment is required in the operation of the sensor, and a device can be easily envisioned which requires merely an LED, two polarizers and an optical detector to catch transmitted light. The system is also label-free, removing stringent requirements of complex binding processes.

This technology can be integrated onto a microfluidic platform to isolate endotoxin and move

it to the confined liquid crystal wells for detection. Since etching is already part of the fabrication processes of many microfluidic chips, the creation of an array of microwells should not add too much additional cost or time to the process. An affinity coated bead capture system could isolate the LPS from media, with microfluidic channels delivering the targeted material to the optical detection system. It is the sincere desire of the author that this work be continued, and its contribution to the improvement of public health realized.

Bibliography

[1] G.L. Mandell, J.E. Bennett, and R. Dolin, editors. *Principles and Practices of Infectious Diseases*, volume 1. Elsevier Inc., 6th edition, 2005.

[2] H. Bloch. The inventor of the stethoscope - Rene Laennec. *Journal Of Family Practice*, 37(2):191–191, 1993.

[3] W. Einthoven. The string galvanometer and the human electrocardiogram (reprinted from proceedings of the koninklijke nederlandse akademie van wetenschappen, vol 6, pg 107-115, 1904). *Proceedings Of The Koninklijke Nederlandse Akademie Van Wetenschappen*, 100(3-4):91–99, 1997.

[4] Biography of Hans Berger. Online, 2006.

[5] U.S. Department of Health and Human Services, Centers for Disease Control and Prevention. National hospital ambulatory medical care survey, 2003.

[6] World Heath Organization. Revised Global Burden of Disease 2002 Estimates, 2004.

[7] N. B. King. The influence of anxiety: September 11, bioterrorism, and American public health. *Journal Of The History Of Medicine And Allied Sciences*, 58(4):433–441, 2003.

[8] N. Khardori. Bioterrorism and bioterrorism preparedness: Historical perspective and overview. *Infectious Disease Clinics Of North America*, 20(2):179–211, 2006.

[9] P. N. Prasad. Emerging opportunities at the interface of photonics, nanotechnology and biotechnology. *Molecular Crystals And Liquid Crystals*, 446:1–10, 2006.

[10] J. Chin-Dusting, J. Mizrahi, G. Jennings, and D. Fitzgerald. Finding improved medicines: the role of academic-industrial collaboration. *Nature Reviews Drug Discovery*, 4(11):891–897, 2005.

[11] K. C. Norris. Translational research: Moving scientific advances into the real-world setting. *Ethnicity and Disease*, 15(3):363–364, 2005.

[12] Joe Naiman. Where physics and biology meet. *Materials Today*, 8(12):52, 2005.

[13] T. B. Crist, A. I. Schafer, and R. A. Walsh. Translating basic discoveries into better health care: The APM's recommendations for improving translational research. *American Journal Of Medicine*, 116(6):431–434, 2004.

[14] D. W. Slaaf and A. A. H. J. Sauren. Integration of the sciences and engineering with biomedical disciplines. The 5-year biomedical engineering program at Eindhoven University of Technology in collaboration with Maastricht University, the Netherlands.

[15] H. Mori. Novel optical compensators of negative birefringence for wide-viewing-angle twisted-nematic liquid-crystal displays. *Japanese Journal Of Applied Physics Part 1-Regular Papers Short Notes and Review Papers*, 36(3A):1068–1072, 1997.

[16] P. Van de Witte, S. Stallinga, and Jamm van Haaren. Viewing angle compensators for liquid crystal displays based on layers with a positive birefringence. *Japanese Journal Of Applied Physics Part 1-Regular Papers Short Notes and Review Papers*, 39(1):101–108, 2000.

[17] H. Mada and T. Sonoda. A proposal on and verification of surface alignment of liquid-crystals aligned by frictional rubbing. *Japanese Journal Of Applied Physics Part 2-Letters*, 32(9A):L1245–L1247, 1993.

[18] A. Mosley, B. M. Nicholas, and P. A. Gass. Surface alignment of liquid-crystals by rubbed polymer layers. *Displays*, 8(1):17–21, 1987.

[19] K. W. Chien and H. P. D. Shieh. Time-multiplexed three-dimensional displays based on directional backlights with fast-switching liquid-crystal displays. *Applied Optics*, 45(13):3106–3110, 2006.

[20] M. X. Gu, II Smalyukh, and O. D. Lavrentovich. Directed vertical alignment liquid crystal display with fast switching. *Applied Physics Letters*, 88(6), 2006. 061110.

[21] M. Schaechter, N.C. Engleberg, B.I. Eisenstein, and G. Medoff, editors. *Mechanisms of Microbial Disease*. Lippincott Williams and Wilkins, third edition, 1999.

[22] E. Yacoub-George, L. Meixner, W. Scheithauer, A. Koppi, S. Drost, H. Wolf, C. Danapel, and K. A. Feller. Chemiluminescence multichannel immunosensor for biodetection. *Analytica Chimica Acta*, 457(1):3–12, 2002.

[23] M. Ogilvie. Molecular techniques should not now replace cell culture in diagnostic virology laboratories. *Reviews In Medical Virology*, 11(6):351–354, 2001.

[24] B. Carman. Molecular techniques should now replace cell culture in diagnostic virology laboratories. *Reviews In Medical Virology*, 11(6):347–349, 2001.

[25] D. M. Dragsted, B. Dohn, J. Madsen, and J. S. Jensen. Comparison of culture and pcr for detection of bordetella pertussis and bordetella parapertussis under routine laboratory conditions. *Journal Of Medical Microbiology*, 53(8):749–754, 2004.

[26] P. A. G. Tilley, M. V. Kanchana, I. Knight, J. Blondeau, N. Antonishyn, and H. Deneer. Detection of bordetella pertussis in a clinical laboratory by culture, polymerase chain reaction, and direct fluorescent antibody staining; accuracy, and cost. *Diagnostic Microbiology And Infectious Disease*, 37(1):17–23, 2000.

[27] S. Yang and R. E. Rothman. PCR-based diagnostics for infectious diseases: uses, limitations, and future applications in acute-car setttings. *The Lancet*, 4:337–348, 2004.

[28] M. A. Pfaller. Molecular approaches to diagnosing and managing infectious diseases: Practicality and costs. *Emerging Infectious Diseases*, 7(2):312–318, 2001.

[29] J. Wang. From dna biosensors to gene chips. *Nucleic Acids Research*, 28(16):3011–3016, 2000.

[30] C. E. Corless, M. Guiver, R. Borrow, V. Edwards-Jones, A. J. Fox, and E. B. Kaczmarski. Simultaneous detection of neisseria meningitidis, haemophilus influenzae, and streptococcus pneumoniae in suspected cases of meningitis and septicemia using real-time pcr. *Journal of Clinical Microbiology*, 39(4):1553–1558, 2001.

[31] Y. S. Boriskin, P. S. Rice, R. A. Stabler, J. Hinds, H. Al-Ghusein, K. Vass, and P. D. Butcher. DNA microarrays for virus detection in cases of central nervous system infection. *Journal of Clinical Microbiology*, 42(12):5811–5818, 2004.

[32] M. J. Espy, J. R. Uhl, L. M. Sloan, J. E. Rosenblatt, F. R. Cockerill, and T. F. Smith. Detection of vaccinia virus, herpes simplex virus, varicella-zoster virus, and bacillus anthracis DNA by lightcycler polymerase chain reaction after autoclaving: Implications for biosafety of bioterrorism agents. *Mayo Clinic Proceedings*, 77(7):624–628, 2002.

[33] J. R. Uhl, C. A. Bell, L. M. Sloan, M. J. Espy, T. F. Smith, J. E. Rosenblatt, and F. R. Cockerill. Application of rapid-cycle real-time polymerase chain reaction for the detection of microbial pathogens: The mayo-roche rapid anthrax test. *Mayo Clinic Proceedings*, 77(7):673–680, 2002.

[34] C. E. Corless, M. Guiver, R. Borrow, V. Edwards-Jones, A. J. Fox, E. B. Kaczmarski, and K. J. Mutton. Development and evaluation of a 'real-time' RT-PRC for the detection of enterovirus and parechovirus RNA in CSF and throat swab samples. *Journal of Medical Virology*, 67:555–562, 2002.

[35] A. K. Deisingh and M. Thompson. Sequences of E-coli o157: H7 detected by a PCR-acoustic wave sensor combination. *Analyst*, 126(12):2153–2158, 2001.

[36] M. Tsuruoka, S. Murano, M. Okada, I. Ohiso, and T. Fujii. The extremely rapid oligonucleotide hybridization and high throughput detection of microbial gene sequences using fluorescence polarization. *Biosensors and Bioelectronics*, 16(9-12):695–699, 2001.

[37] J. G. Lee, K. H. Cheong, N. Huh, S. Kim, J. W. Choi, and C. Ko. Microchip-based one step dna extraction and real-time pcr in one chamber for rapid pathogen identification. *Lab On A Chip*, 6(7):886–895, 2006.

[38] P. Yager, T. Edwards, E. Fu, K. Helton, K. Nelson, M. R. Tam, and B. H. Weigl. Microfluidic diagnostic technologies for global public health. *Nature*, 442(7101):412–418, 2006.

[39] C. Q. Yi, C. W. Li, S. L. Ji, and M. S. Yang. Microfluidics technology for manipulation and analysis of biological cells. *Analytica Chimica Acta*, 560(1-2):1–23, 2006.

[40] K. K. Jain. Nanotechnology in clinical laboratory diagnostics. *Clinica Chimica Acta*, 358(1-2):37–54, 2005.

[41] T. H. Schulte, R. L. Bardell, and B. H. Weigl. Microfluidic technologies in clinical diagnostics. *Clinica Chimica Acta*, 321(1-2):1–10, 2002.

[42] K. B. Mogensen, H. Klank, and J. P. Kutter. Recent developments in detection for microfluidic systems. *Electrophoresis*, 25(21-22):3498–3512, 2004.

[43] F. Su, K. Chakrabarty, and R. B. Fair. Microfluidics-based biochips: Technology issues, implementation platforms, and design-automation challenges. *IEEE Transactions On Computer-Aided Design Of Integrated Circuits And Systems*, 25(2):211–223, 2006.

[44] J. Wang, M. Pumera, M. P. Chatrathi, A. Escarpa, R. Konrad, A. Griebel, W. Dorner, and H. Lowe. Towards disposable lab-on-a-chip: Poly(methylmethacrylate) microchip electrophoresis device with electrochemical detection. *Electrophoresis*, 23(4):596–601, 2002.

[45] R. Gomez-Sjoberg, D. T. Morisette, and R. Bashir. Impedance microbiology-on-a-chip: Microfluidic bioprocessor for rapid detection of bacterial metabolism. *Journal Of Microelectromechanical Systems*, 14(4):829–838, 2005.

[46] G. Medoro, N. Manaresi, A. Leonardi, L. Altomare, M. Tartagni, and R. Guerrieri. A lab-on-a-chip for cell detection and manipulation. *IEEE Sensors Journal*, 3(3):317–325, 2003.

[47] L. Cui, T. Zhang, and H. Morgan. Optical particle detection integrated in a dielectrophoretic lab-on-a-chip. *Journal Of Micromechanics And Microengineering*, 12(1):7–12, 2002.

[48] V. Srinivasan, V. K. Pamula, and R. B. Fair. An integrated digital microfluidic lab-on-a-chip for clinical diagnostics on human physiological fluids. *Lab On A Chip*, 4(4):310–315, 2004.

[49] B. Sepulveda, J. S. del Rio, M. Moreno, F. J. Blanco, K. Mayora, C. Dominguez, and L. M. Lechuga. Optical biosensor microsystems based on the integration of highly sensitive mach-zehnder interferometer devices. *Journal Of Optics A-Pure And Applied Optics*, 8(7):S561–S566, 2006.

[50] W. R. Rodriguez, N. Christodoulides, P. N. Floriano, S. Graham, S. Mohanty, M. Dixon, M. Hsiang, T. Peter, S. Zavahir, I. Thior, D. Romanovicz, B. Bernard, A. P. Goodey, B. D. Walker, and J. T. McDevitt. A microchip CD4 counting method for HIV monitoring in resource-poor settings. *Plos Medicine*, 2(7):663–672, 2005. e182.

[51] W. Vercoutere and M. Akeson. Biosensors for DNA sequence detection. *Current Opinion In Chemical Biology*, 6(6):816–822, 2002.

[52] V. Srinivasan, V. K. Pamula, and R. B. Fair. Droplet-based microfluidic lab-on-a-chip for glucose detection. *Analytica Chimica Acta*, 507(1):145–150, 2004.

[53] A. Rasooly. Moving biosensors to point-of-care cancer diagnostics. *Biosensors and Bioelectronics*, 21(10):1847–1850, 2006.

[54] Z. Du, N. Colls, K. H. Cheng, M. W. Vaughn, and L. Gollahon. Microfluidic-based diagnostics for cervical cancer cells. *Biosensors and Bioelectronics*, 21(10):1991–1995, 2006.

[55] S. H. Lee, D. D. Stubbs, J. Cairney, and W. D. Hunt. Rapid detection of bacterial spores using a quartz crystal microbalance (qcm) immunoassay. *Ieee Sensors Journal*, 5(4):737–743, 2005.

[56] X. D. Su, F. T. Chew, and S. F. Y. Li. Design and application of piezoelectric quartz crystal-based immunoassay. *Analytical Sciences*, 16(2):107–114, 2000.

[57] S. Tombelli, M. Minunni, A. Santucci, M. M. Spiriti, and M. Mascini. A DNA-based piezoelectric biosensor: Strategies for coupling nucleic acids to piezoelectric devices. *Talanta*, 68(3):806–812, 2006.

[58] X. L. Mao, L. J. Yang, X. L. Su, and Y. B. Li. A nanoparticle amplification based quartz crystal microbalance DNA sensor for detection of Escherichia coli O157: H7. *Biosensors and Bioelectronics*, 21(7):1178–1185, 2006.

[59] M. A. Cooper, F. N. Dultsev, T. Minson, V. P. Ostanin, C. Abell, and D. Klenerman. Direct and sensitive detection of a human virus by rupture event scanning. *Nature Biotechnology*, 19(9):833–837, 2001.

[60] M. Zourob, S. Mohr, B. J. T. Brown, P. R. Fielden, M. B. McDonnell, and N. J. Goddard. An integrated metal clad leaky waveguide sensor for detection of bacteria. *Analytical Chemistry*, 77(1):232–242, 2005.

[61] B. T. Cunningham, P. Li, S. Schulz, B. Lin, C. Baird, J. Gerstenmaier, C. Genick, F. Wang, E. Fine, and L. Laing. Label-free assays on the bind system. *Journal Of Biomolecular Screening*, 9(6):481–490, 2004.

[62] B. Cunningham, P. Li, B. Lin, and J. Pepper. Colorimetric resonant reflection as a direct biochemical assay technique. *Sensors And Actuators B-Chemical*, 81(2-3):316–328, 2002.

[63] B. Lin, P. Li, and B. T. Cunningham. A label-free biosensor-based cell attachment assay for characterization of cell surface molecules. *Sensors And Actuators B-Chemical*, 114(2):559–564, 2006.

[64] B. Cunningham, B. Lin, J. Qiu, P. Li, J. Pepper, and B. Hugh. A plastic colorimetric resonant optical biosensor for multiparallel detection of label-free biochemical interactions. *Sensors And Actuators B-Chemical*, 85(3):219–226, 2002.

[65] A. J. Haes and R. P. Van Duyne. A nanoscale optical blosensor: Sensitivity and selectivity of an approach based on the localized surface plasmon resonance spectroscopy of triangular silver nanoparticles. *Journal Of The American Chemical Society*, 124(35):10596–10604, 2002.

[66] R. Ince and R. Narayanaswamy. Analysis of the performance of interferometry, surface plasmon resonance and luminescence as biosensors and chemosensors. *Analytica Chimica Acta*, 569(1-2):1–20, 2006.

[67] C. R. Taitt, G. P. Anderson, and F. S. Ligler. Evanescent wave fluorescence biosensors. *Biosensors and Bioelectronics*, 20(12):2470–2487, 2005.

[68] O. S. Wolfbeis. Fiber-optic chemical sensors and biosensors. *Analytical Chemistry*, 78(12):3859–3873, 2006.

[69] M. J. Bradshaw, E. P. Raynes, J. D. Bunning, and T. E. Faber. The Frank constants of some nematic liquid crystals. *Journal De Physique*, 46(9):1513–1520, 1985.

[70] J. E. Proust, T. Ter-Minassian-Saraga, and E. Guyon. Orientation of a nematic liquid crystal by suitable boundary surfaces. *Solid State Communications*, 11:1227–1230, 1972.

[71] B. Jerome. Surface effects and anchoring in liquid-crystals. *Reports on Progress in Physics*, 54(3):391–451, 1991.

[72] Najm Vanaerle and A. J. W. Tol. Molecular-orientation in rubbed polyimide alignment layers used for liquid-crystal displays. *Macromolecules*, 27(22):6520–6526, 1994.

[73] K. Ichimura, Y. Suzuki, T. Seki, A. Hosoki, and K. Aoki. Reversible change in alignment mode of nematic liquid-crystals regulated photochemically by command surfaces modified with an azobenzene monolayer. *Langmuir*, 4(5):1214–1216, 1988.

[74] G. P. Crawford, R. J. Ondris-Crawford, S. Zumer, S. Keast, M. Neubert, and J. W. Doane. Alignment and ordering mechanisms at a liquid-crystal solid interface. *Liquid Crystals*, 14(5):1573–1585, 1993.

[75] M. Okulska-Bozek, J. Borycki, T. Prot, and J. Kedzierski. Studies on the alignment of nematic liquid crystals by polyimide layers. *Polimery*, 43(7-8):459–464, 1998.

[76] B. H. Clare, O. Guzman, J. J. de Pablo, and N. L. Abbott. Measurement of the azimuthal anchoring energy of liquid crystals in contact with oligo(ethylene glycol)-terminated self-assembled monolayers supported on obliquely deposited gold films. *Langmuir*, 22(10):4654–4659, 2006.

[77] B. H. Clare, O. Guzman, J. de Pablo, and N. L. Abbott. Anchoring energies of liquid crystals measured on surfaces presenting oligopeptides. *Langmuir*, 22(18):7776–7782, 2006.

[78] J. N. Eakin, Y. Xie, R. A. Pelcovits, M. D. Radcliffe, and G. P. Crawford. Zero voltage freedericksz transition in periodically aligned liquid crystals. *Applied Physics Letters*, 85(10):1671–1673, 2004.

[79] S. P. Gorkhali, S. G. Cloutier, and G. P. Crawford. Two-dimensional vectorial photonic crystals formed in azo-dye-doped liquid crystals. *Optics Letters*, 31(22):3336–3338, 2006.

[80] M. Slavinec, G. D. Crawford, S. Kralj, and S. Zumer. Determination of the nematic alignment and anchoring strength at the curved nematic-air interface. *Journal Of Applied Physics*, 81(5):2153–2156, 1997. 0021-8979.

[81] P. Chiarelli, S. Faetti, and L. Fronzoni. Experimental-measurement of the director orientation at the free-surface of a nematic liquid-crystal. *Lettere Al Nuovo Cimento*, 36(3):60–64, 1983.

[82] S. Krishnaswamy and R. Shashidhar. Experimental studies of the surface tension of nematic liquid crystals. *Molecular Crystals and Liquid Crystals*, 35(3-4):253–259, 1976.

[83] M. G. J. Gannon and T. E. Faber. Surface-tension of nematic liquid-crystals. *Philosophical Magazine A-Physics Of Condensed Matter Structure Defects And Mechanical Properties*, 37(1):117–135, 1978.

[84] H. Kasten and G. Strobl. Nematic wetting at the free-surface of 4-cyano-4'-n-alkyl-biphenyls. *Journal of Chemical Physics*, 103(15):6768–6774, 1995.

[85] E. M. Delrio, M. M. T. Dagama, E. Demiguel, and L. F. Rull. Surface-induced alignment at model nematic interfaces. *Physical Review E*, 52(5):5028–5039, 1995. Times Cited: 32 A.

[86] C. Biensan, B. Desbat, and J. M. Turlet. Molecular orientation of a cyanobiphenyl liquid crystal in freely suspended films and at the air-water interface. *Thin Solid Films*, 284:293–296, 1996.

[87] T. Martynski. Liquid crystalline binary mixtures at the air-water interface. *Colloids And Surfaces A-Physicochemical And Engineering Aspects*, 198:179–185, 2002. Sp. Iss. SI.

[88] J. C. Loudet, P. Barois, P. Auroy, P. Keller, H. Richard, and P. Poulin. Colloidal structures from bulk demixing in liquid crystals. *Langmuir*, 20(26):11336–11347, 2004.

[89] E. B. Kim, O. Guzman, S. Grollau, N. L. Abbott, and J. J. de Pablo. Interactions between spherical colloids mediated by a liquid crystal: A molecular simulation and mesoscale study. *Journal Of Chemical Physics*, 121(4):1949–1961, 2004.

[90] J. M. Brake, M. K. Daschner, Y. Y. Luk, and N. L. Abbott. Biomolecular interactions at phospholipid-decorated surfaces of liquid crystals. *Science*, 302:2094–2097, 2003.

[91] J. M. Brake, A. D. Mezera, and N. L. Abbott. Active control of the anchoring of 4 '-pentyl-4-cyanobiphenyl (5CB) at an aqueous-liquid crystal interface by using a redox-active ferrocenyl surfactant. *Langmuir*, 19(21):8629–8637, 2003.

[92] N. A. Lockwood and N. L. Abbott. Self-assembly of surfactants and phospholipids at interfaces between aqueous phases and thermotropic liquid crystals. *Current Opinion In Colloid and Interface Science*, 10(3-4):111–120, 2005.

[93] D. A. Higgins, J. E. Hall, and A. Xie. Optical microscopy studies of dynamics within individual polymer-dispersed liquid crystal droplets. *Accounts of Chemical Research*, 38:137–145, 2005.

[94] R. D. Polak, G. P. Crawford, B. C. Kostival, J. W. Doane, and S. Zumer. Optical determination of the saddle-splay elastic-constant K(24) in nematic liquid-crystals. *Physical Review E*, 49(2):R978–R981, 1994.

[95] C. Tsakonas, A. J. Davidson, C. V. Brown, and N. J. Mottram. Multistable alignment states in nematic liquid crystal filled wells. *Applied Physics Letters*, 90, 2007.

[96] D. K. Hwang and A. D. Rey. Optical modeling of liquid crystal biosensors. *The Journal of Chemical Physics*, 125, 2006.

[97] G. P. Crawford, R. Ondriscrawford, S. Zumer, and J. W. Doane. Anchoring and orientational wetting transitions of confined liquid-crystals. *Physical Review Letters*, 70(12):1838–1841, 1993.

[98] P. A. Kossyrev and G. P. Crawford. The birefringent texture of nematic liquid crystals confined to capillary tubes with square cross-section. *Molecular Crystals And Liquid Crystals*, 351:379–385, 2000.

[99] S. V. Shiyanovskii, O. D. Lavrentovich, T. Schneider, T. Ishikawa, II Smalyukh, C. J. Woolverton, G. D. Niehaus, and K. J. Doane. Lyotropic chromonic liquid crystals for biological sensing applications. *Molecular Crystals And Liquid Crystals*, 434:587–598, 2005.

[100] J. M. Brake, M. K. Daschner, and N. L. Abbott. Formation and characterization of phospholipid monolayers spontaneously assembled at interfaces between aqueous phases and thermotropic liquid crystals. *Langmuir*, 21(6):2218–2228, 2005.

[101] E. B. Kim, N. Lockwood, M. Chopra, O. Guzman, N. L. Abbott, and J. J. de Pablo. Interactions of liquid crystal-forming molecules with phospholipid bilayers studied by molecular dynamics simulations. *Biophysical Journal*, 89(5):3141–3158, 2005.

[102] N. A. Lockwood, J. J. de Pablo, and N. L. Abbott. Influence of surfactant tail branching and organization on the orientation of liquid crystals at aqueous-liquid crystal interfaces. *Langmuir*, 21(15):6805–6814, 2005.

[103] N. A. Lockwood, K. D. Cadwell, F. Caruso, and N. L. Abbott. Formation of polyelectrolyte multilayer films at interfaces between thermotropic liquid crystals and aqueous phases. *Advanced Materials*, 18(7):850–854, 2006.

[104] Y. Y. Luk, S. F. Campbell, N. L. Abbott, and C. J. Murphy. Non-toxic thermotropic liquid crystals for use with mammalian cells. *Liquid Crystals*, 31(5):611–621, 2004.

[105] C. J. Woolverton, E. Gustely, L. Li, and O. D. Lavrentovich. Liquid crystal effects on bacterial viability. *Liquid Crystals*, 32(4):417–423, 2005.

[106] O. Guzman, N. L. Abbott, and J. J. de Pablo. Quenched disorder in a liquid-crystal biosensor: Adsorbed nanoparticles at confining walls. *Journal Of Chemical Physics*, 122(18), 2005. 184711.

[107] N. A. Lockwood, J. C. Mohr, L. Ji, C. J. Murphy, S. R. Palecek, J. J. de Pablo, and N. L. Abbott. Thermotropic liquid crystals as substrates for imaging the reorganization of matrigel by human embryonic stem cells. *Advanced Functional Materials*, 16(5):618–624, 2006.

[108] J. Hoogboom, J. Clerx, M. B. J. Otten, A. E. Rowan, T. Rasing, and R. J. M. Nolte. Novel alignment technique for LCD-biosensors. *Chemical Communications*, 23:2856–2857, 2003.

[109] S. R. Kim, R. R. Shah, and N. L. Abbott. Orientations of liquid crystals on mechanically rubbed films of bovine serum albumin: A possible substrate for biomolecular assays based on liquid crystals. *Analytical Chemistry*, 72(19):4646–4653, 2000.

[110] J. S. Lundgren, A. N. Watkins, D. Racz, and F. S. Ligler. A liquid crystal pixel array for signal discrimination in array biosensors. *Biosensors and Bioelectronics*, 15(7-8):417–421, 2000.

[111] T. Araki and H. Tanaka. Surface-sensitive particle selection by driving particles in a nematic solvent. *Journal Of Physics-Condensed Matter*, 18(15):L193–L203, 2006.

[112] J. Y. Fang, W. Ma, J. V. Selinger, and R. Shashidhar. Imaging biological cells using liquid crystals. *Langmuir*, 19(7):2865–2869, 2003.

[113] Y. Y. Luk, M. L. Tingey, K. A. Dickson, R. T. Raines, and N. L. Abbott. Imaging the binding ability of proteins immobilized on surfaces with different orientations by using liquid crystals. *Journal Of The American Chemical Society*, 126(29):9024–9032, 2004.

[114] B. H. Clare and N. L. Abbott. Orientations of nematic liquid crystals on surfaces presenting controlled densities of peptides: Amplification of protein-peptide binding events. *Langmuir*, 21(14):6451–6461, 2005.

[115] Y. Y. Luk, C. H. Jang, L. L. Cheng, B. A. Israel, and N. L. Abbott. Influence of lyotropic liquid crystals on the ability of antibodies to bind to surface-immobilized antigens. *Chemistry Of Materials*, 17(19):4774–4782, 2005.

[116] J. Hoogboom, K. Velonia, T. Rasing, A. E. Rowan, and R. J. M. Nolte. Lcd-based detection of enzymatic action. *Chemical Communications*, 4:434–435, 2006.

[117] M. L. Tingey, S. Wilyana, E. J. Snodgrass, and N. L. Abbott. Imaging of affinity microcontact printed proteins by using liquid crystals. *Langmuir*, 20(16):6818–6826, 2004.

[118] C. H. Jang, M. L. Tingey, N. L. Korpi, G. J. Wiepz, J. H. Schiller, P. J. Bertics, and N. L. Abbott. Using liquid crystals to report membrane proteins captured by affinity microcontact printing from cell lysates and membrane extracts. *Journal Of The American Chemical Society*, 127(25):8912–8913, 2005.

[119] Y. Choi, Y. Lee, H. Kwon, and S. Lee. Optical detection of the ligand-receptor binding by anchoring transitions of liquid crystals. *Materials Science and Engineering*, (24):237–240, 2004.

[120] S. L. Helfinstine, O. D. Lavrentovich, and C. J. Woolverton. Lyotropic liquid crystal as a real-time detector of microbial immune complexes. *Letters In Applied Microbiology*, 43(1):27–32, 2006.

[121] L. A. Tercero Espinoza, K. R. Schumann, Y. Y. Luk, B. A. Israel, and N. L. Abbott. Orientational behavior of thermotropic liquid crystals on surfaces presenting electrostatically bound vesicular stomatitis virus. *Langmuir*, 20(6):2375–2385, 2004.

[122] C. H. Jang, L. L. Cheng, C. W. Olsen, and N. L. Abbott. Anchoring of nematic liquid crystals on viruses with different envelope structures. *Nano Letters*, 6(5):1053–1058, 2006.

[123] B.R. Acharya, K.M. Anhalt, N.L. Abbott, and B.A. Israel. Detection of viruses using liquid crystals. *Molecular Crystals and Liquid Crystals*, 2006. (submitted for publication).

[124] A.W. Artenstein. Bioterrorism and biodefense. In J. Cohen and W.G. Powderly, editors, *Infectious Diseases*, pages 99–107. Mosby, London, 2nd edition, 2003.

[125] P. G. de Gennes and J. Prost. *The Physics of Liquid Crystals*. Oxford Science, Oxoford, 2nd edition, 1993.

[126] C. Blanc, D. Svensek, S. Zumer, and M. Nobili. Dynamics of nematic liquid crystal disclinations: The role of the backflow. *Phys Rev Lett*, 95(9):097802, 2005.

[127] J. B. Fournier and P. Galatola. Modeling planar degenerate wetting and anchoring in nematic liquid crystals. *Europhysics Letters*, 72(3):403–409, 2005.

[128] A. N. Beris and B. J. Edwards. *Thermodynamics of Flowing Systems*. Oxford University Press, New York, 1994.

[129] W. H. Press, B. P. Flannery, S. A. Teukolsky, and W. T. Vetterling. *Numerical Recipes*. Cambridge University Press, Cambridge, 1986.

[130] R. Ondriscrawford, E. P. Boyko, B. G. Wagner, J. H. Erdmann, S. Zumer, and J. W. Doane. Microscope textures of nematic droplets in polymer dispersed liquid-crystals. *Journal Of Applied Physics*, 69(9):6380–6386, 1991.

[131] E. T. Rietschel, T. Kirikae, F. U. Schade, U. Mamat, G. Schmidt, H. Loppnow, A. J. Ulmer, U. Zahringer, U. Seydel, F. Dipadova, M. Schreier, and H. Brade. Bacterial, endotoxin - molecular relationships of structure to activity and function. *Faseb Journal*, 8(2):217–225, 1994.

[132] L. Thomas. *The Lives of a Cell. Notes of a Biology Watcher*. The Viking Press, New York, 1974.

[133] C. Galanos, O. Luderitz, E. T. Rietschel, O. Westphal, H. Brade, L. Brade, M. Freudenberg, U. Schade, M. Imoto, H. Yoshimura, S. Kusumoto, and T. Shiba. Synthetic and natural

Escherichia-coli free lipid-A express identical endotoxic activities. *European Journal of Biochemistry*, 148(1):1–5, 1985.

[134] P. O. Magalhaes, A. M. Lopes, P. G. Mazzola, C. Rangel-Yagui, T. C. V. Penna, and A. Pessoa. Methods of endotoxin removal from biological preparations: A review. *Journal of Pharmacy and Pharmaceutical Sciences*, 10(3):388–404, 2007.

[135] N. Ohno and D. C. Morrison. Lipopolysaccharide interaction with lysozyme - binding of lipopolysaccharide to lysozyme and inhibition of lysozyme enzymatic-activity. *Journal of Biological Chemistry*, 264(8):4434–4441, 1989.

[136] L. L. Yu, M. Y. Tan, B. Ho, J. L. Ding, and T. Wohland. Determination of critical micelle concentrations and aggregation numbers by fluorescence correlation spectroscopy: Aggregation of a lipopolysaccharide. *Analytica Chimica Acta*, 556(1):216–225, 2006.

[137] D. Heumann and T. Roger. Initial responses to endotoxins and gram-negative bacteria. *Clinica Chimica Acta*, 323(1-2):PII S0009–8981(02)00180–8, 2002.

[138] R. C. Bone, R. A. Balk, F. B. Cerra, R. P. Dellinger, A. M. Fein, W. A. Knaus, R. M. H. Schein, W. J. Sibbald, J. H. Abrams, G. R. Bernard, J. W. Biondi, J. E. Calvin, R. Demling, P. J. Fahey, C. J. Fisher, C. Franklin, K. J. Gorelick, M. A. Kelley, D. G. Maki, J. C. Marshall, W. W. Merrill, J. P. Pribble, E. C. Rackow, T. C. Rodell, J. N. Sheagren, M. Silver, C. L. Sprung, R. C. Straube, M. J. Tobin, G. M. Trenholme, D. P. Wagner, C. D. Webb, J. C. Wherry, H. P. Wiedemann, and C. H. Wortel. American-college of chest physicians society of critical care medicine consensus conference - definitions for sepsis and organ failure and guidelines for the use of innovative therapies in sepsis. *Critical Care Medicine*, 20(6):864–874, 1992.

[139] G. S. Martin, D. M. Mannino, S. Eaton, and M. Moss. The epidemiology of sepsis in the United States from 1979 through 2000. *New England Journal Of Medicine*, 348(16):1546–1554, 2003.

[140] D. B. Chalfin, M. E. B. Holbein, A. M. Fein, and G. C. Carlon. Cost-effectiveness of monoclonal-antibodies to gram-negative endotoxin in the treatment of gram-negative sepsis in ICU patients. *Journal Of The American Medical Association*, 269(2):249–254, 1993.

[141] T. M. Perl, L. A. Dvorak, T. Hwang, and R. P. Wenzel. Long-term survival and function after suspected gram-negative sepsis. *Journal Of The American Medical Association*, 274(4):338–345, 1995.

[142] L. Genfa, Z. Jiang, Z. Hong, Y. M. Zheng, L. X. Wang, W. Guo, H. Ming, D. L. Jiang, and L. Z. Wei. The screening and isolation of an effective anti-endotoxin monomer from radix paeoniae rubra using affinity biosensor technology. *International Immunopharmacology*, 5(6):1007–1017, 2005.

[143] Y. G. Kim, C. S. Lee, W. J. Chung, E. Kim, D. S. Shin, J. H. Rhim, Y. S. Lee, B. G. Kim, and J. H. Chung. Screening of LPS-specific peptides from a phage display library using epoxy beads. *Biochemical And Biophysical Research Communications*, 329(1):312–317, 2005.

[144] C. J. C. de Haas, P. J. Haas, K. P. M. van Kessel, and J. A. G. van Strijp. Affinities of different proteins and peptides for lipopolysaccharide as determined by biosensor technology. *Biochemical And Biophysical Research Communications*, 252(2):492–496, 1998.

[145] Y. Y. Goh, B. Ho, and J. L. Ding. A novel fluorescent protein-based biosensor for gram-negative bacteria. *Applied And Environmental Microbiology*, 68(12):6343–6352, 2002.

[146] Y. Y. Goh, V. Frecer, B. Ho, and J. L. Ding. Rational design of green fluorescent protein mutants as biosensor for bacterial endotoxin. *Protein Engineering*, 15(6):493–502, 2002.

[147] E. A. James, K. Schmeltzer, and F. S. Ligler. Detection of endotoxin using an evanescent wave fiber-optic biosensor. *Applied Biochemistry And Biotechnology*, 60(3):189–202, 1996.

[148] M. Yang and J. Chen. Self-assembled monolayer based quartz crystal biosensors for the detection of endotoxins. *Analytical Letters*, 3(11):1775–1784, 2002.